Chemical Science

ROYAL SOCIETY OF CHEMISTRY

REVIEW

View Article Online
View Journal | View Issue

Cite this: *Chem. Sci.*, 2024, **15**, 13

f-Element heavy pnictogen chemistry

Jingzhen Du, [ab] Philip J. Cobb,[b] Junru Ding,[a] David P. Mills *[b] and Stephen T. Liddle *[b]

The coordination and organometallic chemistry of the f-elements, that is group 3, lanthanide, and actinide ions, supported by nitrogen ligands, *e.g.* amides, imides, and nitrides, has become well developed over many decades. In contrast, the corresponding f-element chemisty with the heavier pnictogen analogues phosphorus, arsenic, antimony, and bismuth has remained significantly underdeveloped, due largely to a lack of suitable synthetic methodologies and also the inherent hard(f-element)–soft(heavier pnictogen) acid–base mismatch, but has begun to flourish in recent years. Here, we review complexes containing chemical bonds between the f-elements and heavy pnictogens from phosphorus to bismuth that spans five decades of endeavour. We focus on complexes whose identity has been unambiguously established by structural authentication by single-crystal X-ray diffraction with respect to their synthesis, characterisation, bonding, and reactivity, in order to provide a representative overview of this burgeoning area. By highlighting that much has been achieved but that there is still much to do this review aims to inspire, focus and guide future efforts in this area.

Received 26th September 2023
Accepted 22nd November 2023

DOI: 10.1039/d3sc05056d

rsc.li/chemical-science

1. Introduction

Due to their widespread and important applications in magnetic materials,[1,2] electronic devices,[3,4] bioimaging,[5,6] synthesis,[7,8] catalysis,[9,10] materials science[11,12] and nuclear technologies,[13,14] there has been burgeoning interest in the fundamental chemistry of the f-elements over the past few decades. Since f-element metal ions, that is group 3, lanthanide, and actinide ions, are hard Lewis acids with typically large radii and high coordination numbers, they preferentially bind with hard bases (by the hard–soft-acid-base definition); the chemical bonds of these ions are understood to be predominantly ionic, thus their solution chemistry is dominated by N-, O-, and halide-donor ligands.[15] With ever-developing synthetic methods

[a]*College of Chemistry, Zhengzhou University, Zhengzhou, 450001, China*
[b]*Department of Chemistry and Centre for Radiochemistry Research, The University of Manchester, Oxford Road, Manchester, M13 9PL, UK. E-mail: david.mills@manchester.ac.uk; steve.liddle@manchester.ac.uk*

Jingzhen Du

Jingzhen Du received his BSc in 2013 from Shangqiu Normal University. Before moving to the University of Manchester as a President's Doctoral Scholarship PhD student in 2016 to investigate actinide nitride chemistry with Prof. Steve Liddle, he had a few years research training in Prof. Liang Deng's Group working on organometallic d-block compounds at Shanghai Institute of Organic Chemistry. In 2020, he received his PhD degree from the University of Manchester and continued as a Postdoctoral researcher in the Liddle group. In 2023, he started his independent career at Zhengzhou University. His research interests are organometallic f-block complexes with unusual structures, properties, and reactivities.

Philip J. Cobb

Philip Cobb gained his PhD in 2018 from the University of Manchester after conducting a research project on the chemistry of uranyl chemistry under the supervision of Prof. Steve Liddle. He then spent 2 years researching f-element complexes at Manchester before moving into the nuclear industry.

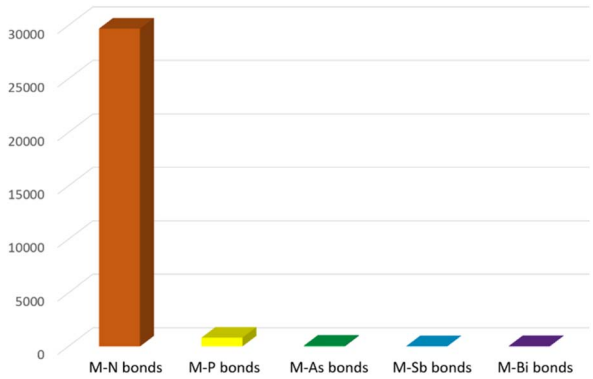

Fig. 1 Bar graph summarising the number of molecular structures deposited into the CCDC by 10-08-2023 for any type of f-element pnictogen bond. Total numbers: M–N = 29 713, M–P = 817, M–As = 67, M–Sb = 21, M–Bi = 28.

and characterisation techniques, molecular non-aqueous f-element chemistry has developed in recent years, and under non-aqueous conditions f-element complexes with novel linkages involving softer donor atoms can be accessed and investigated.[16] More peripherally, but still relevant, it is known that softer donor ligands can effect better selectivity in extraction processes, so the study of such linkages can provide bonding benchmarks of wider relevance.[17] For group 15, the pnictogens, f-element chemistry is well developed for nitrogen ligands, *e.g.* amides, imides, and nitrides, but this is not the case for the heavier congeners phosphorus, arsenic, antimony, and bismuth.[18–20] To illustrate the point, a search of the Cambridge Structural Database (CSD, 10th August 2023†)[21] for any type of crystallographically characterised chemical bond between the f-elements and any pnictogen reveals a stark picture, Fig. 1. There are almost thirty thousand complexes with f-element nitrogen bonds, over 30 times the total number of 933 for f-element heavier pnictogen complexes. Furthermore, below phosphorus there are only 67, 21, and 28 examples of f-element bonds to arsenic, antimony, and bismuth, respectively, with most of those examples reported in the last decade.

The above data parallel transition metal chemistry in many regards, though are a more extreme picture reflecting that stabilisation of the heavier and softer pnictogen ligands multiply bonded at large and hard Lewis acidic f-element metal ions is certainly more challenging. However, f-element pnictinidene and pnictido complexes remain of interest since in addition to being heavy amide, imide, and nitride analogues, they are isoelectronic congeners of transition metal alkyls, carbenes, and carbynes, respectively, that have developed into excellent catalysts for various organic transformations[22] or as precursors to inorganic materials.[23] Furthermore, whilst f-element phosphorus and arsenic multiple bonding is precedented, f-element antimony or bismuth multiple bonds are conspicuous by their absence.[20] Indeed, as group 15 is descended the pnictide ions become increasingly electropositive and metal-like, which increases the challenges of pairing electropositive f-element and increasingly large pnictogen metal ions together to form weak and highly polarised metal–metal bonds. Thus, well-defined molecules are of vital importance to study the inherent physicochemical properties and nature of covalency in f-element ligand bonds. This in turn could benefit the development of new synthetic methods, ligand design, catalytic

† Shortly after the census date of this review, reports of a yttrium-bismolyl complex and a yttrium-bismuth cluster were published by Demir and co-workers, and an account of rare-earth phosphinidene complexes was published by Chen and co-workers. See ref. 156–158 for details.

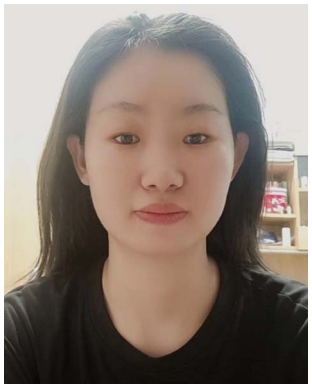

Junru Ding

Junru Ding received her MSc degree at Zhengzhou University in 2023, and then began her PhD investigating f-block organometallic chemistry under the supervision of Prof. Jingzhen Du at the College of Chemistry, Zhengzhou University.

David P. Mills

David P. Mills is a Professor of Inorganic Chemistry in the Department of Chemistry at The University of Manchester, where he started his independent career as a Lecturer in 2012. His current research interests are focussed on the synthesis, characterisation, and applications of coordinatively unsaturated complexes with unusual electronic structures and bonding motifs, mainly with the f-block elements.

Stephen T. Liddle

Steve Liddle is Professor and Head of Inorganic Chemistry and Co-Director of the Centre for Radiochemistry Research at the University of Manchester Department of Chemistry, which are positions he has held since 2015. His research interests broadly encompass the physical-inorganic chemistry of the f-elements, with particular interests in synthesis, reactivity, magnetism, small molecule activation, and catalysis.

Table 1 ^{31}P NMR chemical shifts of reported f-element complexes with phosphorus ligands in this review

Complex name	^{31}P NMR (ppm)	Solvent	Ref.
[Y(Cp″)$_2$(THF)(PHSi^{t}Bu$_3$)] (**5**)	−181.1	C_6D_6	44
[Y(Cp″)$_2${(μ-PH$_2$)(μ-Li[tmeda])}$_2$(Cl)}] (**6**)	−218.5	Toluene-d_8	45
[Yb(Cp*)$_2${(PCHCMeCMeCHC)$_2$}] (**8c**)	191.6	THF-d_8	48
[Yb(Cp*)$_2${(PCHCMeCMeCHC)$_2$}] (**8c**)	178.2	Toluene-d_8	48
[{Lu(PNP^{iPr})(μ-PMes)}$_2$] (**9**)	186.8	C_6D_6	50
[{Lu(PNP^{iPr})(μ-PMes)}$_2$] (**9**)	18.1	C_6D_6	50
[{Nd(μ-PDipp)(I)(THF)$_3$}$_2$] (**10**)	−168	C_6D_6	51
[{Sc(PNP^{iPr})(μ-PTripp)}$_2$] (**13**)	227.4	C_6D_6	53
[{Sc(PNP^{iPr})(μ-PTripp)}$_2$] (**13**)	7.0	C_6D_6	53
[Sc(PNP^{iPr})(μ-PDmp)(μ-Br)Li] (**14**)	9.8	C_6D_6	53
[Sc(PNP^{iPr})(μ-PDmp)(μ-Br)Li] (**14**)	8.0/13.2	C_6D_6	53
[Sc(PNP^{iPr})(μ-PDmp)(μ-Br)Li(DME)] (**15**)	56.1	C_6D_6	53
[Sc(PNP^{iPr})(μ-PDmp)(μ-Br)Li(DME)] (**15**)	10.8/5.6	C_6D_6	53
[{Sc(NCCN^{iPr})(μ-PXyl}$_2$] (**16**)	183.8	C_6D_6	54
[{Sc(NCCN^{iPr})(μ-PXyl)(DMAP)}$_2$] (**17**)	181.3	C_6D_6	54
[Sc(NCCN^{iPr})(2,2′-bipy){η^2-P$_2$(Xyl)$_2$}] (**18**)	30.0/25.9	C_6D_6	54
[{Sc(NCCN^{iPr})}$_2$(μ-S){μ-η^2-P$_2$(Xyl)$_2$}] (**19S**)	−79.0	C_6D_6	54
[{Sc(NCCN^{iPr})}$_2$(μ-Se){μ-η^2-P$_2$(Xyl)$_2$}] (**19Se**)	−72.2	C_6D_6	54
[{Sc(NCCNiPr)}$_2$(μ-Te){μ-η^2-P$_2$(Xyl)$_2$}] (**19Te**)	−60.1	C_6D_6	54
[Sc(NCCN^{Dipp})(Me){P(H)Dipp}] (**20**)	−90.9	C_6D_6	55
[{Sc(NCCN^{Dipp})}$_2$(μ-CH$_2$)(μ-PDipp)] (**21**)	84.1	C_6D_6	55
[{Y[PhC(NDipp)$_2$](μ$_2$-Me)}$_3$(μ$_3$-Me)(μ$_3$-PPh)] (**26Y**)	138.8	C_6D_6	56
[{Lu[PhC(NDipp)$_2$](μ$_2$-Me)}$_3$(μ$_3$-Me)(μ$_3$-PPh)] (**26Lu**)	103.4	C_6D_6	56
[{Y[PhC(NDipp)$_2$]}$_3$(μ$_2$-Me)$_2$(μ$_3$-Me)(μ$_2$,η^2:η^3-PC$_6$H$_4$)] (**27Y**)	262.48	C_6D_6	56
[{Lu[PhC(NDipp)$_2$]}$_3$(μ$_2$-Me)$_2$(μ$_3$-Me)(μ$_2$,η^2:η^3-PC$_6$H$_4$)] (**27Lu**)	192.52	C_6D_6	56
[{Y(Cp^{Me})$_2$}$_3$(μ-PMes)$_3$Li][Li(THF)$_4$]$_2$ (**28Y**)	57.24	C_6D_6	58
[Sc(NCCN^{Dipp}){PP(EDA^{Dipp})}] (**29**)	412.0	C_6D_6	59
[Sc(NCCN^{Dipp}){PP(EDA^{Dipp})}] (**29**)	157.2	C_6D_6	59
[Sc(NCCN^{Dipp}){PP(EDA^{Dipp})}] (**29**)	402.3	THF-d_8	59
[Sc(NCCN^{Dipp}){PP(EDA^{Dipp})}] (**29**)	158.5	THF-d_8	59
[Sc(NCCN^{Me}){PP(EDA^{Dipp})}] (**30**)	324.8	C_6D_6	59
[Sc(NCCN^{Me}){PP(EDA^{Dipp})}] (**30**)	169.0	C_6D_6	59
[Sc(NCCN^{Me}){PP(EDA^{Dipp})}] (**30**)	312.2	THF-d_8	59
[Sc(NCCN^{Me}){PP(EDA^{Dipp})}] (**30**)	166.8	THF-d_8	59
[Sc(NCCN^{Me}){(μ-PB)[N(Dipp)CHCHN(Dipp)]}(μ-Cl)K]$_2$ (**35**)	11.4	Toluene-d_8	60
[Sc(NCCN^{Me}){(μ-PB)[N(Dipp)CHCHN(Dipp)]}(μ-Cl){K(DB18C6)}] (**36**)	19.6	Toluene-d_8	60
[Sc(NCCN^{Me}){N(^{i}Pr)C(PB{N(Dipp)CHCHN(Dipp)})N(^{i}Pr)}] (**37**)	−103.1	C_6D_6	60
[Y(Tp^{tBu,Me})(Me)(HPDipp)] (**38Y**)	−117.8	C_6D_6	61
[Y(Tp^{tBu,Me})(PDipp)(DMAP)$_2$] (**40**)	−5.5	C_6D_6	61
[{Y(I)}{Y[μ$_3$-P(Dipp)](μ-I)(THF)}$_4$(μ$_6$-P){K(C$_7$H$_8$)}] (**41**)	347.4	C_6D_6	62
[{Y(I)}{Y[μ$_3$-P(Dipp)](μ-I)(THF)}$_4$(μ$_6$-P){K(C$_7$H$_8$)}] (**41**)	154.7	C_6D_6	62
[{Y(I)}{Y[μ$_3$-P(Dipp)](μ-I)(THF)}$_4$(μ$_6$-P){K(THF)}] (**42**)	346.6	C_6D_6	62
[{Y(I)}{Y[μ$_3$-P(Dipp)](μ-I)(THF)}$_4$(μ$_6$-P){K(THF)}] (**42**)	154.3	C_6D_6	62
[{Y(I)}{Y(I)(THF)}$_2${Y(THF)$_2$}$_2$(μ-I)[μ$_3$-P(Dipp)]$_4$(μ$_5$-P)] (**43**)	358.8	THF-d_8	62
[{Y(I)}{Y(I)(THF)}$_2${Y(THF)$_2$}$_2$(μ-I)[μ$_3$-P(Dipp)]$_4$(μ$_5$-P)] (**43**)	148.4	THF-d_8	62
[{Y(I)}{Y(I)(THF)}$_2${Y(NCCN^{iPr})}$_2$(μ-I)[μ$_3$-P(Dipp)]$_4$(μ$_5$-P)] (**44**)	400.7	THF-d_8	62
[{Y(I)}{Y(I)(THF)}$_2${Y(NCCN^{iPr})}$_2$(μ-I)[μ$_3$-P(Dipp)]$_4$(μ$_5$-P)] (**44**)	176.3/172.9	THF-d_8	62
[{Y(THF)}{Y(μ-I)(THF)}$_2${Y(THF)}{Y(Cp*)}(μ$_3$-I)(μ-I)[μ$_3$-P(Dipp)]$_4$(μ$_6$-P){K(THF)}] (**45**)	300.9	THF-d_8	62
[{Y(THF)}{Y(μ-I)(THF)}$_2${Y(THF)}{Y(Cp*)}(μ$_3$-I)(μ-I)[μ$_3$-P(Dipp)]$_4$(μ$_6$-P){K(THF)}] (**45**)	72.8 to 130.4	THF-d_8	62
[{Sc(NN^{fc})}$_3$P$_7$] (**47Sc**)	−131.4 to 23.2	C_6D_6	64
[{Y(NN^{fc})(THF)}$_3$P$_7$] (**47Y**)	−130.4 to −20.4	C_6D_6	64
[{Sm(DippForm)$_2$}$_2$(μ^2-η^4:η^4-P$_4$)] (**48**)	453	C_6D_6	67
[{Y(DippDBD)(THF)}$_2$(P$_3$)][K(18C6)(toluene)] (**49**)	−273.01	THF-d_8	68
[Th(Cp*)$_2$(PPh$_2$)$_2$] (**50**)	143	C_6D_6	79
[Th(Cp*)$_2$(μ-PPh$_2$)$_2$Ni(CO)$_2$] (**51**)	177	C_6D_6	79
[Th(Cp*)$_2$(μ-PPh$_2$)$_2$Pt(PMe$_3$)] (**52**)	149.3	Toluene-d_8	80
[Th(Cp*)$_2$(μ-PPh$_2$)$_2$Pt(PMe$_3$)] (**52**)	−3.3	Toluene-d_8	80
[Th(Cp*)$_2$(PHTripp)$_2$] (**53**)	1.66	C_6D_6	81
[Th(Tren^{TIPS})(PH$_2$)] (**54Th**)	−144.08	C_6D_6	83
[U(Tren^{TIPS})(PH$_2$)] (**54U**)	595.07	C_6D_6	82
[Th(Tren^{TCHS})(PH$_2$)] (**55Th**)	−133.01	THF-d_8	84
[U(Tren^{TCHS})(PH$_2$)] (**55U**)	605.91	THF-d_8	84
[{Th(Cp*)$_2$}$_2${μ-P[(2,6-CH$_2$CHCH$_3$)$_2$-4-^{i}PrC$_6$H$_2$]}] (**57**)	161.9	C_6D_6	81

Table 1 (*Contd.*)

Complex name	^{31}P NMR (ppm)	Solvent	Ref.
[{Th(Cp*)$_2$(μ-PTripp)(μ-PHTripp)(K)}$_2$] (**58**)	171.91	THF-d_8	87
[{Th(Cp*)$_2$(μ-PTripp)(μ-PHTripp)(K)}$_2$] (**58**)	−110.54	THF-d_8	87
[Th(Cp*)$_2$(PTripp)}(PHTripp)][K(2,2,2-cryptand)] (**59**)	177.86	THF-d_8	87
[Th(Cp*)$_2$(PTripp)}(PHTripp)][K(2,2,2-cryptand)] (**59**)	−106.99	THF-d_8	87
[{Th(Cp^{tt})$_2$(PMes*}(ClK)}$_2$](**60**)	108.79	C_6D_6	93
[Th(Cp^{tt})$_2$(PMes*)(μ-Cl){K(18C6)}] (**61**)	133.5	C_6D_6	93
[U(Cp*)$_2$(PMes*)(OPMe$_3$)] (**62**)	71.06	C_6D_6	95
[U(Cp*)$_2$(PMes*)(OPMe$_3$)] (**62**)	−59.84	C_6D_6	95
[Th(Cp^{ttt})$_2$(PMes*)] (**63**)	145.7	C_6D_6	97
[{U(Tren^{TIPS})(μ-PH)}{K(2,2,2-cryptand)}] (**66**)	2460.4	C_6D_6	82
[Th(Tren^{TIPS})(PH)][Na(12C4)$_2$] (**67**)	198.8	C_6D_6	83
[Th(Tren^{TCHS})(PH)][Na(2,2,2-cryptand)] (**69Th**)	266.16	THF-d_8	84
[U(Tren^{TCHS})(PH)][Na(2,2,2-cryptand)] (**69U**)	2628.50	THF-d_8	84
[{Th(Tren^{TIPS})}$_2$(μ-P)][Na(12C4)$_2$] (**70**)	553.5	THF-d_8	83
[{Th(Tren^{TIPS})}$_2$(μ-PH)] (**71Th**)	145.7	C_6D_6	83
[Th(Tren^{TIPS})(OCP)] (**74Th**)	−339.91	C_6D_6	110
[U(Tren^{TIPS})(OCP)] (**74U**)	−319.96	C_6D_6	109
[{Th(Tren^{TIPS}) }$_6$(μ-OC$_2$P$_3$)$_2$(μ-OC$_2$P$_3$H)$_2$Rb$_4$] (**76**)	217.99 to 261.14	C_6D_6	110
[{Th(Cp^{tt})$_2$}$_2$(μ^2-η^4-P$_6$)] (**77**)	−41.9 to 125.3	Toluene-d_8	111
[{Th(Cp^{tt})$_2$}(μ^2-η^3-P$_3$){Th(Cp^{tt})$_2$Cl}] (**78**)	−94.5 to −69.7	CD_2Cl_2	111
[{U(Cp*)(C$_8$H$_6$(Si^{i}Pr$_3$)$_2$)}$_2$(μ^2-η^4-P$_4$)] (**79**)	718	C_6D_6	112
[{Th(Cp″)$_3$}$_2$(μ^2-η^2-P$_4$)] (**80**)	−246.55 to 323	C_6D_6	113

transformations, and materials precursors. Reflecting the growing nature of this field, there have been a number of excellent but very general or ligand-specific review articles and book chapters covering the historical developments of some of the subtopics,[20,24–29] but recent developments justify a broad but detailed review specifically focussed on this topic.

This review highlights the most notable achievements in the field of f-element heavy pnictogen chemistry from phosphorus to the heaviest abundant main group element bismuth up to August 2023. In line with the criteria for reviews, a representative selection, rather than a complete literature survey, is presented, and discussions concentrate on structurally characterised molecules. We aim to highlight the major advances involving all heavy pnictogen ligand types, with the exception of phospholyl and arsolyl ligands, which were reviewed in 2021,[30] and $(OCE)^-$ (E = P, As) ligands, which were reviewed in 2019 and are normally O-bound unless the E centre decisively directs the chemistry;[31] several other previous reviews have separately covered the ligand classes that comprise this review.[20,24–29] Here we present current challenges to inspire researchers and focus and guide future efforts of the field to develop f-element heavy pnictogen chemistry more rapidly in the future. In this review, we include the group 3 elements scandium, yttrium, and lanthanum under the heading of lanthanide sections for convenience. ^{31}P NMR chemical shifts for P-bound complexes covered in this review are compiled in Table 1.

2. Nomenclature

Metal heavy pnictogen nomenclature depends upon the pnictogen identity, charge and binding mode. The prefix is determined by the pnictogen identity; the general prefix is 'pnict-', whilst bonds involving phosphorus, arsenic, antimony and bismuth begin with 'phosph-', 'ars-', 'stib-', and 'bism-', respectively. The suffix denotes the charge of the pnictogen and binding mode; the suffix 'ide' is used for a terminally bound pnictogen bearing a formal −1 charge, whereas a terminal pnictogen with a −2 charge ends with '-inidene'. A bridging pnictogen with a −2 charge has the suffix '-inidiide', and lastly a pnictogen bearing a −3 charge ends with '-ido', independent of the binding mode. This gives the four bonding types: pnictide (I), pnictinidiide (II), pnictinidene (III) and pnictido (IV), Fig. 2. Exceptions to these rules are seen for $(As)^{3-}$ and $(R_2As)^-$ ligands, which are given the prefix 'arsen-' to give the respective terms arsenido and arsenide when bound to metal centres. An additional exception is made for the parent phosphide $(H_2P)^-$, which is given the unique moniker 'phosphanide'. However, within some f-element pnictinidiide and pnictido examples, the ligands can be bridged by more than two metal centres to form more complex bonding modes which are not presented in Fig. 2, but will be discussed with specific examples in the following sections.

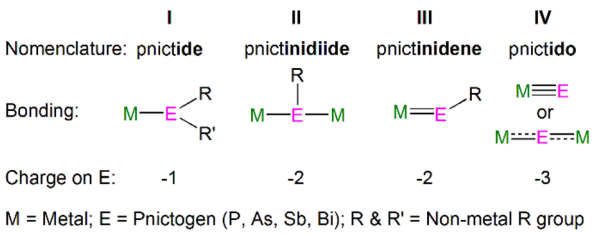

Fig. 2 General nomenclature for pnictogen metal bonding.

3. Synthetic methodologies for generating f-element pnictogen bonds

Precise synthetic strategies can vary depending on the type of pnictogen reagents and f-element precursors, but a pnictogen donor ligand is commonly installed on an f-element metal centre in one of the following general ways:

(1) Dative coordination of a neutral phosphorus or arsenic ligand to form an adduct with an f-element complex that has an available vacant coordination site; this tends to not be the case for antimony or bismuth, which need to be negatively charged to coordinate to an f-element metal centre.

(2) Salt elimination/metathesis of alkali metal pnictogen anions with an f-element halide (or halide equivalent) precursor to produce a polarised-covalent f-element pnictogen linkage.

(3) Alkane elimination between a primary or secondary pnictogen precursor and f-element alkyl (or cyclometallate) complex exploiting the acidic nature of the proton on the pnictogen atom.

(4) Oxidising highly reducing low-valent f-elements with pnictogen compounds.

(5) Combining salt and alkane elimination approaches using a primary pnictide alkali metal salt to react with an f-element alkyl and halide starting material (mainly used to produce metal–ligand multiple bonds).

4. Lanthanide phosphorus complexes

The past few decades have seen significant progresses in f-element phosphorus chemistry, with many novel f-element phosphorus motifs isolated and investigated.[20,24–29] The neutral, soft phosphine donor tends to form weak dative bonding interactions to hard f-element metal ions, though this can be overcome by incorporating P-donor centres into polydentate ligands as demonstrated separately by Fryzuk and Lu,[32–34] and such complexes were reviewed previously, so these compounds are not included here.[20,26,32–34] This section discusses recent advances in f-element complexes containing phosphide/phosphanide, phosphorin, phosphinidiide/phosphinidene, phosphido, and inorganic polyphosphorus ligands.

4.1 Lanthanide phosphide complexes

Due to the large size of the metal ions, lanthanide phosphide complexes tend to form multi-nuclear species with bridging phosphide ligands; mono-nuclear complexes are therefore relatively rare and usually require bulky stabilising phosphorus substituents as demonstrated by Izod.[35–37] The first mononuclear lanthanide phosphide complex [Tm{P(SiMe$_3$)$_2$}$_3$(THF)$_2$] (**1Tm**) was reported by Rabe and co-workers in 1995, Fig. 3; this was prepared from the reaction of [TmI$_3$(THF)$_{3.5}$] with three equivalents of KP(SiMe$_3$)$_2$ in THF *via* salt elimination.[38] The molecular structure of **1Tm** exhibits the five-coordinate thulium centre in a distorted trigonal bipyramidal geometry with two axial THF molecules and three equatorial bis(trimethylsilyl)phosphide ligands. The Tm–P bond distances

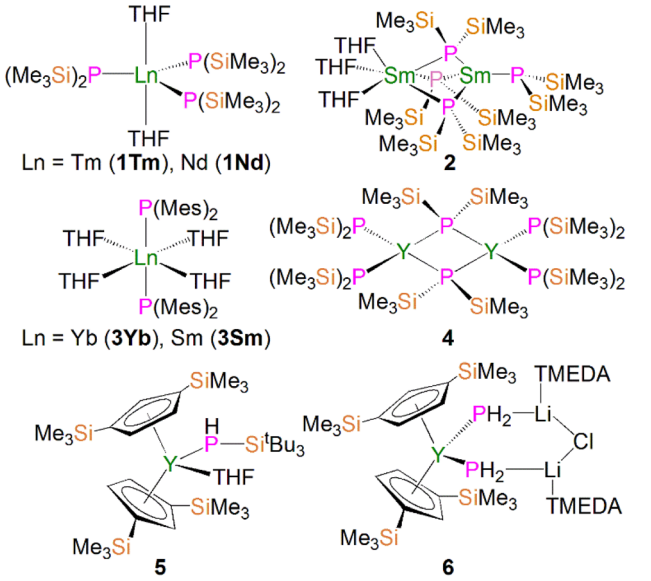

Fig. 3 Examples of lanthanide–phosphide complexes **1–6**.

of 2.709(1) and 2.701(2) Å are typical of single bonds. Subsequently, the isostructural neodymium analogue [Nd{P(SiMe$_3$)$_2$}$_3$(THF)$_2$] (**1Nd**) was isolated using the same synthetic approach, Fig. 3. The Nd–P bond lengths of 2.80(4) and 2.83(3) Å are slightly longer than those in **1Tm**, attributed to the larger metal radii of Nd than Tm in the same coordination environment.[39] However, because of the paramagnetic metal centres, no resonances were observed in their ^{31}P NMR spectra. However, the similar reaction of the divalent samarium precursor [SmI$_2$(THF)] with two equivalents of KP(SiMe$_3$)$_2$ in THF produced dinuclear and asymmetric [Sm{P(SiMe$_3$)$_2$}{μ-P(SiMe$_3$)$_2$}$_3$Sm(THF)$_3$] (**2**).[40] Using a similar salt elimination method, Nief and co-workers showed that monomeric divalent lanthanide phosphide complexes could be accessed by isolation of [Ln{P(Mes)$_2$}$_2$(THF)$_4$] (Ln = Yb, **3Yb**, Sm, **3Sm**; Mes = 2,4,6-Me$_3$C$_6$H$_2$), Fig. 3, where the metal centres adopt octahedral geometries with two axial bis(mesityl)phosphide ligands and four equatorial THF molecules.[41,42] According to the +2 oxidation state, the Sm–P bond of 3.034(2) Å in **3Sm** is significantly longer than those of trivalent **1Ln**. In 1997, Rabe and co-workers also reported the synthesis and molecular structures of the first examples of divalent lanthanide phosphide complexes containing primary phosphide ligands, [Ln{HP(Mes*)}$_2$(THF)$_4$] (Ln = Yb, Eu; Mes* = 2,4,6-^{t}Bu$_3$C$_6$H$_2$), which also exhibit octahedral metal centres.[43]

In 2002, Westerhausen and co-workers isolated a dinuclear yttrium phosphide complex [Y{P(SiMe$_3$)$_2$}$_2${μ-P(SiMe$_3$)$_2$}]$_2$ (**4**) and a mono-nuclear yttrium phosphide complex [Y(Cp″)$_2$(THF)(PHSi^{t}Bu$_3$)] (**5**, Cp″ = 1,3-(SiMe$_3$)$_2$C$_5$H$_3$), Fig. 3.[44] The latter contains one primary phosphide ligand stabilised by the sterically demanding Cp″ ligands paired with the bulky phosphorus substituents. With the convention of using a Cp″ centroid as a ligating point, the molecular structure of **5** revealed that the metal centre adopts a pseudo-tetrahedral geometry and the Y–P

bond distance is 2.770(1) Å. Complex **5** is diamagnetic and the ^{31}P NMR spectrum exhibits a doublet of doublets resonance at −181.1 ppm with $^{1}J_{YP}$ and $^{1}J_{PH}$ values of 144.0 and 201.0 Hz, respectively. Phosphanide complexes featuring the $(PH_2)^-$ ligand are exceedingly rare for f elements. Although actinide phosphanide complexes with terminal An–PH_2 linkages are known (see below), isostructural analogues still remain rare for lanthanides. The only relevant example is the yttrium complex $[Y(Cp'')_2\{(\mu\text{-}PH_2)(\mu\text{-}Li[tmeda])\}_2(Cl)\}]$ (**6**), Fig. 3, which contains two $(PH_2)^-$ groups that bridge to two lithium cations.[45] It was found that **6** is unstable in both solid and solution states, and decomposes under argon atmosphere at room temperature to produce PH_3 as well as a small amount of H_2PSiMe_3, reflecting the synthetic challenge of stabilising terminal lanthanide-PH_2 species.

4.2 Lanthanide phosphorin and biphosphinine complexes

In 1997, Cloke and co-workers reported the synthesis and molecular structure of the bis(2,4,6-tri-*tert*-butyl-phosphorin) holmium(0) complex $[Ho(\eta^6\text{-}Ttp)_2]$ (**7**), Fig. 4, prepared by co-condensation of holmium vapor with an excess of 2,4,6-tri-*tert*-butyl-phosphorin at −196 °C followed by further work-up and recrystallisation.[46] The remarkable thermostability of **7** ($T_{sublimation}$ = 160 °C, 10^{-5} mbar, 90% recovery) arises from the better π-acceptor capability for phosphorin over arenes, which was confirmed by optical and magnetic data for **7**. The structure of **7** was found to exhibit extensive disorder, with the P-atoms equally disordered over the three possible positions of each phosphorin ligand, so no preference for *syn* or *anti* conformations could be inferred.

During 2014 to 2016 Nocton, Clavaguéra, and co-workers reported biphosphinine complexes of the general formula $[Ln(L)_2\{(PCHCMeCMeCHC)_2\}]$ (Ln = Tm, L = $\{P(CBu^tCMe)_2\}$, **8a**; Ln = Sm or Yb, L = Cp*, C_5Me_5, **8b**, **8c**),[47,48] Fig. 4. In these complexes the biphosphinine ligands are formally radical anions but the extent of electron transfer for the Yb complex was ambiguous, with characterisation data intermediate to closed or fully open shell formulations. The Tm–P, Sm–P, and Yb–P distances were found to be 2.825/2.862(2), 2.909(2)/2.927(2), and 2.872(2)/2.938(2) Å, consistent with the radii of the lanthanide ions. We note that this work followed on from prior work on P-methylated phosphinine ligands with chelating side arms from Arliguie, Mézailles, and co-workers; however, in those complexes the anion charge partially delocalises into the C_5P rings, resulting in rather long M–P bonds (~3 Å for Ce, Nd, and U) that are between dative phosphines and covalent phosphides,[49] thus we do not discuss them further.

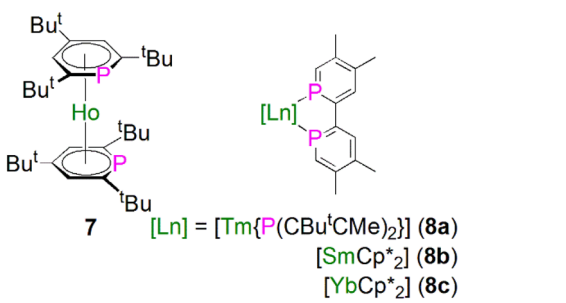

Fig. 4 Lanthanide complexes containing phosphorin ligands **7** and **8**.

4.3 Lanthanide phosphinidiide complexes

Unlike their d-transition metal counterparts, lanthanide–pnictogen multiple bonds are relatively rare as a result of the valence orbital spatial and energy mismatch of 4f metal ions and pnictogen ligands. Most lanthanide pnictinidenes form bridging dimeric pnictinidiide complexes where the "Ln=Pn" moiety is stabilised through additional interactions with adjacent rare earth metal centres or electropositive alkali metal cations.[26] This section describes the progresses made in isolation of a handful of lanthanide pnictinidiide complexes before the terminal phosphinidene species was finally secured very recently.

In 2008, Kiplinger and co-workers synthesised the first bridging phosphinidiide lanthanide complex $[Lu\{(PNP^{iPr})(\mu\text{-}PMes)\}_2]$ (**9**, PNP^{iPr} = $[\{2\text{-}(^iPr_2P)C_6H_4\}_2N]^-$) by protonolysis of $[(PNP^{iPr})Lu(CH_2SiMe_3)_2]$ with $MesPH_2$, in 52% yield, Scheme 1.[50] Complex **9** exhibits an asymmetric Lu_2P_2 core, with two short [2.5973(15)/2.6031(16) Å] and two long [2.6527(16)/2.6724(14) Å] Lu–P bonds. The sum of the angles about the phosphorus atoms range from 358.9 to 356.5°, which indicates that the phosphorus lone pairs possibly π-donate to the Lu ions. The authors concluded that the structural data for **9** suggested

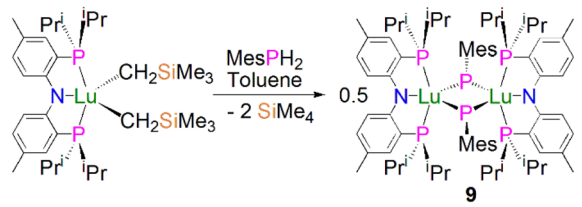

Scheme 1 Synthesis of Lu–phosphinidiide complex **9**.

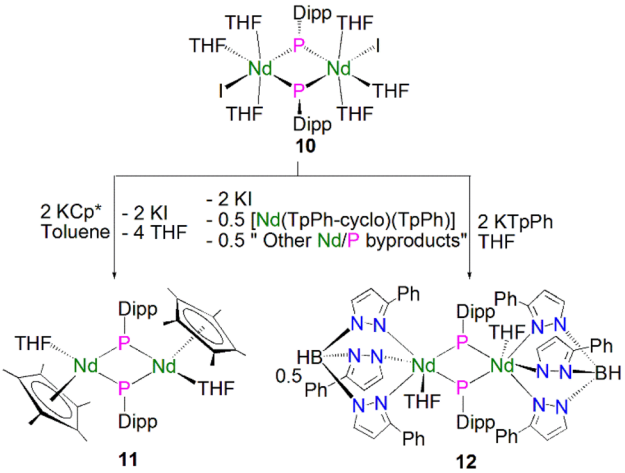

Scheme 2 Synthesis of Nd–phosphinidiide complexes **10**–**12**.

that the complex formed *via* the dimerisation of a transient terminal phosphinidene species, [Lu(PNP^{iPr})(PMes)].

Soon afterwards, Chen and co-workers reported the synthesis of the first early lanthanide phosphinidiide complex, [{Nd(I)(μ-PDipp)(THF)$_3$}$_2$] (**10**, Dipp = 2,6-^{i}Pr$_2$C$_6$H$_3$), *via* the concomitant salt elimination and silyl redistribution reaction of [NdI$_3$(THF)$_{3.5}$] with two equivalents of KP(SiMe$_3$)(Dipp) to eliminate one equivalent of P(SiMe$_3$)$_2$(Dipp) and two equivalents of KI, Scheme 2.[51] The Nd(III) ions in **10** exhibits pseudo-octahedral geometries, with the two bridging phosphinidiides forming an asymmetric Nd$_2$P$_2$ core that is analogous to the Ln$_2$P$_2$ core of **9**, with Nd–P bond distances of 2.7314(15) and 2.7769(16) Å. In common with **9**, the phosphorus atoms in **10** are trigonal planar, with the sum of bond angles equalling 359.1°. The authors carried out preliminary investigations into the reactivity of **10**, establishing that it reacts in a similar fashion to carbenes with substrates such as benzophenone to give a phosphaalkene.

In 2010 Chen and co-workers later expanded the range of neodymium phosphinidiide complexes, utilising **10** in salt metathesis reactions with two equivalents of either KCp* or KTp^{Ph} (KHB(3-Ph-N$_2$C$_3$H$_2$)$_3$) to yield the phosphinidiide complexes [{Nd(Cp*)(μ-PDipp)(THF)}$_2$] (**11**) and [{Nd(Tp^{Ph})(μ-PDipp)(THF)}$_2$] (**12**), respectively, Scheme 2.[52] Complex **11** was isolated as the major product in a yield of 52%. Complex **12**, however, was initially isolated as a crystalline mixture with the cyclometallated complex [Nd(Tp^{Ph}-*cyclo*)(TpPh)], with purification of the two complexes performed *via* the manual separation of crystals. The solid-state structure of **11** revealed that there is a loss of the trigonal planar geometry of the bridging phosphinidiides, indicated by the decrease of the sum of bond angles of the phosphorus atom to 349.2(3)° when compared to complexes **12** [358.9(4)°] and **10** [359.1°], which could be a result of the coordination of the sterically demanding Cp* ligand. Complex **11** exhibits an analogous Nd$_2$P$_2$ core to that of **10**, with inequivalent Nd–P distances of 2.7456(11) and 2.7827(10) Å, whilst **12** demonstrates a more regular core geometry with Nd–P distances of 2.7808(16) and 2.7911(15) Å. The molecular structure of **12** exhibits one inverted pyrazolyl group on each Tp^{Ph} ligand, which is a result of isomerisation of the ligand *via* a 1,2-shift to relieve steric buttressing between the Tp^{Ph} ligand and the phosphinidiide Dipp group.

In 2010, Mindiola and co-workers reported that the reaction of the sterically demanding phosphide precursor, LiPH(Tripp) (Tripp = 2,4,6-^{i}Pr$_3$C$_6$H$_2$), with [Sc(PNP^{iPr})(Me)(Br)] yielded the bridging phosphinidiide dinuclear scandium complex

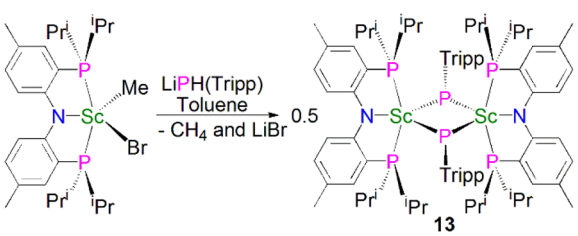

Scheme 3 Synthesis of Sc–phosphinidiide complex **13**.

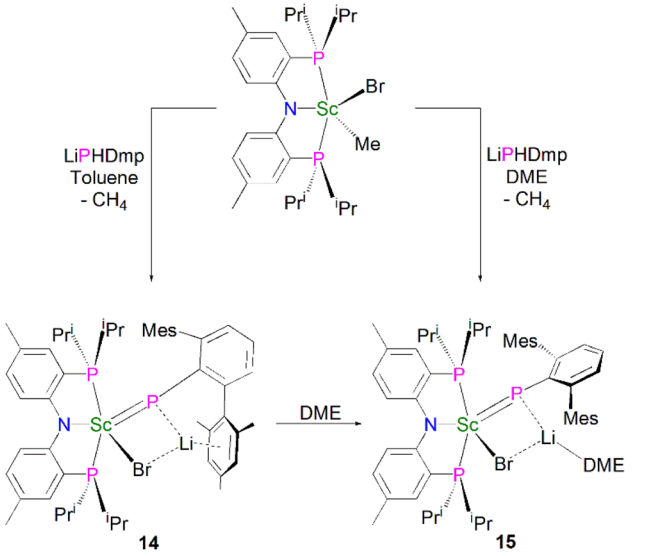

Scheme 4 Synthesis of Sc–phosphinidiide complexes **14** and **15**.

[{Sc(PNP^{iPr})(μ-PTripp)}$_2$] (**13**), Scheme 3, again *via* the elimination of one equivalent each of methane and lithium bromide.[53] The authors postulated that **13** formed *via* aggregation of a transient terminal scandium phosphinidene species, [Sc(PNP^{iPr})(PTripp)]. The molecular structure of **13** revealed an asymmetric four-membered Sc$_2$P$_2$ ring core, with similar Sc–P bond distances of 2.5446(8) and 2.5527(10) Å. Based on the crystallographic data for **13** the authors proposed that the phosphorus lone pairs are delocalised around the Sc$_2$P$_2$ core.

Mindiola and co-workers subsequently disclosed the first mononuclear rare earth phosphinidiide complexes. The Li-capped complexes [Sc(PNP^{iPr})(μ-PDmp)(μ-Br)Li(DME)$_n$] (Dmp = 2,6-Mes$_2$C$_6$H$_3$; n = 0, **14**; n = 1, **15**) were prepared from the concomitant salt metathesis and protonolysis reactions of the bulky primary phosphide lithium salt, LiPHDmp with [(PNP^{iPr})Sc(Me)(Br)], eliminating methane as the driving force, to give **14** (55%) and **15** (47%), Scheme 4.[53] The exact product depends on the reaction solvent; complex **15** was also synthesised by the addition of a stoichiometric amount of DME to **14** (21%). Single crystal X-ray diffraction studies revealed that both **14** and **15** have short Sc–P bond lengths of 2.338(2) and 2.3732(18) Å, respectively. Calculations performed on **15** indicated that the Sc=P bond has significant multiple bond character with a Mayer bond order of 1.46. The authors varied the reaction

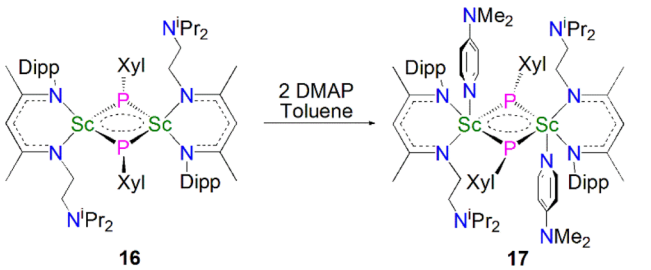

Scheme 5 Synthesis of Sc–phosphinidiide complexes **16** and **17**.

conditions for the synthesis of **14** and **15** to investigate if the elimination of LiBr was possible. However, heating reaction mixtures up to 100 °C did not liberate the occluded LiBr.

In 2013, Maron, Chen and co-workers utilised a similar one-pot salt metathesis and protonolysis methodology with the reaction of KPHXyl (Xyl = 2,6-$Me_2C_6H_3$) with [Sc(NCCN^{iPr})(Me)(Cl)] (NCCN^{iPr} = MeC(NDipp)CHC(Me)(NCH$_2$CH$_2$N^{i}Pr$_2$) yielding the bridging phosphinidiide dinuclear scandium complex [{Sc(NCCN^{iPr})(μ-PXyl}$_2$] (**16**, 74%), *via* the elimination of KI and methane, Scheme 5.[54] In contrast with the previously reported Sc–phosphinidiide complex **13**, the Sc_2P_2 core in **16** is more symmetric with Sc–P distances of 2.522(1) and 2.528(1) Å. They also attempted to synthesise a terminal Sc–phosphinidene complex by reacting **16** with a strongly donating ligand, DMAP (DMAP = 4-NMe_2-C_5H_4N) to break the dimer up; however, this resulted in the formation of the adduct [{Sc(NCCN^{iPr})(μ-PXyl)(DMAP)}$_2$] (**17**) in a 90% yield. The authors noted that **17** was the major product if an excess of DMAP (four equivalents) was added to **16**. Whilst **17** retains its Sc_2P_2 core, the Sc–P bonds are longer than **16** at 2.540(1) and 2.589(1) Å, reflecting the increased Sc coordination numbers.

Maron, Chen and co-workers showed that **16** exhibits notable redox chemistry; for example, the addition of three equivalents of 2,2′-bipyridine (2,2′-bipy) results in the oxidative coupling of two phosphinidiide fragments to form a diphosphanide Sc-complex [Sc(NCCN^{iPr})(2,2′-bipy){η^2-P$_2$(Xyl)$_2$}] (**18**), with the single electron reduction of two molecules of 2,2′-bipy affording [Sc(NCCN^{iPr})(2,2′-bipy·)$_2$] as a side product, Scheme 6. Similarly, the oxidative coupling of the two (PXyl)$^{2-}$ ligands to (P$_2$(Xyl)$_2$)$^{2-}$ promotes the reduction of elemental selenium/tellurium or Ph_3P=E (E = Se or S) to S^{2-}, Se^{2-} or Te^{2-}, yielding the bridging chalcogenido complexes [{Sc(NCCN^{iPr})}$_2$(μ-E){μ-η^2-P$_2$(Xyl)$_2$}] (**19E**, E = S, Se or Te). The authors also found that **16** readily undergoes nucleophilic addition chemistry with a range of unsaturated allene, nitrile, isocyanide, and CS_2 substrates to generate the corresponding organophosphorus scandium complexes. In follow-up work they reported that **16** could readily cleave the boron–oxygen bonds in pinacol–borane and catecholborane to give complexes featuring a newly-generated ligand (HB{P(Xyl)}$_2$)$^{2-}$, demonstrating the reactive nature of the Sc-phosphinidiide species due to the highly ionic Sc–P bonding interaction.[54]

In 2015, Maron, Chen and co-workers found that thermal decomposition of the scandium phosphide precursor [Sc(NCCN^{Dipp})(Me){P(H)Dipp}] (**20**, NCCN^{Dipp} = {MeC(NDipp)}$_2$CH) supported by the NCCN^{Dipp} scaffold afforded the scandium phosphinidiide complex [{(NCCN^{Dipp})Sc}$_2$(μ-CH$_2$)(μ-PDipp)] (**21**). However, this reaction also gave a diphosphide by-product [(NCCN^{Dipp}){P(H)Dipp}$_2$] in a 1 : 1 ratio with **21**. An optimal route was then implemented by reacting one equivalent of **20** with [Sc(NCCN^{Dipp})(Me)$_2$], giving **21** in a 77% yield, Scheme 7.[55] Complex **21** exhibits Sc–P bond lengths of 2.495(1) and 2.508(1) Å, which are shorter than other scandium bridging phosphinidiide complexes. Interestingly, there is an up-field shift of the phosphinidiide moiety resonances in the ^{31}P NMR spectrum of **21** to 84.1 ppm, *cf.* **13** (227.4 ppm) and **16** (183.8 ppm), which is presumably due to one of the bridging phosphinidiide units being replaced by a methylidene fragment.

In the same publication Maron, Chen and co-workers conducted a reactivity study of **21**; this revealed that, in contrast with the previously reported complex **16**, the phosphinidiide ligand in **21** is relatively unreactive, with all small molecules reacting at the adjacent methylidene centre, Scheme 8. The reaction of **21** with either CO_2, PhCN, ^{t}BuNC or CS_2 resulted in

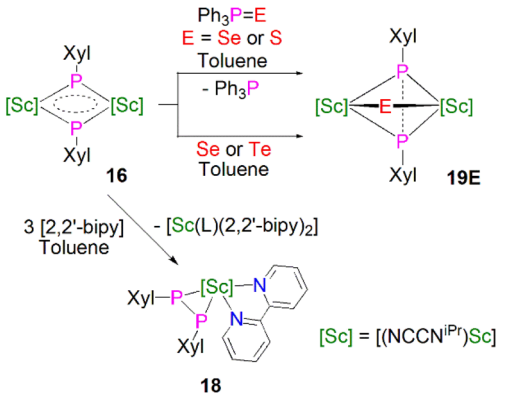

Scheme 6 Selected redox reactions of **16**.

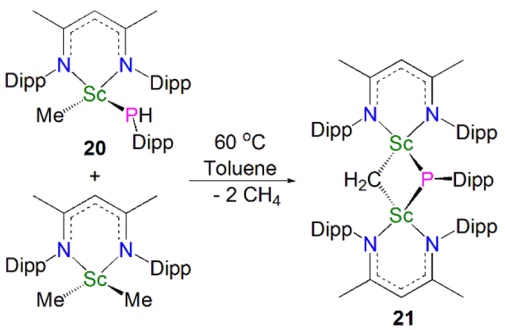

Scheme 7 Synthesis of the Sc–phosphinidiide complex **21**.

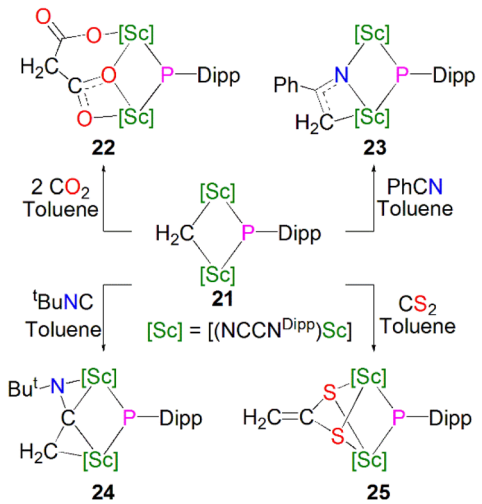

Scheme 8 Reactivity of Sc–phosphinidiide complex **21**.

insertion of the unsaturated functional group into the Sc–CH_2 bonds to give the bridging phosphinidiide complexes [{Sc(NCCN^{Dipp})}$_2$(L){μ-P(Dipp)}] (L = μ-O-COCH$_2$CO$_2$, **22**; μ-N-C(Ph)(CH$_2$), **23**; μ-C(CH$_2$)(N^{t}Bu), **24**; or (μ-S)$_2$CCH$_2$, **25**). Complexes **22–25** all demonstrate similar Sc–P distances between 2.4922(13) and 2.588(2) Å. DFT studies of **21** indicated that the lack of reactivity of the Sc–P bond was possibly due to its increased covalency when compared to the Sc–C bonds in the same complex.[55]

Zhou, Luo, Zhang and co-workers later expanded the number of structurally characterised lanthanide phosphinidiide complexes *via* the protonolysis reactions of [{Ln[PhC(NDipp)$_2$](μ$_2$-Me)}$_3$(μ$_3$-Me)(μ$_3$-CH$_2$)] (Ln = Y, Lu) and one equivalent of $PhPH_2$ to give the clusters [{Ln[PhC(NDipp)$_2$](μ$_2$-Me)}$_3$(μ$_3$-Me)(μ$_3$-PPh)] (Ln = Lu, **26Lu**, 92%; Ln = Y, **26Y**, 90%), Scheme 9.[56] These clusters exhibit a rare μ^3-bridging mode of the phosphinidiide between three rare earth metal ions, which is in contrast to most other rare earth phosphinidiide complexes where a μ^2-bridging mode is observed. Complex **26Y** exhibits one long [2.9432(12) Å] and two short [2.7142(11) and 2.7317(12) Å] Y–P bond lengths. The longer distance is within the range of previously reported dative R$_2$P:→Ln(III) interactions. Once the change in metal radii is accounted for, this rationale can be applied to **26Lu**, which exhibits similar asymmetric bonding between the phosphinidiide and three bonded Ln(III) ions, with Lu–P distances of 2.902(2), 2.684(2) and 2.639(2) Å. Both complexes contain P–C bonds that are bent out of the Ln$_3$ plane (Lu: 49.3°; Y: 59.1°); this differs from analogous transition metal bridging phosphinidiide complexes where the P–C bond is approximately perpendicular to the M$_3$ plane. In common with other rare earth phosphinidiide complexes, the authors reported that complexes **26Ln** exhibited reactivity towards unsaturated molecules such as ketones, thiones, or isothiocyanates, where the complex undergoes phospha–Wittig chemistry, with the exchange of the phosphinidene for an oxo or a sulfido group. Upon heating complexes **26Ln** in toluene, an additional molecule of methane was eliminated to yield the μ$_2$-bridging phosphinidiide complexes [{Ln[PhC(NDipp)$_2$]}$_3$(μ$_2$-Me)$_2$(μ$_3$-Me)(μ$_2$,η^2:η^3-PC$_6$H$_4$)], **27Ln**, in high yields (Ln = Lu, 94%; Y, 91%). Complex **27Lu** exhibits Lu–P distances of 2.649(4)/2.644(4) Å, which is a similar range to that of the two shorter Lu–P bonds in **26Lu**, whilst **27Y** displays a range of Y–P distances [2.698(2)/2.692(2) Å] that are shorter than those seen for **26Y**. The authors have additionally reported the crystal structure of the yttrium bridging phosphinidiide complex [{Y(PhC[NDipp]$_2$)(μ-Me)}$_2$(μ$_3$-CCCPh)(μ,η^2:η^3-PC$_6$H$_4$)],[57] which exhibits Y–P bond distances of 2.701(3) and 2.700(3) Å; these are statistically indistinguishable from the corresponding distances seen in **27Y**. However, the synthetic route and additional characterisation data for this complex have not been reported to date.

In 2015, Layfield and co-workers synthesised the bridging phosphinidiide lanthanide complexes [{Ln(Cp^{Me})$_2$}$_3$(μ-PMes)$_3$-Li] [Li(THF)$_4$]$_2$ (**28Ln**; Ln = Y or Dy; Cp^{Me} = C$_5$H$_4$Me), Scheme 10.[58] The deprotonation reactions of the bridging lanthanide phosphides, [{Ln(Cp^{Me})$_2$(μ-PHMes}$_3$] (Ln = Y or Dy), with three equivalents of *n*-butyl-lithium gave **28Y** and **28Dy**, in yields of 56% and 64%, respectively, in addition to three equivalents of butane gas. The solid-state structures of **28Ln** exhibit central Ln$_3$P$_3$ cores in a chair-like configuration, and the phosphinidiide units are capped with a single lithium ion. The authors reported longer Y–P bond distances for **28Y** [2.7869(12)–2.8268(13) Å] than the yttrium complex **27Y**, which is possibly due to the coordination a lithium ion to the three

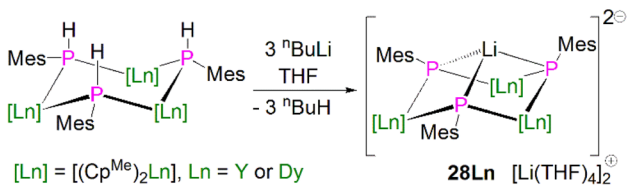

Scheme 10 Synthesis of Y- and Dy–phosphinidiide complexes **28Ln**.

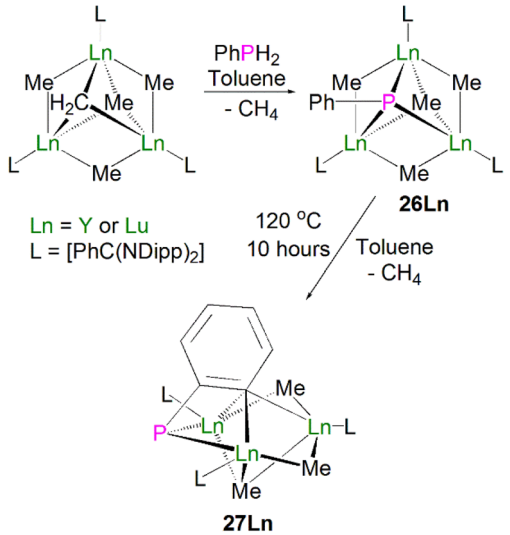

Scheme 9 Synthesis of Lu- and Y–phosphinidiide complexes **26Ln**–**27Ln**.

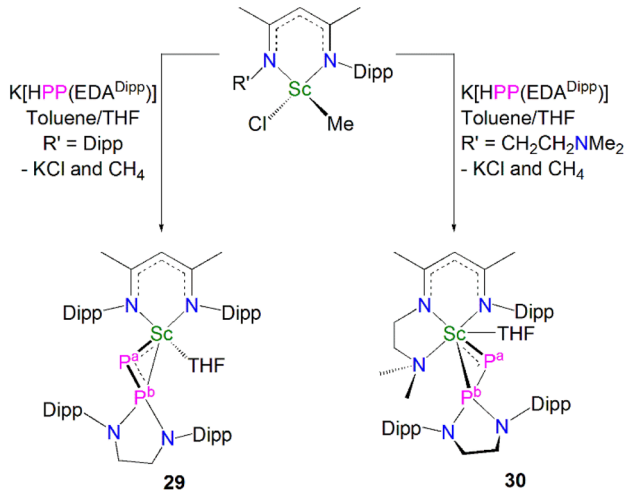

Scheme 11 Synthesis of the Sc–phosphinophosphinidene complexes **29** and **30**.

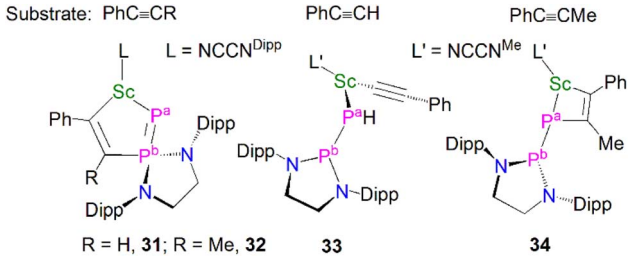

Fig. 5 Reactivity of Sc–phosphinophosphinidene complexes **29** and **30** to give **31–34**.

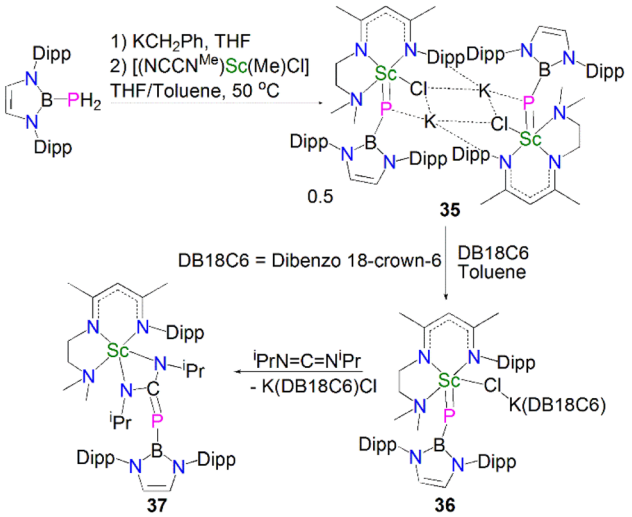

Scheme 12 Synthesis and reactivity of a terminal Sc–phosphinidene complexes **36**.

phosphinidiide units. Complex **28Dy** exhibits Dy–P bond distances of 2.7850(15)–2.8249(15) Å, which are shorter than the range of distances seen for the phosphide precursor [{Dy(Cp^{Me})$_2$(μ-PHMes}$_3$] [2.926(6)–2.951(6) Å], which is likely due to increasing negative charge localised at the phosphorous atom resulting in stronger electrostatic bonding.

In 2020, Maron, Chen and co-workers utilised the phosphinophosphinidene ligand [PP{N(Dipp)CH$_2$CH$_2$N(Dipp)}]$^{2-}$ (PP{EDA^{Dipp}}$^{2-}$) in the one-pot salt metathesis and protonolysis reactions of [Sc(NCCN^R)(Me)(Cl)] (NCCN^R = DippNC(Me)CHC(Me)NR′; R = Me (see **33** below) R′ = CH$_2$CH$_2$NMe$_2$ or Dipp) with one equivalent of K[HPP{EDA^{Dipp}}] to afford the Sc phosphinophosphinidene complexes [Sc(NCCN^R){PP(EDA^{Dipp})}] (R = Dipp, **29**, 54%; R = Me, **30**, 67%), with elimination of one equivalent each of methane and potassium chloride, Scheme 11.[59] Due to the poor stability of the K[HPP{EDA^{Dipp}}] ligand precursor, it was synthesised *in situ* from the phosphine derivative and benzyl potassium. Complex **29** exhibits a shorter Sc–P phosphinidene bond distance [2.448(1) Å] when compared to **30** [2.484(1) Å], which the authors attributed to the increase in coordination number of the scandium centre from five to six.

Complex **29** displays interesting reactivity towards unsaturated small molecules such as alkynes when compared to **30**.[59] The reaction of **29** with one equivalent of PhC≡CR (R=H or Me) gave [Sc(NCCN^{Dipp}){η^2-P=P(EDA^{Dipp})CR = CPh}], Fig. 5, (R = H, **31**; R = Me, **32**), which was surprising as reactions with unsaturated molecules typically occur at the more nucleophilic centre, *i.e.* the phosphinidene (P^a-phosphorus). Indeed, the authors reported that **30** reacts as expected at the phosphinidene centre with the same alkynes PhC≡CR to yield [(NCCN^{Me})Sc{P(H)P(EDA^{Dipp})}(C≡CPh)] (**33**) and [(NCCN^{Me})Sc{η^2-PP(EDA^{Dipp})MeC = CPh}] (**34**). The calculated reaction pathways for **29** and **30** with PhC≡CH illustrated that the interesting reactivity at the P^b-phosphorus in the case of **29** was a consequence of the coordinated THF blocking the access of reactants to the P^a-phosphinidene centre.

4.4 Lanthanide phosphinidene complexes

Whilst there were many lanthanide metal phosphinidiide complexes reported in the past two decades, a bona fide terminal phosphinidene complex for any lanthanide metal remained elusive for decades. A breakthrough in this field was achieved very recently; in 2021, Maron, Chen and co-workers reported the synthesis and molecular structure of the first terminal scandium phosphinidene complex, Scheme 12.[60]

Building on their Sc–phosphinophosphinidene work, Maron, Chen and co-workers reacted the boronylphosphine H$_2$PB{N(Dipp)CHCHN-(Dipp)} with KCH$_2$Ph to give *in situ*-generated K[HPB{N(Dipp)CHCHN(Dipp)}], which was treated with [Sc(NCCN^{Me})(Me)(Cl)] in a THF/toluene mixture to afford a K/Sc heterometallic phosphinidiide complex **35** after heating at 50 °C for 24 h. Dimeric **35** could be converted to a terminal monomeric boronylphosphinidene complex **36** as a dark purple solid in 83% yield by reacting with dibenzo-18-crown-6 in toluene. The solid-state structure confirmed the boronylphosphinidene ligand of **36** adopts an end-on coordination even though the chloride ligand is still bridged between the Sc and K metal centres. The Sc–P bond length in **36** (2.381(1) Å) is close to that in **35** (2.397(2) Å) but shorter than that in the scandium phosphinophosphinidene complex **30** (2.484(1) Å). The ^{31}P{^{1}H} NMR spectrum for **36** at 25 °C shows a very broad signal, but data recorded at −30 °C gave a sharper resonance at 19.6 ppm. DFT studies on **36** revealed a three-centre two-electron (3c-2e) Sc–P–B σ bond with a strong Sc–P π-interaction. In line with the nucleophilic nature of the phosphinidene ligand, a preliminary reactivity study showed that **36** reacted with *N*,*N*′-diisopropylcarbodiimide at room temperature *via* a [2 + 2]-addition fashion to give a four-membered scandium metallaheterocycle complex, [Sc(NCCN^{Me}){N(^{i}Pr)C(PB{N(Dipp)CHCHN(Dipp)})N(^{i}Pr)}] (**37**) in 82% yield.

Very recently, Sirsch, Anwander and co-workers reported the synthesis and molecular structure of the first terminal yttrium phosphinidene complex, Scheme 13.[61] The reactions of H$_2$PDipp with the lanthanide dimethyl complexes [Ln(Tp^{tBu,Me})(Me)$_2$] (Ln = Y, Dy, Ho; Tp^{tBu,Me} = HB(2-Me-4-^{t}Bu-N$_2$C$_3$H)$_3$) afforded the corresponding phosphide complexes [(Tp^{tBu,Me})Ln(Me)(HPDipp)] (**38Ln**, Ln = Y, Dy, Ho). Addition of DMAP to **38Ln** gave the corresponding DMAP adducts [(Tp^{tBu,Me})Ln(Me)(HPDipp)(DMAP)] (**39Ln**, Ln = Y, Dy, Ho);

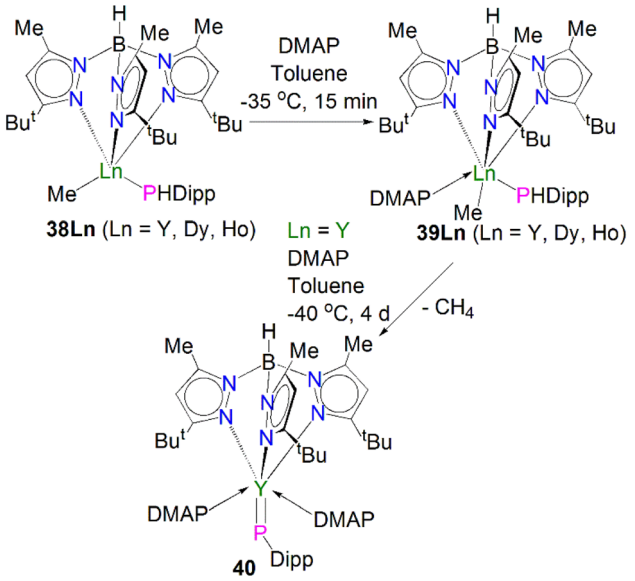

Scheme 13 Synthesis of a terminal Y–phosphinidene complex **40**.

addition of a further equivalent of DMAP to **38Y** produced [Y(Tp^{tBu,Me})(PDipp)(DMAP)$_2$] (**40**). Overall, **40** was prepared *via* a double-deprotonation approach previously established by Anwander for terminal lanthanide imido complexes. However, attempts to synthesise the Dy and Ho phosphinidene analogues using the similar strategy were unsuccessful. Moreover, the Lewis acid-stabilised yttrium phosphinidiide [Y(Tp^{tBu,Me})[(μ-PDipp)(μ-Me)AlMe$_2$] was prepared by addition of H_2PDipp to the solution of [Y(Tp^{tBu,Me})(Me)(AlMe$_4$) in toluene. However, cleavage of trimethylaluminum within this phosphinidiide complex to target a terminal phosphinidene was unsuccessful as well. The solid-state structure of **40** revealed a short Y–P distance of 2.4855(7) Å, which is in between the sum of single and double covalent bond radii of Y and P (2.74 and 2.32 Å, respectively), indicating multiple bonding character. The ^{31}P NMR spectrum of **40** exhibits a very weak signal at −5.5 ppm with a maximum $^1J_{YP}$ coupling constant of 282 Hz, which is shifted to lower frequency compared to that of [Y(Tp^{tBu,Me})[(μ-PDipp)(μ-Me)AlMe$_2$] at −52.2 ppm, suggesting the increase of electron density at the yttrium centre in **40**. A computational study of **40** confirmed the highly polarised covalent multiple bond of Y=PDipp linkage and revealed one σ- and two π-type Y–P interactions with a Wiberg bond index (WBI) of 1.37. The successful isolation and characterisation of terminal phosphinidenes **36** and **40** indicates that it should be possible to access terminal phosphinidene species with other lanthanides with the right supporting ligands combined with suitable phosphinidene group transfer methodologies and reagents.

4.5 Lanthanide phosphido complexes

In common with their pnictinidene derivatives, there are relatively few examples of f-element, and hence lanthanide, heavy pnictido complexes. To date the only structurally authenticated complexes to feature f-element pnictido bonding are with phosphorus or arsenic, with the pnictogen bridging between

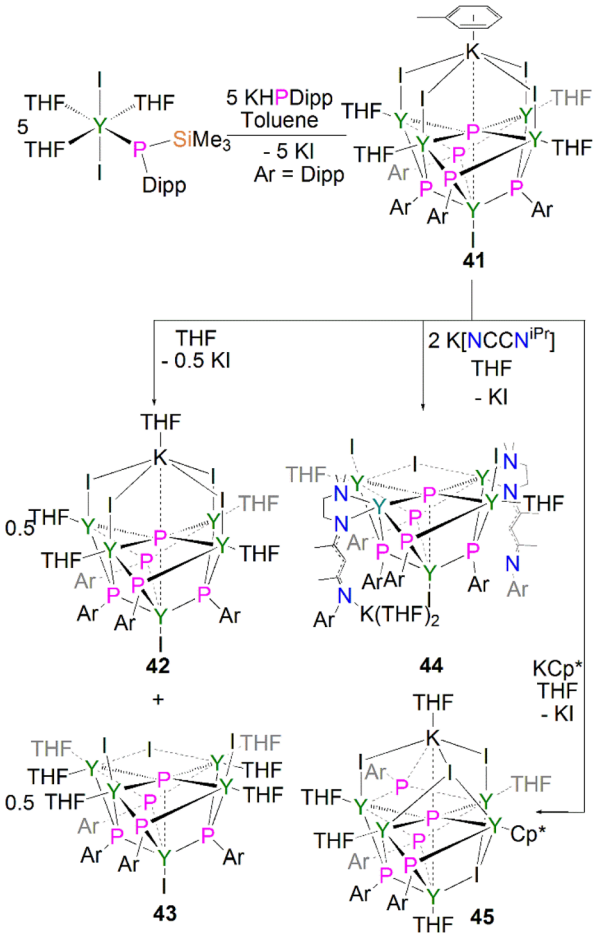

Scheme 14 Synthesis of yttrium phosphido complexes **41**–**45**.

two or more metal centres.[20] There have been no structurally authenticated f-element stibido or bismuthido derivatives to date, therefore they are highly sought-after synthetic targets. For lanthanide metal complexes, only a few clusters were reported containing phosphido ligand.

In 2011, Chen and co-workers reported the first structurally authenticated rare earth phosphido complex, [{Y(I)}{Y[μ$_3$-P(Dipp)](μ-I)(THF)}$_4$(μ$_6$-P){K(C$_7$H$_8$)}] (**41**) *via* a salt elimination/protonolysis protocol, Scheme 14.[62] The reaction of [Y{P(SiMe$_3$)(Dipp)}(I)$_2$(THF)$_3$] with one equivalent of K[P(H)Dipp] gave **41** in a 33% yield. The product formed depends upon the reaction solvent; dissolution of **41** in THF results in the loss of half an equivalent of potassium iodide and the conversion of **41** to half an equivalent each of the THF adduct, [{Y(I)}{Y[μ$_3$-P(Dipp)](μ-I)(THF)}$_4$(μ$_6$-P){K(THF)}] (**42**), and the potassium–free complex [{Y(I)}{Y(I)(THF)}$_2$}{Y(THF)$_2$}$_2$(μ-I)[μ$_3$-P(Dipp)]$_4$(μ$_5$-P)] (**43**). The authors attempted to displace the yttrium-bound THF molecules by exposing **41** to potassium salts of NCCN^{iPr} and Cp*, yielding the corresponding phosphido complexes [{Y(I)}{Y(I)(THF)}$_2$}{Y(NCCN^{iPr})}$_2$(μ-I)[μ$_3$-P(Dipp)]$_4$(μ$_5$-P)] (**44**) and [{Y(THF)}{Y(μ-I)(THF)}$_2$}{Y(THF)}{Y(Cp*)}(μ$_3$-I)(μ-I)[μ$_3$-P(Dipp)]$_4$(μ$_6$-P){K(THF)}] (**45**), respectively.[62] The phosphido centres in complexes **41**–**45** are stabilised through interactions with five yttrium ions where bridging phosphinidiide ligands

are present as well. In the cases of **41**, **42** and **45** an additional interaction with a potassium ion is present, rendering the phosphido bridging modes as either $(\mu_5\text{-P})^{3-}$ or $(\mu_6\text{-P})^{3-}$. The phosphido ions in **41–45** lie in the plane of the four equatorial yttrium ions with near-linear mean Y_{eq}–P–Y_{eq} bond angles [164.89(6)–175.6(2)°], giving the phosphido centres octahedral or square pyramidal geometries (depending upon the coordination of a potassium ion). The four equatorial Y_{eq}–P bond distances found in **41–45** [range: 2.6720(11)–2.8787(14) Å] are shorter than the axial Y_{ax}–P distances [range: 2.885(2)–3.179(2) Å]. The phosphido cores in **41–45** exhibit ^{31}P NMR resonances between 300.9 and 400.7 ppm, which are shifted downfield compared to their phosphinidiide counterparts in these clusters [72.8–176.3 ppm].

4.6 Lanthanide polyphosphorus complexes

This class of lanthanide complexes are normally synthesised by the reactions of reducing low valent lanthanide precursors with P_4 or transition metal polyphosphorus compounds *via* redox methods.[26] In 2009, Roesky and co-workers reported the synthesis and molecular structure of the first molecular lanthanide metal polyphosphorus complex $[\{Sm(Cp^*)_2\}_4P_8]$ (**46**)[63] prepared by diffusion of P_4 vapour into a toluene solution of solvent-free samarocene involving a four electron transfer process, Fig. 6. The solid-state structure of **46** revealed a very rare structure that can be seen as a realgar-type P_8^{4-} ligand, which is isoelectronic with the P_4S_4 molecule, trapped in a cage of four $[Sm(Cp^*)_2]$ cations. The Sm–P bond distances of **46** range from 2.997(2) Å to 3.100(2) Å.

A few years later, Diaconescu and co-workers reported another rare earth metal P_8 cluster $[\{Sc(NN^{fc})\}_4P_8]$ (NN^{fc} = 1,1-fc(NSi^{t}BuMe$_2$)$_2$, fc = ferrocenylene) prepared by the reaction of the scandium naphthalendiide complex $[\{Sc(NN^{fc})\}_2(\mu\text{-}C_{10}H_8)]$ with P_4.[64] The core P_8^{4-} ligand in this molecule is very similar to that in **46**. Interestingly, using excess P_4 in the reactions with $[\{Sc(NN^{fc})\}_2(\mu\text{-}C_{10}H_8)]$ and $[\{Y(NN^{fc})(THF)\}_2(\mu\text{-}C_{10}H_8)]$ yielded the P_7 complexes $[\{(NNfc)Ln(THF)_n\}_3P_7]$ (**47Ln**, Ln = Sc, n = 0; Ln = Y, n = 1), respectively, Fig. 6. Complexes **47Ln** are the first examples of rare earth metal Zintl P_7 compounds prepared from P_4 activation directly. The solid-state structures of **47Sc** and **47Y** revealed that the P_7^{3-} units in both cases are similar to the molecular structure of the inorganic salt Li_3P_7. The ionic interactions between the rare earth metals and the Zintl P_8^{4-} or P_7^{3-} units above was confirmed by DFT calculations.

Although actinide-P_5 and P_6 complexes are known,[20] and indeed *cyclo*-P_5 complexes are well-known for transition metals, such species remain rare for the lanthanides.[26] Examples of lanthanide-P_5/P_6 complexes have been stabilised by transition metals, resulting in 3d/4d-4f clusters. For instance, the first lanthanide complex containing *cyclo*-P_5 bridged by lanthanide and transition metals, $[\{Fe(Cp^*)\}(\mu\text{-}P_5)\{Sm(DPIP)(THF)_2\}]$ (DPIP = 2,5-bis{*N*-(2,6-diisopropylphenyl) iminomethyl}pyrrolyl), was prepared from the reaction of $[Sm(DPIP)(I)(THF)_3]$ with one equivalent of $[Fe(Cp^*)(\mu\text{-}P_5)]$ in THF in the presence of potassium-naphthalenide.[65] Interestingly, whilst dinuclear $[\{Fe(Cp^*)\}(\mu\text{-}P_5)\{Sm(DPIP)(THF)_2\}]$ was obtained when the product was recrystallised from THF and toluene, recrystallisation from toluene and pentane gave tetranuclear $[\{Fe(Cp^*)(\mu\text{-}P_5)Sm(DPIP)\}_2]$. In contrast, reacting samarocenes with $[Fe(Cp^*)(\mu\text{-}P_5)]$ produced $[\{Fe(Cp^*)\}_2(\mu\text{-}P_{10})\{Sm(Cp^*)_2\}_2]$ (R = Me or ^{n}Pr) containing a $[P_{10}]^{4-}$ unit, which was also the first example of a 3d-P_{10}-4f complex.[66] Well-defined *cyclo*-P_3 and -P_4 lanthanide complexes have been reported more recently. For example, in 2018, Roesky and co-workers reported the lanthanide *cyclo*-P_4 complex $[\{Sm(DippForm)_2\}_2(\mu^2\text{-}\eta^4\text{:}\eta^4\text{-}P_4)]$ (**48**, DippForm = {(NDipp)$_2$-CH}) by the reduction of P_4 with the divalent precursor $[Sm(DippForm)_2(THF)_2]$, Fig. 6.[67] In 2019, Zhang, Zhou and co-workers reported the lanthanide *cyclo*-P_3 complex $[K(18C6)(toluene)][\{Y(DippDBD)(THF)\}_2(P_3)]$ (**49**, DippDBD = *N*,*N*′-2,6-diisopropylphenyl-1,4-diazabutadiene), with the central P_3^{3-} trianion bridging two Y(III) metal ions, prepared by alkyl migration of an organosubstituted *cyclo*-P_4R_2 precursor followed by encapsulation of K^+ cation with 18-crown-6 reagent, Fig. 6.[68] Very recently, using a redox synthetic strategy, Roesky and co-workers reported another two *cyclo*-P_3 and -P_4 inverse sandwich complexes for lanthanides supported by a xanthene-diamide ligand.[69] Lastly, diphosphorus (P_2) complexes, which are heavy N_2 analogues, remain elusive for lanthanides because of the synthetic challenges of making and stabilising P_2.[69]

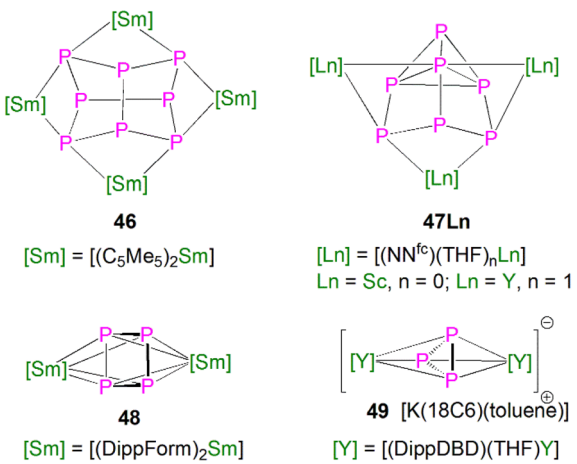

Fig. 6 Rare earth metal polyphosphorus complexes **46–49**.

5. Actinide phosphorus complexes

Although actinide–nitrogen chemistry is well-developed over several decades, this is not the case for actinide–phosphorus chemistry.[16,20] Nevertheless, actinide–phosphorus chemistry is the most developed compared with the analogous lanthanide chemistry, likely because actinides can deploy 5f and 6d orbitals in bonding to form more covalent chemical bonds than lanthanides. In this section, seminal examples in actinide phosphorus chemistry are highlighted, noting that after initial work on phosphine derivatives that remains contemporaneous,[70,71] binding phosphines to amides has supported metal–metal bonds.[72–75]

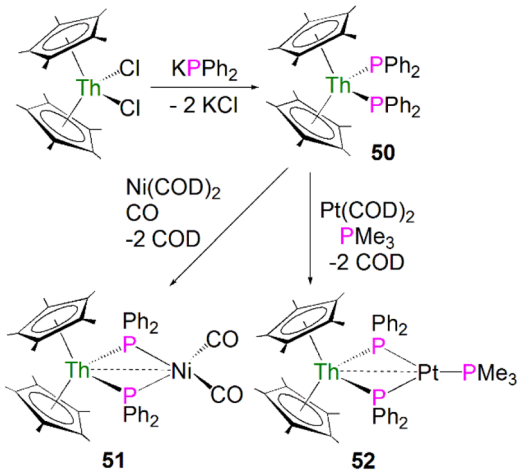

Scheme 15 Synthesis of Th phosphide complexes **50–52**.

5.1 Actinide phosphide complexes

In terms of actinide complexes containing metal–phosphorus single bond interactions, monoanionic charged phosphide ligands can have stronger interactions with actinide metal centres than neutral phosphine ligands, which only form dative bonds to actinide ions.[20] Furthermore, some actinide phosphide complexes are useful precursors to novel linkages such as actinide–metal and -ligand multiple bonds (see below), low-valent U–P bonds,[76] and hydrophosphination catalysts.[77,78]

The first examples of actinide phosphide complexes were reported in 1985 by Ryan and co-workers. The mononuclear complex $[Th(Cp^*)_2(PPh_2)_2]$ (**50**) was prepared by a salt metathesis reaction between $[Th(Cp^*)_2(Cl)_2]$ and potassium diphenylphosphide, Scheme 15.[79] Importantly, the phosphide ligands are able to coordinate to transition metals as well, supporting actinide and transition metal interactions, making it possible to investigate actinide–metal bonding. Treatment of **50** with $[Ni(COD)_2]$ (COD = 1,5-cyclooctadiene) under a CO atmosphere, or $[Pt(COD)_2]$ in the presence of PMe_3, led to the formation of the heterobimetallic compounds $[Th(Cp^*)_2(\mu\text{-}PPh_2)_2Ni(CO)_2]$ (**51**)[79] and $[Th(Cp^*)_2(\mu\text{-}PPh_2)_2Pt(PMe_3)]$ (**52**)[80] in moderate yields, respectively, Scheme 15. The $^{31}P\{^1H\}$ NMR spectrum for **51** exhibits a signal at 177 ppm, which is shifted downfield from the resonance for **50** found at 143 ppm. In contrast, the ^{31}P NMR spectrum for **52** shows a doublet at 149.3 ppm, and a triplet at −3.3 ppm. These were attributed to the $[PPh_2]^-$ and PMe_3 ligands, respectively. Both resonances contain coupling to Pt, suggesting a direct interaction between the phosphorus atoms of both ligands and the transition metal. The solid-state structure of **51** revealed the Th–P bond lengths to be 2.869(4) and 2.900(4) Å, which are close to the Th–P distance of 2.866(7) Å found in the mononuclear starting material **50**. The Th–P bond lengths in **52** are unexceptional and are similar to those in **50**. The distance between the thorium and nickel atoms in **51** was found to be 3.206(2) Å, which is longer than the sum of the covalent single bond radii of Th and Ni (2.85 Å). In contrast, in **52** the distance between the thorium and platinum centres was found to be 2.984(1) Å, which is similar to the sum of the covalent single bond radii of Th and Pt (2.98 Å). The metal–metal bonding interactions in **51** and **52** were interpreted as a weak, donor–acceptor dative bonds from the low-valent electron-rich Ni(0) and Pt(0) ions to the electron-poor thorium(IV) ions.

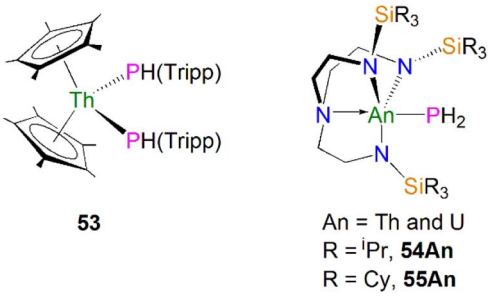

Fig. 7 Actinide phosphide and phosphanide complexes **53-55An**.

As well as actinide phosphide complexes with secondary phosphide ligands, there are also some actinide complexes containing primary phosphide ligands, which could potentially be used to access actinide phosphorus multiple bonds. For example, in 2015 Walensky and co-workers reported the thorium bisphosphide complex $[Th(Cp^*)_2(PHTripp)_2]$ (**53**, Tripp = 2,4,6-^{i}Pr$_3$C$_6$H$_2$), prepared by the reaction of $H_2PTripp$ with the thorium dimethyl precursor $[Th(Cp^*)_2(CH_3)_2]$ in a 2 : 1 stoichiometric ratio *via* an alkane elimination method, Fig. 7.[81] The Th–P bond distances in **53** (2.8754(6) and 2.8830(6) Å) are very close to those in **50–52**, indicative of typical single bond interactions. However, the $^{31}P\{^1H\}$ NMR spectrum of **53** has a resonance at 1.66 ppm, whereas the $^{31}P\{^1H\}$ resonances in **50–52** range from 143 to 177 ppm. Complex **53** is a useful precursor to thorium phosphinidiide and phosphinidene complexes (see below). Unlike complexes **50–53**, which contain bulky phosphide substituents, by using bulky triamidoamine ligand frameworks Liddle, Scheer, and co-workers synthesised the first actinide parent phosphanide complexes $[An(Tren^R)(PH_2)]$ ($Tren^R = \{N(CH_2CH_2NR)_3\}^{3-}$, R = TIPS, triisopropylsilyl, An = Th and U, **54An**; R = TCHS, tricyclohexylsilyl, An = Th and U, **55An**), Fig. 7.[82–84] Complexes **54An** were prepared by salt metathesis reactions of the corresponding actinide precursors with $NaPH_2$,[82,84] whilst **55An** were synthesised by protonation of their respective terminal parent phosphinidene complexes due to the lack of suitable actinide precursors for salt metathesis reactions.[84] These four terminal phosphanide complexes are the only known examples to date for any f-element. The solid-state structures of **54An** and **55An** revealed trigonal-bipyramidal metal geometries with the parent phosphide group well-protected by the bulky silyl substituents. The An–P bond distances are 2.982(2), 2.883(2), 3.0360(15), and 2.8725(13) Å for **54Th**, **54U**, **55Th**, and **55U**, respectively, which are slightly longer than the respective sum of the single bond covalent radii for thorium and phosphorus (2.86 Å) and uranium and phosphorus (2.81 Å). Due to the P–H coupling, the ^{31}P NMR spectra for **54Th**, **54U**, **55Th**, and **55U** exhibit triplet resonates at −144.1, 595.0, −133.0 and 605.9 ppm, respectively. As expected,

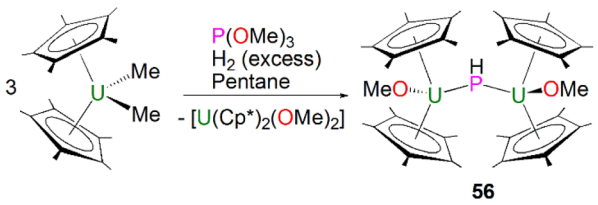

Scheme 16 Synthesis of the U–phosphinidiide complex **56**.

the resonances for uranium complexes are significantly shifted owing to the paramagnetic nature of $5f^2$ uranium(IV). These phosphanide complexes have proven to be key precursors to access actinide–phosphorus multiple bonds (see below).

5.2 Actinide phosphinidiide complexes

Phosphinidiide complexes can be viewed as polynuclear forms of phosphinidene complexes where the phosphinidene ligands are bridged between two or more electropositive metal ions to enhance the stability of the reactive moiety. As discussed above, phosphinidiide complexes are also more common than terminal phosphinidenes for both lanthanides and actinides, but some phosphinidiide complexes can still have metal–phosphorus multiple bonding character.

The first crystallographically characterised actinide phosphinidiide complex was isolated in 1984 by Marks, Day and co-workers, as a parent $(HP)^{2-}$ unit bridging two uranium(IV) centres. Mixing three equivalents of $[U(Cp^*)_2(Me)_2]$ with one equivalent of $P(OCH_3)_3$ and excess hydrogen gave $[\{U(Cp^*)_2(OMe)\}_2(\mu\text{-}PH)]$ (**56**) in yields of 42%, Scheme 16.[85] The authors additionally prepared $[\{Th(Cp^*)_2(OMe)\}_2(\mu\text{-}PH)]$ in an analogous manner. Marks and Day postulated that the mechanism for the synthesis of **56** proceeded *via* an actinide hydride. To confirm this, additional reactions were conducted in the absence of hydrogen or utilising $[An(Cp^*)_2(H)_2]_2$ as starting materials. The former showed no detectable reaction, whilst the latter gave **56**. Complex **56** exhibits two U–P distances of 2.743(1) Å and a U–P–U angle of 157.7(2)°. The IR spectrum of **56** confirmed the presence of the parent phosphinidiide, with a PH stretching mode at 2193 cm^{-1} ($\upsilon_{P-H}/\upsilon_{P-D} = 1.39$). Liddle, Scheer, and co-workers also reported diactinide parent phosphinidiide complexes supported by triamidoamine ligands,[86] which will be discussed in the phosphido section below for comparison purposes.

In 2015 Walensky and co-workers utilised the bis-Cp* framework to synthesise the bridging thorium phosphinidiide complex $[\{Th(Cp^*)_2\}_2\{\mu\text{-}P[(2,6\text{-}CH_2CHCH_3)_2\text{-}4\text{-}^iPrC_6H_2]\}]$ (**57**, 63%) by the protonolysis of two equivalents of $[Th(Cp^*)_2(Me)_2]$ with one equivalent of H_2PTripp at 90–95 °C, Scheme 17.[81] Complex **57** exhibits Th–P bond distances of 2.8083(9) and 2.8186(9) Å, which are marginally shorter than those observed for the thorium phosphide complex **53** (2.8755(6) and 2.8829(7) Å) due to the bridging mode of the phosphinidiide.

Walensky and co-workers also derivatised **53** to synthesise the bridging phosphide/phosphinidiide thorium complex $[\{Th(Cp^*)_2(\mu\text{-}PTripp)(\mu\text{-}PHTripp)(K)\}_2]$ (**58**), Scheme 17,[87] which paved the way to a number of derivatives.[88–92] The reaction of **53** with one equivalent of $KN(SiMe_3)_2$ gave **58** in a yield of 64% *via* the elimination of one equivalent of $HN(SiMe_3)_3$. It was found that if the deprotonation reaction was conducted in the presence of 2.2.2-cryptand the monomeric phosphide/phosphinidene complex $[K(2.2.2\text{-cryptand})][Th(Cp^*)_2(\text{-}PTripp)\}(PHTripp)]$ (**59**) was obtained.[87] Complex **58** exhibits Th–P distances of 2.6957(10) Å, whilst **59** demonstrates a shorter Th–P bond length of 2.6024(9) Å, which is a result of the encapsulation of the potassium ion allowing more electron

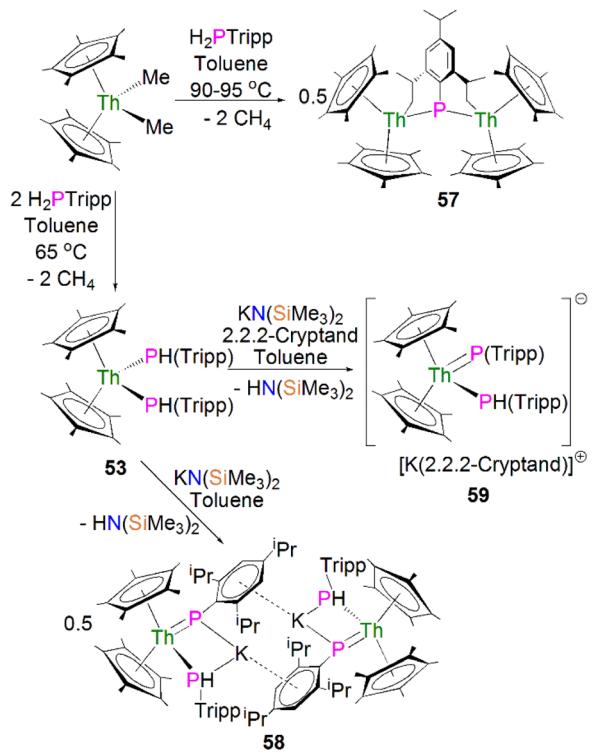

Scheme 17 Synthesis of Th–phosphinidiide complexes **57** and **58** and phosphinidene **59**.

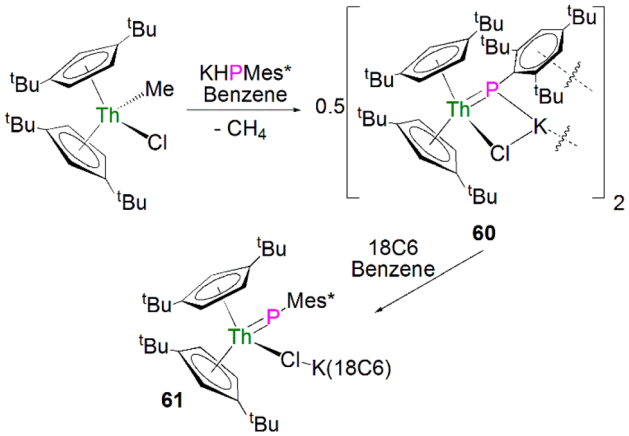

Scheme 18 Synthesis of thorium phosphinidiide and phosphinidene complexes **60** and **61**.

density to be donated from the phosphorous atom to the thorium centre.

Recently, Walter, Ding, Zi and co-workers reported the salt metathesis/protonolysis reaction of one equivalent each of [Th(Cp^{tt})$_2$(Me)(Cl)] (Cp^{tt} = 1,3-^{t}Bu$_2$-C$_5$H$_3$) and KPH(Mes*) to synthesise the dinuclear phosphinidiide complex [{Th(Cp^{tt})$_2$(-PMes*}(ClK)}$_2$] (**60**) in 78% yield, Scheme 18, with elimination of one equivalent each of methane and potassium chloride.[93] The authors reported that **60** could be converted to the mononuclear terminal phosphinidene complex [Th(Cp^{tt})$_2$(PMes*)(μ-Cl){K(18C6)}] (**61**, 92%) by the addition of 18-crown-6.[93] The solid-state structure of **60** and **61** revealed that **60** exhibits a slightly shorter Th–P distance of 2.560(1) Å and a more acute Th–P–C^{Ar} angle of 162.6(2)° than found in **61** (2.582(1) Å; Th–P–C^{Ar} angles = 171.3(1)°) which is most likely a result of the removal of the interaction between phosphorus and the potassium cation from **60** to **61**. The authors reported that all four complexes **58–61** exhibit ^{31}P{^{1}H} NMR resonances in the range 108.8 to 177.85 ppm.

5.3 Actinide phosphinidene complexes

Although uranium imido chemistry is well-developed,[18] actinide complexes containing heaver pnictogen An = PnR (An = actinide; Pn = P, As, Sb, Bi) multiple bonds are scarce.[20] To date, there are few complexes containing An=PnR double bonds outside of cryogenic matrix isolation conditions, but only with P or As ligands, not for Sb and Bi ligands. Also, there is no example of a terminal actinide heavy pnictido An≡Pn triple bond isolated under ambient conditions. Even for d-block metals there are relatively few structurally characterised terminal metal pnictinidene complexes (~50), far fewer than their imido counterparts (>3000).[94] Actinide pnictinidene complexes normally require kinetic stabilisation by sterically demanding ancillary ligands, coupled with bulky pnictinidene substituents (*cf.* **59** and **61**).

In 1996, Burns and co-workers reported the first example of a terminal uranium phosphinidene complex utilising the sterically demanding Cp* supporting ligand. The salt elimination/protonolysis reaction of one equivalent each of [U(Cp*)$_2$(Me)(Cl)] and KHP(Mes*) in the presence of OPMe$_3$ gave [U(Cp*)$_2$(PMes*)(OPMe$_3$)] (**62**), in yields of up to 62%, Scheme 19 (top).[95] Complex **62** exhibits a U–P distance of 2.562(3) Å, which is shorter than the bridging phosphinidiide U–P distance in **56** or, for example, the U–P distance in the phosphide complex [U(Cp*)$_2${P(SiMe$_3$)$_2$}(Cl)] (2.789(4) Å).[96] The authors postulated that the U–P–C^{Ar} angle of 143.7(3)° in **62** was due to crystal packing forces, or a result of the combination of heavy main group elements generally adopting bent geometries in addition to the preferred linear geometry required to minimise P–U π-overlap.

In 2018, using sterically demanding cyclopentadienyl ligands, Walter, Ding, Zi and co-workers reported a base-free terminal thorium phosphinidene [Th(Cp^{ttt})$_2$(PMes*)] (**63**, Cp^{ttt} = 1,2,4-^{t}Bu$_3$-C$_5$H$_2$), Scheme 19 (bottom).[97] Complex **63** was prepared by a similar salt metathesis/protonolysis reaction that was employed to prepare **62**; reaction of one equivalent each of [Th(Cp^{ttt})$_2$(Me)(I)] and KPH(Mes*) produced **63** in high yield (80%), with elimination of one equivalent each of methane and potassium iodide. The molecular structure of **63** further confirmed a base-free terminal phosphinidene species with a short Th–P bond distance (2.536(2) Å). The ^{31}P{^{1}H} NMR spectrum of **63** shows one resonance at 145.7 ppm, which is close to those for **59** and **61**. Calculations probing the Th=P bonding of **63** and the theoretical monomeric model of **63** suggest more covalency in this linkage than related imido complexes. The authors additionally treated the thorium complexes **63** with a wide range of unsaturated substrates to probe the reactivity of Th–P double bond. In general, the actinide metallocene phosphinidene motif has proven practicable to effect with a range of cyclopentadienyl substituents.[98–105]

From the above examples, it is clear that sterically demanding cyclopentadienyl ligands have proven effective at stabilising actinide phosphinidiide and phosphinidene complexes, but sterically demanding triamidoamine ligands

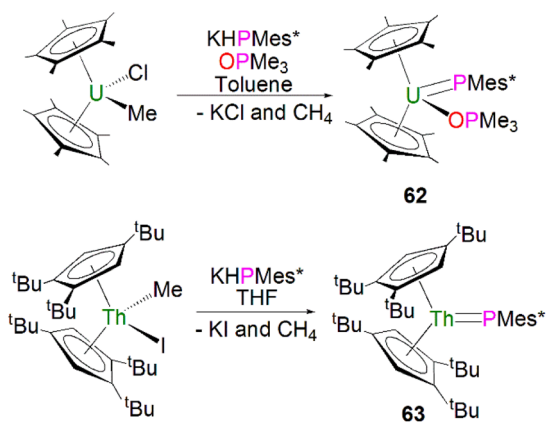

Scheme 19 Synthesis of terminal uranium and thorium phosphinidene complexes **62** (top) and **63** (bottom).

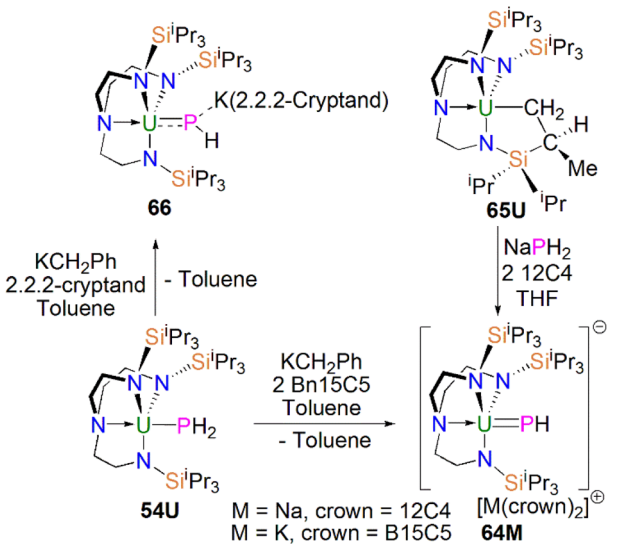

Scheme 20 Synthesis of uranium phosphinidene and phosphinidiide complexes **64M** and **66**.

have in parallel extended this chemistry into a new regime. Following the successful isolation of terminal uranium nitrides supported by the Tren^{TIPS} ligand (Tren^{TIPS} = {N(CH$_2$CH$_2$NSi^{i}Pr$_3$)$_3$}$^{3-}$) in 2012 and 2013,[106,107] Liddle, Scheer, and co-workers utilised this bulky ligand framework to stabilise the first terminal uranium parent phosphinidene in 2014, Scheme 20. The reaction of **54U** with one equivalent of benzyl potassium and two equivalents of benzo-15-crown-5 ether (B15C5) yielded the terminal parent uranium(IV) phosphinidene complex [K(B15C5)$_2$][U(Tren^{TIPS})(PH)] (**64K**).[82] The synthesis of the sodium analogue [Na(12C4)$_2$][U(Tren^{TIPS})(PH)] (**64Na**) was achieved by reaction of the uranium cyclometallate complex [U{N(CH$_2$CH$_2$NSi^{i}Pr$_3$)$_2$(CH$_2$CH$_2$NSi^{i}Pr$_2$C(H)MeCH$_2$)}] (**65U**) with one equivalent of NaPH$_2$ and two equivalents of 12-crown-4 ether (12C4).[86] The authors reported that the treatment of **54U** with one equivalent each of KCH$_2$Ph and 2.2.2-cryptand gave the contact ion pair phosphinidiide complex [{U(Tren^{TIPS})(μ-PH)}{K(2.2.2-cryptand)}] (**66**).[82] The solid-state structures revealed that the terminal phosphinidene complexes **64M** and phosphinidiide **66** exhibit U–P distances ranging from 2.613(2) to 2.685(2) Å, which are shorter than that in the parent phosphide precursor **54U** (2.883(2) Å). The authors reported that the IR spectrum of **64K** exhibits a P–H stretch of 2360 cm^{-1}. The U–P bond lengths in **64M** are longer than those observed for **62** (2.562(3) Å) lying between the sum of the covalent single and double bond radii for uranium and phosphorus (2.81 Å and 2.36 Å, respectively); this reflects the sterically demanding nature of Tren^{TIPS} and indicates polarised covalent U=P interactions that is confirmed by DFT calculations.

In 2016, Liddle, Scheer, and co-workers utilised the Tren^{TIPS} ligand framework to stabilise terminal thorium parent phosphinidene analogues. The two methodologies used to synthesise the uranium complexes **64M** were adapted to prepare the terminal phosphinidene thorium complex [Na(12C4)$_2$][Th(Tren^{TIPS})(PH)] (**67**), Scheme 21.[83] Complex **67** could be synthesised either through deprotonation of **54Th** with one equivalent of NaCH$_2$Ph and two equivalents of 12C4, or by the reaction of the thorium cyclometallate complex [Th{N(CH$_2$CH$_2$NSi^{i}Pr$_3$)$_2$(CH$_2$CH$_2$NSi^{i}Pr$_2$C(H)MeCH$_2$)}] (**65Th**) with one equivalent of NaPH$_2$ and two equivalents of 12C4 in yields of up to 38%. Complex **67** is isostructural with the uranium phosphinidene complex **64Na**.

The Th–P bond length of 2.758(2) Å in **67** is *ca.* 0.22 Å shorter than that of the Th–PH$_2$ bond in **54Th** (2.982(2) Å), but is longer than the U=P double distance of 2.613(2) Å in **64K**, suggesting a more polarised double bond interaction for Th=PH linkage. This is in accord with a smaller Th–P Mayer bond order of 1.67 in **67** than that of 1.92 in **64K**. The Th=P–H angle of 67.45(8)° in **67** indicates an 'agostic-type' interaction between the metal ion and the electron density of the P–H bond, whereas this interaction was not observed in **64K**, which has a U=P–H angle of 118.8(9)°. The ^{31}P NMR spectrum for **67** has a doublet resonance at 198.8 ppm due to P–H coupling, further confirming the presence of [PH]$^{2-}$ group at thorium. By contrast, because of the strong paramagnetic shielding from the uranium(IV) centre, no resonance was observed in the ^{31}P NMR spectra for **64M**.

Protonation of reactive actinide–carbon bonds has proven to be an effective strategy for constructing actinide–pnictogen multiple bonds. In 2022, Liddle, Scheer, and co-workers developed a bulky Tren^{TCHS} ligand ({N(NCH$_2$CH$_2$NSiCy$_3$)$_3$}$^{3-}$) to prepare two new terminal actinide phosphinidene complexes, Scheme 22. Reaction of the cyclometallate actinide complexes [An{N(CH$_2$CH$_2$NSiCy$_3$)$_2$(CH$_2$CH$_2$NSiCy$_2$[CHCH$_2$CH$_2$CH$_2$CH$_2$CH])}] (**68An**, An = Th, U) with NaPH$_2$ in the presence of 2.2.2-cryptand in THF afforded [Na(2.2.2-cryptand)][An(Tren^{TCHS})(PH)] (**69An**, An = U, Th).[84] The molecular structures of **69An** confirmed the presence of terminal phosphinidenes, with the (HP)$^{2-}$ ligand well-protected by the super bulky tricyclohexylsilyl groups. The An–P bond distances of 2.7237(9) and 2.6381(12) Å for **69Th** and **69U**, respectively are statistically invariant to those in **67** and **64M**, indicating multiple bonding interactions in these An=PH linkages with polarised covalent interactions supported by DFT studies. The 'agostic-type' interaction between the An ion and the

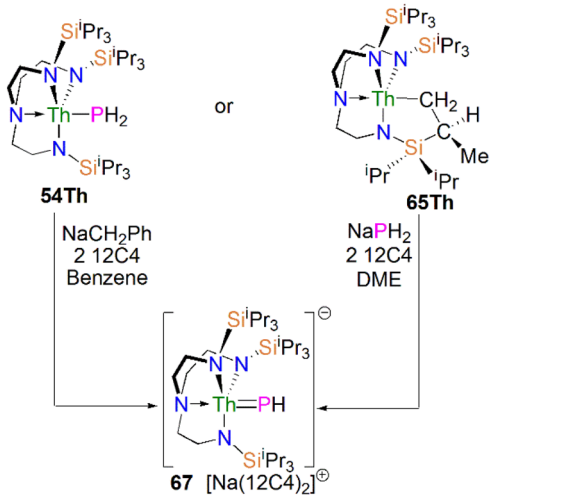

Scheme 21 Synthesis of thorium phosphinidene complex **67**.

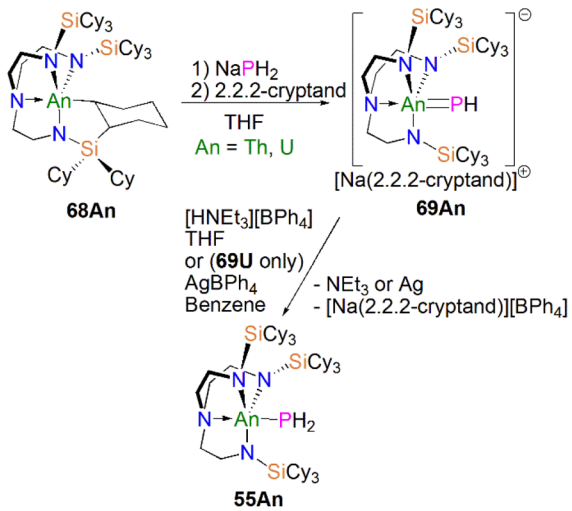

Scheme 22 Synthesis of thorium and uranium phosphinidene complexes **69An** and phosphanide complexes **55An**.

phosphinidene ligand was observed in both structures, with An–P–H angles of 65.83(17)° and 65.23(13)°, respectively. In addition, absorptions corresponding to P–H stretches at 2072 and 2070 cm^{-1} for **69Th** and **69U**, respectively, were observed in their ATR-IR spectra. The An=P vibrations are also observed in the Raman spectra of **69Th** and **69U** at 306 and 296 cm^{-1}, respectively. The ^{31}P NMR spectrum for **69U** exhibits a broad resonance at 2629 ppm due to the paramagnetic uranium(IV) centre, while this is not observed in **64M**. Similar to **67**, **69Th** exhibits a doublet resonance at 266.2 ppm in its ^{31}P NMR spectrum due to P–H coupling.

Reflecting the basic and nucleophilic nature of **69An**, Liddle, Scheer, and co-authors additionally found that treatment of **69An** with $[HNEt_3][BPh_4]$, as a proton source, in THF resulted in the isolation of the phosphanide complexes **55An** in good yields, Scheme 22,[84] which have similar bond metrics to **54An**.[82] Alternatively, **55U** could be prepared by oxidation of **69U** with $AgBPh_4$ in benzene. The formation of **55U** in these oxidation reactions may involve a transient U(V)=PH species (or valence isomer, *e.g.* U(IV)=P˙H), which then abstracts a proton (or H˙) in the reaction mixture due to the HSAB mismatch of U and P. This reactivity contrasts to the disproportionation observed for $Tren^{TIPS}$-supported U(V)=NH chemistry, which produces U(IV)–NH_2 amide and U(VI)≡N nitride products.[108] These reactivity outcomes reflect the periodic differences between nitrogen and phosphorus, and that when the latter is paired with electropositive metals P-based electrons can become involved in redox reactions as found in the reactivity of **16**.

5.4 Actinide phosphido complexes

Actinide phosphido complexes remain exceeding rare. There are only a few bridging dinuclear complexes isolated in recent years with no examples of terminal actinide heavy pnictido An≡Pn triple bond isolated under ambient conditions to date.[20]

In 2016, Liddle, Scheer, and co-workers reported the first example of an actinide–phosphido complex $[Na(12C4)_2][\{Th(Tren^{TIPS})\}_2(\mu\text{-}P)]$ (**70**), where the phosphido ligand bridges two thorium centres, Scheme 23.[83] Complex **70** was also the first such f-element phosphido species, and was prepared by the reaction of two equivalents of **65Th** with $NaPH_2$ in the presence of two equivalents of 12C4 in up to 57% yield. Alternatively, **70** can be synthesised by the stoichiometric reaction of **67** with **65Th**. The authors additionally reported the synthesis of the bridging phosphinidiide complex $[\{Th(Tren^{TIPS})\}_2(\mu\text{-}PH)]$ (**71Th**) in a 40% yield, either by treatment of **54Th** with one equivalent of **65Th**, or the reaction of two equivalents each of **65Th** with $NaPH_2$, eliminating one equivalent of 'Na_2PH'. However, attempts to prepare **70** by deprotonation of **71Th** were unsuccessful. Complex **70** has a symmetrical ThPTh core with Th–P bond distances of 2.740(2) and 2.735(2) Å, which are shorter than those in **71Th** (2.898(2) Å) but compares well to that of the terminal phosphinidene **67** (2.7584(18) Å), and lies between the sum of the covalent single and double bond radii for thorium and phosphorus (2.86 and 2.45 Å, respectively), suggesting multiple bonding interactions in the ThPTh linkage. The ^{31}P NMR spectra for **71Th** and **70** exhibit doublet and singlet resonances at 145.7, and 553.5 ppm, confirming the presence of $(HP)^{2-}$ and P^{3-}, respectively.

Subsequently, in 2017 Liddle, Scheer, and co-authors reported that addition of one equivalent of KCH_2Ph to a mixture of **54U** and $[U(Tren^{TIPS})(THF)][BPh_4]$ gave the bridging diuranium phosphinidiide complex $[\{U(Tren^{TIPS})\}_2(\mu\text{-}PH)]$ (**71U**)[86] that is isostructural to **71Th**, Scheme 24. Importantly, the authors found that deprotonation of **71U** with benzyl potassium in the presence of two equivalents of B15C5 produced the diuranium(IV/IV) phosphido compound $[K(B15C5)_2][\{U(Tren^{TIPS})\}_2(\mu\text{-}P)]$ (**72K**), Scheme 24;[86] recall that this method did not work for **71Th**.[84] Complex **72K** was found to rapidly decompose, which was attributed to steric overload, and so,

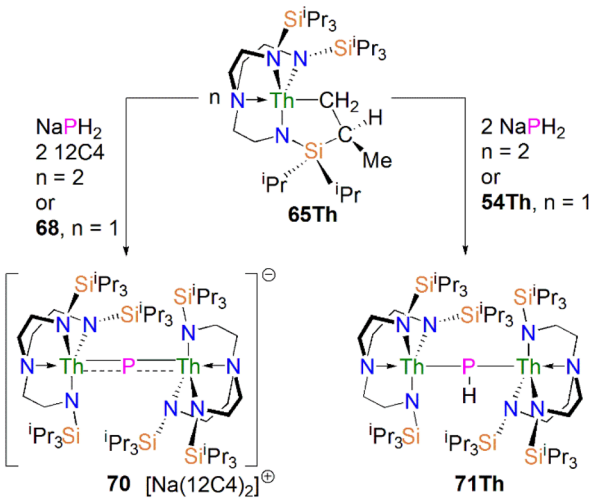

Scheme 23 Synthesis of bridging thorium phosphinidiide and phosphido complex **70** and **71Th**.

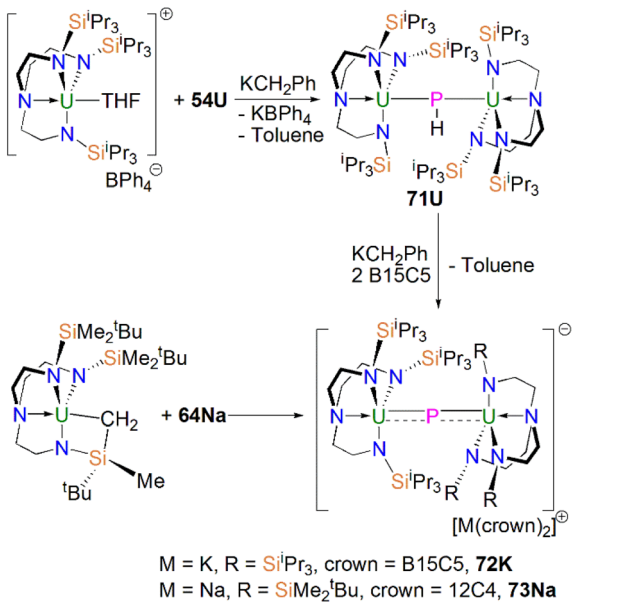

Scheme 24 Synthesis of bridging uranium phosphinidiide and phosphido complexes **71U**-**73Na**.

seeking a more stable combination, the slightly less bulky and asymmetric sodium analogue of **72K**, $[Na(12C4)_2][\{U(Tren^{TIPS})\}\{U(Tren^{DMBS})\}(\mu\text{-}P)]$ (**73Na**; $Tren^{DMBS}$ = $\{N(CH_2CH_2NSiMe_2{}^tBu)_3\}^{3-}$) was prepared[86] by the reaction of one equivalent each of **64Na** with the cyclometallate complex $[U\{N(CH_2CH_2NSiMe_2{}^tBu)_2(CH_2CH_2NSi(Me)(CH_2)(^tBu))\}]$, which is a less sterically demanding Tren ligand compared to $Tren^{TIPS}$.

Unlike **70** which is stable, **72K** and **73Na** are to various extents unstable in solution, in line with the paucity of such phosphido species, which resulted in both complexes being isolated in relatively low yields of 29% and <5% for **73Na** and **72K**, respectively. Interestingly, **73Na** exhibits an asymmetric UPU core, with two U–P bond distances of 2.657(2) and 2.713(2) Å, and the shorter U–P distance is the $Tren^{TIPS}$ ligated unit. In contrast, **72K** has a symmetric core with statistically indistinguishable U–P bond lengths of 2.653(4) and 2.665(4) Å, which are shorter than those in the phosphinidiide **71U** (2.8187(12) and 2.8110(12) Å). Calculations on **72K** and **73Na** suggested that the U–P bond are less covalent than the terminal phosphinidene species **64M**. This is reflected by smaller U–P Mayer bond orders of 1.41/1.43 and 1.44/1.66 for **72K** and **73Na**, respectively, when compared to $[\mathbf{64K}]^-$ (1.92). DFT calculations also suggest that the Th–P bonds in **70** are more polarised and ionic than the U–P bonds in **72K** and **73Na**, as evidenced by smaller Th–P Mayer bond orders of 1.26 and 1.28 for $[\mathbf{70}]^-$. However, these An–P Mayer bond orders are nearly twice that of the single U–N_{amide} bonds (~0.71), suggesting that these An–P bonds are polarised multiple bond interactions.

5.5 Actinide 2-phosphaethynolate complexes

Transition metal 2-phosphaethynolate $(OCP)^-$ complexes have proven to be useful precursors to prepare phosphido complexes *via* redox or photolysis process.[31] Recently, Liddle, Scheer, and co-workers reported the two new actinide–OCP complexes $[An(Tren^{TIPS})(OCP)]$ (**74An**, An = Th and U) and their reduction chemistry.[109,110] Reduction of **74U** with KC_8 in the presence of 2.2.2-cryptand gives $[K(2.2.2\text{-cryptand})][\{U(Tren^{TIPS})\}_2\{\mu\text{-}\eta^2(OP):\eta^2(CP)\text{-}OCP\}]$ (**75**), Scheme 25.[109] Although there was no phosphido species isolated from this reduction, the coordination mode of this trapped OCP-ligand is unique, and derives from a novel highly reduced and bent carbene-like form of this ligand with a bridging P-centre and the most acute P–C–O angle of ~127° in any complex to date. The mixed valence diuranium(III/IV) formulation is supported by the characterisation data and DFT calculations, where back-bonding from uranium gives a highly reduced form of the OCP unit that is perhaps best described as a uranium stabilised $(OCP)^{2-}$ radical dianion. In contrast, reduction of **74Th** with KC_8 or CsC_8 produced the phosphinidiide C–H bond activation product $[\{Th(Tren^{TIPS})\}Th\{N(CH_2CH_2NSiPr^i{}_3)_2[CH_2CH_2SiPr^i{}_2CH(Me)CH_2C(O)\mu\text{-}P]\}]$ and the oxo complex $[\{Th(Tren^{TIPS})(\mu\text{-}OCs)\}_2]$. Surprisingly, using RbC_8 for the reduction afforded a hexathorium complex, $[\{Th(Tren^{TIPS})\}_6(\mu\text{-}OC_2P_3)_2(\mu\text{-}OC_2P_3H)_2Rb_4]$ (**76**), which contains four five-membered $[C_2P_3]$ phosphorus heterocycles *via* a [2 + 2 + 1] cycloaddition, Scheme 25.[110] In addition, this hexathorium complex can be converted to the oxo complex $[\{Th(Tren^{TIPS})(\mu\text{-}ORb)\}_2]$ and the known cyclometallated complex **65Th** at 80 °C, *via* an otherwise hidden example of reductive cycloaddition reactivity in the chemistry of 2-phosphaethynolate. From the above examples it can be seen that the reduction chemistry of 2-phosphaethynolate for actinides can be quite complicated.

5.6 Actinide polyphosphorus complexes

Similar to most polyphosphorus complexes, actinide polyphosphorus complexes are most often prepared from P_4 and low-valent actinide compounds.[20] In 1991, Scherer and co-workers reported the first examples of actinide polyphosphorus complexes, $[\{Th(Cp^{tt})_2\}_2(\mu^2\text{-}\eta^4\text{-}P_6)]$ (**77**) and $[\{Th(Cp^{tt})_2\}(\mu^2\text{-}\eta^3\text{-}P_3)\{Th(Cp^{tt})_2Cl\}]$ (**78**), prepared by treatment of $[Th(Cp^{tt})_2(\eta^4\text{-}C_4H_6)]$ with P_4 at 100 °C in the absence or presence of, $MgCl_2$, respectively, Fig. 8.[111] The solid-state structures of **77** and **78** revealed distinct structural differences: a bicyclic $P_6{}^{4-}$ ligand is bridged by two thorium(IV) centres in **77**, whilst *cyclo*-$P_3{}^{3-}$ is bridged in **78**, with Th–P bond distances between 2.840(7) and 2.921(7) Å. The ^{31}P NMR

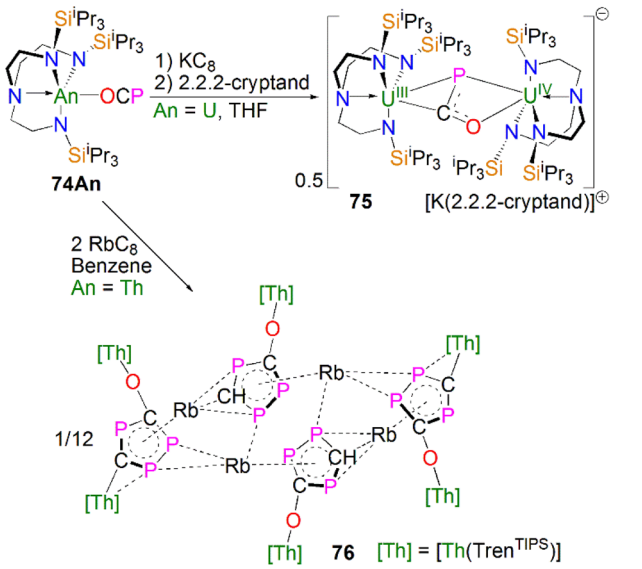

Scheme 25 Reduction of actinide–OCP complexes **74An** to produce actinide complexes **75** and **76**.

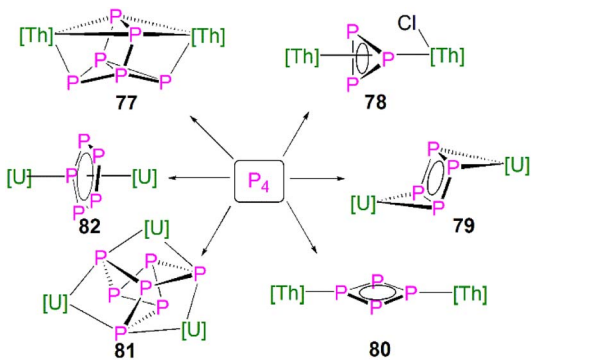

Fig. 8 Core structures for reported actinide polyphosphorus complexes **78**–**82** prepared from P_4.

spectrum for 77 exhibits resonances at 125.3, 18.4 and −41.9 ppm. In contrast, the ^{31}P NMR spectrum for **78** shows temperature-dependent features; at room temperature, there is one resonance at −75.7 ppm, however, at 193 K, two resonances at −69.7 and −94.5 ppm were observed, indicating two unique phosphorus environments at low temperature.

This area progressed little over 20 years until in 2011 Cloke, Green and co-workers isolated the *cyclo*-P_4 uranium complex $[\{U(Cp^*)(C_8H_6(Si^iPr_3)_2)\}_2(\mu^2\text{-}\eta^4\text{-}P_4)]$ (**79**), Fig. 8, from the reaction of the U(III) complex $[U(Cp^*)(C_8H_6(Si^iPr_3)_2)(THF)]$ with half an equivalent of P_4.[112] The molecular structure of **79** revealed a diuranium structure where each of the uranium metal centres interacts with the *cyclo*-P_4 ligand in an η^2-fashion. The P_4 ligand forms a chair-like structure with the two uranium atoms, with U–P bond distances of 2.9763(12) and 2.9773(12) Å, respectively, which are typical single bond character. In addition, the P–P bond distances of 2.152(2) and 2.149(2) Å within the bridging *cyclo*-P_4 unit suggest the dianionic charge of the P_4 ligand. There is only a single resonance at 718 ppm in the $^{31}P\{^1H\}$ NMR spectrum of **79**. In 2016, Mills and co-workers reported another actinide *cyclo*-P_4 complex, $[\{Th(Cp'')_3\}_2(\mu^2\text{-}\eta^2\text{-}P_4)]$ (**80**), Fig. 8, by reacting the Th(III) complex $[Th(Cp'')_3]$ with P_4.[113] The solid-state structure of **80** revealed a planar $(P_4)^{2-}$ ligand bridging two thorium centres *via* two individual η^1 bonding interactions. The Th–P bond distances of 2.919(4) Å indicates Th–P single bond interactions and the short P–P bond distances of only 2.051(9) Å are 0.1 Å shorter than those in **79**, suggesting that the bonding within the *cyclo*-P_4 ligand is closer to double bond character, which might be due to the η^1 coordination mode and the lack of Th–P π-bonding. The ^{1}H NMR spectrum was diagnostic of a diamagnetic complex, reflecting that the reduction of the P_4 arises from the oxidation of the Th(III) precursor to two Th(IV) centres; the ^{31}P NMR spectrum of **80** suggests the presence of two different phosphorus environments with two triplet signals at 227.59 and 328.86 ppm, respectively, with a P–P coupling constant of *ca*. 400 Hz.

In 2013, Liddle and co-workers reported that reaction of the diuranium(V) arene complex $[\{U(Ts^{Tol})\}_2(\mu_2\text{-}\eta^6\text{:}\eta^6\text{-}C_6H_5CH_3)]$ (Ts^{tol} = $HC(SiMe_2NAr)$, Ar = 4-MeC_6H_4) with one equivalent of P_4 resulted in the formation and isolation of the triuranium Zintl cluster $[\{U(Ts^{Tol})\}_3(\mu^3\text{-}\eta^3\text{-}P_7)]$ (**81**),[114] Fig. 8. The solid-state structure of **81** revealed a P_7^{3-} trianion cluster capped on three of its faces by three TS^{Tol}-uranium cation fragments. The U–P bond lengths of **81** are in the range of 2.949(2)–3.031(2) Å, which are comparable to the U–P cluster distances discussed above. Interestingly, **81** reacts with a variety of halide reagents, such as Me_3SiCl, LiCl, MeI, and PhI, to afford P_7R_3 products with subsequent reduction of the U component closing the synthetic cycle.

Extending the reactivity of P_4 with other U(III) complexes, Liddle and co-workers reported that treatment of $[U(Tren^{TIPS})]$ with 0.25 equivalents of P_4 reproducibly gives the actinide inverted sandwich *cyclo*-P_5 complex $[\{U(Tren^{TIPS})\}_2(\mu\text{-}\eta^5\text{:}\eta^5\text{-}cyclo\text{-}P_5)]$ (**82**),[115] Fig. 8. All previous examples of *cyclo*-P_5 complexes were stabilised by transition metals, but the isolation of **82** indicates that *cyclo*-P_5 can also be stabilised by hard actinide ions. Moreover, the characterisation data are consistent with **82** being a diuranium(IV) complex, and thus the *cyclo*-P_5 unit in **82** is formally a radical dianion rather than the usual monoanion form. The molecular structure of **82** revealed quite long U–P bond distances spanning the range 3.250(6)–3.335(6) Å, which are longer than the sum of the single bond covalent radii of U and P (2.81 Å), perhaps owing to the sterically demanding nature of $Tren^{TIPS}$ ligands combined with the bridging η^5-bound (per U) nature of the *cyclo*-P_5 unit in **82**. DFT studies on **82** indicates the principal bonding in the $U(P_5)U$ unit is polarised δ-bonding, whilst the isolobal cyclopentadienyl ligand normally interacts with metals *via* σ- and π-bonding interactions with minimal δ-interaction. In a related study, Zhu, Maron, and co-workers investigated the reactivity of P_4 with U(III) supported by a tertiary phosphine-appended Tren ligand, resulting in a diuranium product containing a P_4 chain.[116]

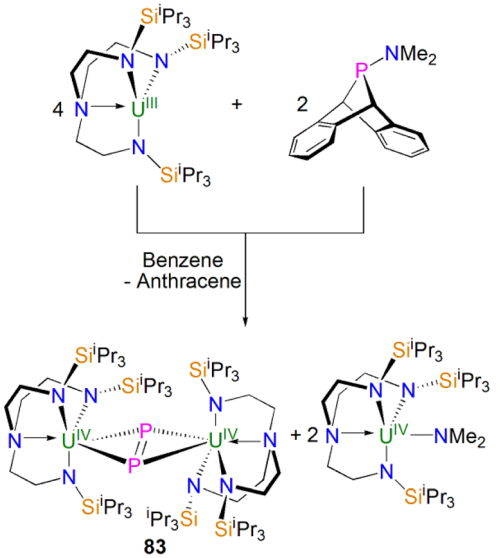

83

Scheme 26 Synthesis of uranium diphosphorus complex **83**.

In 2021, Liddle and co-workers reported the synthesis and structure of a side-on bound diphosphorus U(IV) complex, $[\{U(Tren^{TIPS})\}_2(\mu\text{-}\eta^2\text{:}\eta^2\text{-}P_2)]$ (**83**), Scheme 26, by reacting the 7λ^3-(dimethylamino)phosphadibenzonorbornadiene P-atom transfer reagent (anthracene-$PNMe_2$) with $[U(Tren^{TIPS})]$.[117] The by-product, $[U(Tren^{TIPS})(NMe_2)]$, was isolated from the reaction mixture by fractional crystallisation, accounting for the fate of the NMe_2 unit. Complex **83** is the first diphosphorus complex for any f-element complex, coming after the first f-element dinitrogen complex in 1988.[118] The molecular structure of **83** revealed P–P bond distances of 2.036(2) Å, indicative of P=P double bond character and hence a dianionic P_2^{2-}, which is consistent with a diuanium(IV) formulation confirmed by the characterisation data. The U–P distances of 2.9441(12) and 2.9446(12) Å are longer than the sum of the single bond covalent radii of U and P (2.81 Å), reflecting the side-on bridging mode of the P_2 unit in **83**. Computational results indicated that within the UP_2U motif the in-plane U–P π-bonding dominates with a very weak δ-interaction. It was subsequently found that oxidation of **64M** with $AgBPh_4$ also produces **83** (along with **54U**), which suggests the formation of a transient U(V)=PH linkage that disproportionates to **54U** and U(VI)≡P, the latter of which could dimerise to give the

more stable P–P coupled **83**. In addition, a preliminary reactivity study demonstrated that **83** can be converted to uranium *cyclo*-P_3 complexes $[M(arene)_4][\{U(Tren^{TIPS})_2(\mu\text{-}\eta^3\text{:}\eta^3\text{-}P_3)\}]$ (M = K, Rb, Cs; arene = toluene or benzene); these reactions are low yielding, implying the presence of reactive phosphido intermediates.[107] DFT calculations indicate that uranium moves from π-bonding to P_2 and *cyclo*-P_3 to δ-bonding with *cyclo*-P_5, highlighting the flexibility of the chemical bonding of uranium.

6. Lanthanide heavier pnictogen complexes

Upon descending group 15, the number of f-element heavier pnictogen bonds falls away rapidly, and lanthanide complexes containing heavier pnictogen ligands from As to Bi are much rarer than P analogues. Furthermore, such complexes tend to form multi-centre clusters with bridging pnictogen ligands. Thus, well-defined mononuclear species are sparse. To the best of our knowledge, there are no lanthanide complexes isolated to date with multiple bonding to As, Sb, or Bi.

6.1 Lanthanide arsenic complexes

The first crystallographically characterised complex containing a lanthanide–arsenic bond was reported in 1988 by Schumann and co-workers. It was found that $[Lu(Cp)_2(\mu\text{-}CH_3)_2\{Li(TMEDA)\}]$ (TMEDA = *N*,*N*,*N*′,*N*′-tetramethylethylenediamine) reacted with diphenylarsine in benzene to afford the lanthanide–arsenide complex $[Lu(Cp)_2(\mu\text{-}AsPh_2)_2\{Li(TMEDA)\}]$ (**84**), Fig. 9, *via* methane elimination.[119] The solid-state structure of **84** revealed the Lu–As bond distances are 2.896(2) and 2.870(2) Å, with a As–Lu–As bond angle of 81.14(6)°. By using the reducing nature of Sm(II), Evans and co-worker prepared $[Sm(Cp^*)_2(AsPh_2)]$ (**85**), Fig. 9, by the reaction of two equivalents of $[Sm(Cp^*)_2]$ with $Ph_2AsAsPh_2$ *via* reductive cleavage.[120] This strategy also works for making the phosphide analogue. When dissolved in THF, **85** converts to the THF adduct $[Sm(Cp^*)_2(AsPh_2)(THF)]$, which can ring open THF to produce $[Sm(Cp^*)_2\{O(CH_2)_4AsPh_2\}(THF)]$ under thermolysis conditions.

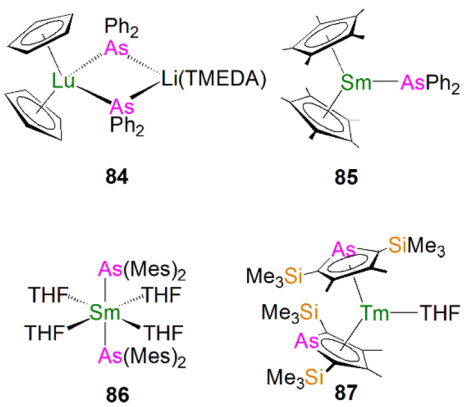

Fig. 9 Selected examples of lanthanide complexes containing metal–arsenide bonds **84**–**87**.

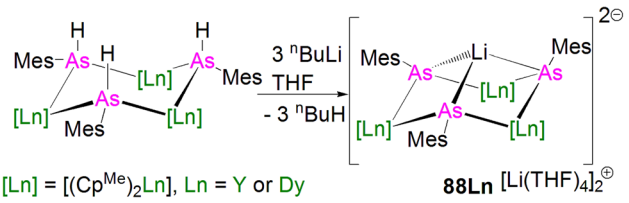

Scheme 27 Synthesis of the yttrium and dysprosium arsinidiide complexes **88Ln**.

In the molecular structure of **85**, there are two independent molecules in unit cell, and the Sm–As bond distances are 2.973(3) and 2.966(3) Å, respectively, which are slightly longer than those seen in **84**. Apart from these Ln(III) arsenide complexes, there are two Ln(II) complexes containing metal–arsenic bonds, where Nief and co-workers reported the preparation of $[Sm(AsMes_2)_2(THF)_4]$ (**86**)[36] and $[Tm(Dsas)_2(THF)]$ (**87**, Dsas = 2,5-bis(trimethylsilyl)-3,4-dimethylarsolide)[121] *via* salt metathesis, Fig. 9.

During 2015 and 2016, Layfield and co-workers synthesised the bridging arsinidiide lanthanide complexes $[\{Ln(Cp^{Me})_2\}_3(\mu\text{-}AsMes)_3Li][Li(THF)_4]_2$ (**88Ln**; Ln = Y, Dy; $Cp^{Me} = C_5H_4Me$; Mes = mesityl), Scheme 27, when investigating the effects of arsinidiide ligands on SMM properties.[122,123] Deprotonation of the bridging lanthanide arsenides $[\{Ln(Cp^{Me})_2\}_3(\mu\text{-}AsHMes)_3]$ (Ln = Y or Dy), with three equivalents of *n*-butyl-lithium gave **88Y** and **88Dy**, in yields of 73% and 77%, respectively, in addition to three equivalents of butane gas. Complexes **88Ln** feature bridging pnictide units, similar to the phosphinidiide clusters **28Ln**. The central Ln_3As_3 core shows a chair-like arrangement that is analogous to the Ln_3P_3 cores in **28Ln**. The authors reported that **88Ln** exhibit Ln–As bond distances (Y: 2.8574(6)–2.8893(7) Å; Dy: 2.8515(6)–2.8908(7) Å) that are shorter than in their arsenide counterparts $[\{Ln(Cp^{Me})_2\}_3(\mu\text{-}AsHMes)_3]$(Ln = Y,

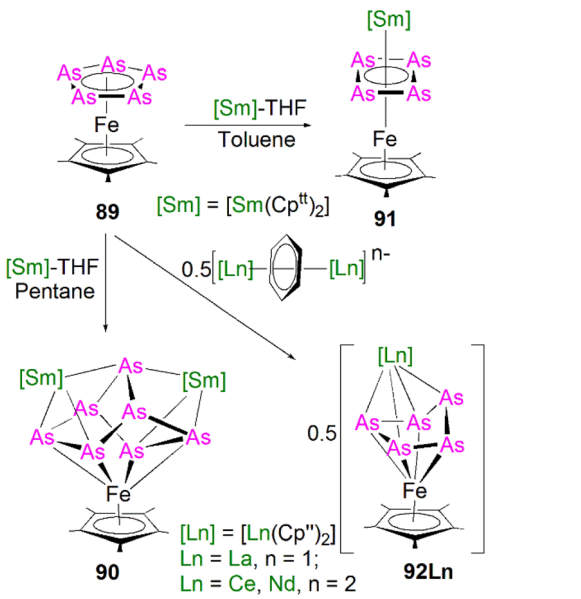

Scheme 28 Synthesis of lanthanide polyarsenide complexes **90**-**92Ln**.

2.977(2)–3.019(2) Å; Dy, 2.984(2)–3.009(2) Å). Computational studies of **88Y** indicated that the Y–As bonding is ionic with a small amount of covalent character, which is greater than the component seen for the yttrium arsenide precursor. The authors reported that **88Dy** demonstrated SMM behaviour at low temperatures (<5 K) with a U_{eff} value of 23(2) cm^{-1} and magnetic hysteresis observed up to 1.8 K. Although the structurally authenticated terminal phosphinidene complex **40** was reported very recently, an analogous lanthanide terminal arsinidene complex still remains elusive.

Due to synthetic difficulties, the chemistry of lanthanide polyarsenide complexes progressed rather slowly until the last decade. In 2016 Roesky and co-workers showed that treatment of [Fe(Cp*)(η^5-As_5)] (**89**) with [Sm(Cp^{tt})$_2$(THF)] gave the first examples of lanthanide polyarsenide complexes, [Sm(Cp″)$_2$(μ-As_7)Fe(Cp*)] (**90**) and [Sm(Cp″)$_2$(μ-η^4-η^4-As_4)Fe(Cp*)] (**91**) by using different solvents, Scheme 28.[124] The solid-state structures of **90** and **91** revealed hetero-trinuclear and -dinuclear 3d/4f clusters with the As_7 and As_4 ligands bridged between multiple metal centres. Complex **90** exhibits a norbornadiene-like structure with two short As–As bonds in the scaffold, whilst **91** is also the first 3d/4f-triple decker sandwich complex with a purely inorganic ligand middle deck. DFT calculations and physical characterisation data indicated that the central As_4 ligand is dianionic, which is isolobal with the 6p-aromatic cyclobutadiene dianion $[C_4H_4]^{2-}$. This is consistent with the As–As bond distances within the *cyclo*-As_4 ligand in **91**, which were found to be in between an As–As single and double bond.

More recent work from the Roesky group has proved that a redox strategy, using [Fe(Cp*)(η^5-As_5)] as an arsenic ligand source to react with low-valent lanthanide starting materials, is an effective way to synthesise new lanthanide polyarsenide complexes. Three new 3d/4f polyarsenide complexes in the separate ion pair form [K(18C6)][Ln(Cp″)$_2$(μ-η^4:η^4-As_5)Fe(Cp*)] (**92Ln**, Ln = La, Ce, Nd) were prepared by the reduction of [Fe(Cp*)(η^5-As_5)] with formally low-valent bridging arene lanthanide compounds in moderate yields, Scheme 28.[125] The molecular structures of **92Ln** are very similar to each other, containing highly reduced As_5 units with an envelope shape. In **92Ln** the Fe centre is η^4-coordinated by the *cyclo*-As_5 unit and the shortest As–As bond distance of 2.3781(6) Å is observed, while the rest of the As–As bonds range from 2.3928(5) Å to 2.4325(5) Å. As expected, Ln–As bond distances vary over a wide range because of the steric constraints and anisotropic charge distribution with in the As_5 ligand. In other work, Roesky and co-workers found that reacting the arsenic source [{Co(Cp‴)}$_2$(μ-η^2:η^2-As_2)$_2$] with samarocenes produced two new mixed 3d/4f polyarsenic complexes [{Co(Cp^{ttt})}$_2$(μ-As)$_4$Sm(Cp^{Me4R})$_2$] (R = Me, *n*-propyl), which represent the first examples of lanthanide complexes with open chain-like polyarsenic ligands.[126]

More recently, Roesky and co-workers found that yellow arsenic (As_4) is also a useful source to introduce polyarsenic ligands to lanthanides. Due to the unstable nature of this As_4 allotrope under ambient conditions, the authors used freshly-prepared As_4 in solution to react with the divalent precursor [Sm(DippForm)$_2$(THF)$_2$]; after workup, red crystals of the *cyclo*-As_4 complex [{Sm(DippForm)$_2$}$_2$(μ-η^4:η^4-As_4)] (**93**),[61] Scheme 29, were obtained as a minor product, which is essentially isostructural to the lanthanide *cyclo*-P_4 complex **48**. Unfortunately, the presence of non-removable impurities hampered further characterisation on **93** because of the instability of As_4 in solution. In parallel work, the authors also explored the reactivity of As_4 with [Sm(Cp*)$_2$]. As both reagents are highly reactive and light sensitive, this reaction was performed with the exclusion of light; after work-up, a few single crystals of [{Sm(Cp*)$_2$}$_2$(μ-η^2:η^2-As_2)] (**94**), Scheme 29, with inseparable side products were isolated.[127] The solid-state structure of **94** revealed a rare diarsenic lanthanide species with the As_2 ligand side-on bound to two samarium centres. The As–As bond distance of 2.278(2) Å indicates As═As double bond character, and hence a dianionic charge on the As_2^{2-} unit. The Sm–As distances of 3.014(1) Å are statistically the same because of the presence of an inversion centre in **94**.

The practical difficulties of working with As_4 solutions has spurred the development of new arsenic starting materials for construction of polyarsenic complexes. Roesky and co-workers reported the preparation for arsenic nanoparticles using a reductive synthetic method developed by Feldmann and co-workers.[128] The elemental As^0 nanoparticles (*nano*-As^0, $d = 7.2 \pm 1.8$ nm) can be formed by the reduction of AsI_3 with a freshly prepared solution of lithium naphthalenide at 0 °C in THF. The *nano*-As^0 can be isolated in a pure form as the LiI by-product is sufficiently soluble in THF and Et_2O to be washed away; this has

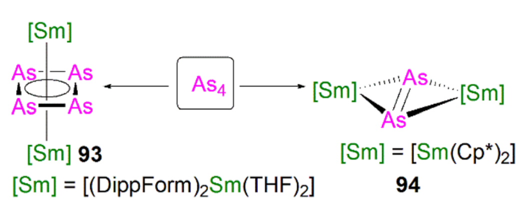

Scheme 29 Synthesis of lanthanide polyarsenide complexes 93 and 94.

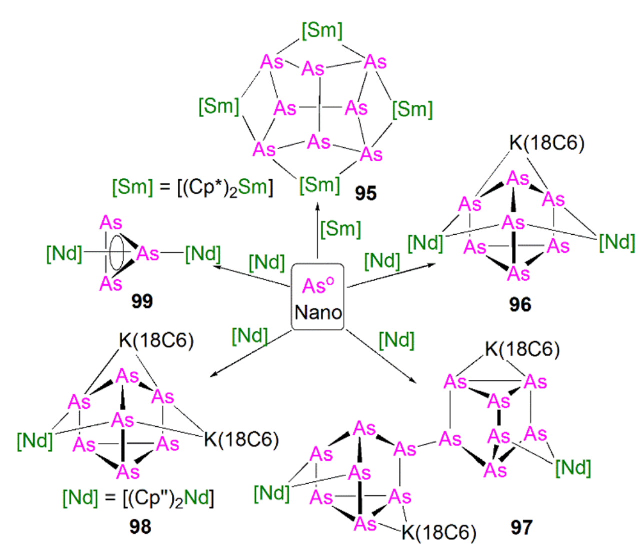

Scheme 30 Synthesis of lanthanide polyarsenic complexes 95–99.

proven very effective at introducing As oligomers to f-elements, Scheme 30. It was reported that **94** could be prepared by the reaction of $[Sm(Cp^*)_2]$ with *nano*-As^0 at 60 °C, but again with inseparable byproducts and in low yield. Interestingly, under harsh conditions, the tetrasamarium polyarsenide cluster $[\{Sm(Cp^*)_2\}_4(\mu\text{-}As_8)]$ (**95**) was reproducibly isolated in yields of 22% as a crystalline solid after work-up.[128] In the molecular structure of **95**, the Sm–As bond distances fall into the small range of 3.0814(10)–3.1734(10) Å, which are slightly longer than those of **94**, and the As–As bond distances are between 2.4044(12) Å and 2.5003(12) Å, suggesting single bonds with angles of 93.52(4)° to 103.68(4)° within the $[As_8]^{4-}$ tetraanionic cage. Very recently, the authors expanded this chemistry, reacting *nano*-As^0 with the dilanthanide inverted arene complexes $[K(18\text{-crown-6})][\{Ln(Cp'')_2\}_2(\mu\text{-}\eta^6\text{:}\eta^6\text{-}C_6H_6)]$ (Ln = La, Ce) and $[[K(18\text{-crown-6})]_2[\{Ln(Cp'')_2\}_2(\mu\text{-}\eta_6\text{:}\eta_6\text{-}C_6H_6)]$ (Ln = Ce, Nd) to give a range of lanthanide Zintl anions **96–99** containing As_3^{3-}, As_7^{3-}, and As_{14}^{4-} ligands, respectively, that were previously not accessible in molecular lanthanide chemistry, Scheme 30.[129] The As_{14}^{4-} unit in **97** is the largest organo-lanthanide-polyarsenic complex to date. The synthesis and characterisation of these diverse polyarsenic lanthanide complexes demonstrated the great utility of *nano*-As^0 for accessing novel molecular polyarsenic clusters.

6.2 Lanthanide antimony complexes

Although there have not been any reports of structurally authenticated f-element-antimony or -bismuth multiple bonds, a relatively small number of lanthanide complexes featuring single bond interactions with these heavy pnictogens have been crystallographically characterised. Lanthanide–antimony or -bismuth bonds are commonly synthesised as clusters with the polyantimony or polybismuth ligands stabilised between multiple metal centres. Complexes containing metal–antimony or -bismuth multiple bonding interaction are also rare for d-block metals; to date, there has been only one single example of a terminal metal stibido complex, $[W^{VI}(Tren^{TMS})(Sb)]$ ($Tren^{TMS}$ = $\{N(CH_2CH_2NSiMe_3)_3\}^{3-}$) with a W≡Sb triple bond (2.526(2) Å), prepared by Scheer and co-workers.[130] No structurally authenticated metal–bismuth multiple bonds are known both for d-block and f-block metals. In 1992, Evans and co-workers reported the synthesis of a complex featuring Sm–Sb interactions. The reaction of one equivalent each of $[Sm(Cp^*)_2]$ and $Sb(^nBu)_3$ afforded the samarium antimony Zintl ion complex $[\{Sm(Cp^*)_2\}_3(\mu\text{-}\eta^2\text{:}\eta^2\text{:}\eta^1\text{-}Sb_3)(THF)]$ (**100**), Scheme 31.[131] Complex **100** exhibits five Sm–Sb bonds in the range of 3.162(1)–3.205(1) Å.

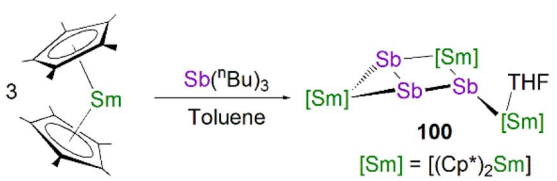

Scheme 31 Synthesis of samarium polyantimony complex **100**.

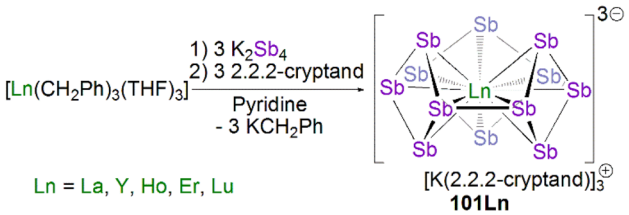

Scheme 32 Synthesis of lanthanide Zintl polyantimony complexes **101Ln**. Ln–Sb interactions are omitted for clarity.

Surprisingly, there were no further reports of lanthanide–antimony bonds until in 2016 a wide range of lanthanide–polyantimony clusters emerged. Sun, Boldyrev and co-workers reported the synthesis of lanthanide(III) complexes with three Zintl Sb_4^{2-} units $[K(2.2.2\text{-cryptand})]_3[Ln(\eta^4\text{-}Sb_4)_3]$ (**101Ln**; Ln = La, Y, Ho, Er, Lu).[132] Complexes **101Ln** were synthesised *via* the reaction of $[Ln(CH_2C_6H_5)_3(THF)_3]$ (Ln = La, Y, Ho, Er, Lu) with three equivalents each of K_2Sb_4 and 2.2.2-cryptand in pyridine, Scheme 32. The five complexes exhibit two types of Ln–Sb bond distances, with equatorial Ln–Sb_{eq} distances of ~3.4 Å and shorter non-equatorial Ln–Sb_{ne} distances of ~3.2 Å. The authors noted that the Ln–Sb bond distances decrease from lanthanum to lutetium due to the lanthanide contraction (Ln–Sb_{ne}: 3.2461(5), 3.0932(10), 3.0843(9) and 3.0643(11) Å for La, Ho, Er and Lu respectively). Calculations on **101Ln** indicated that the Sb_4 units are aromatic in nature, similar to cyclobutadienyl.

In 2017, Layfield and co-workers reported the synthesis of lanthanide stibide complexes which contain either a bridging stibide or a Zintl-like $[Sb_4Mes_3]^{3-}$ moiety. The bridging stibide $[\{Ln(Cp^{Me}{}_2)\}_3(\mu\text{-}SbHMes\}_3)]$ (**102Ln**, Ln = Y, Dy) was synthesised *via* the reaction of three equivalents each of $[Ln(Cp^{Me})_3]$ and $MesSbH_2$, Scheme 33.[133] Complexes $[\{Ln(Cp^{Me}{}_2)\}_3\{\mu\text{-}(SbMes)_3\text{-}Sb\}]$ (**103Ln**, Ln = Y, Dy) were synthesised *via* two different routes, the first of which involved the reaction of three equivalents each of $[Ln(Cp^{Me})_3]$ and *n*-butyl lithium with four

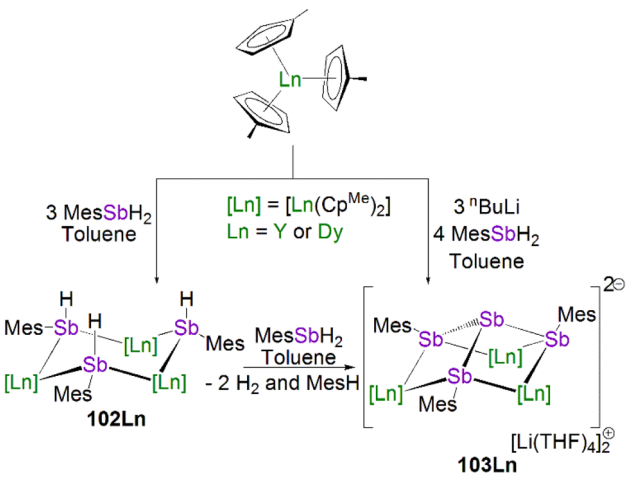

Scheme 33 Synthesis of lanthanide polyantimony complexes **102Ln** and **103Ln**.

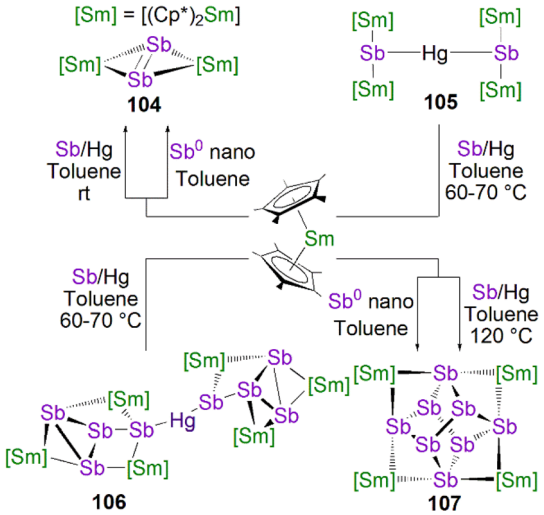

Scheme 34 Synthesis of samarium polyantimony complexes **104**–**107**.

equivalents of $MesSbH_2$; however, stibine dehydrocoupling to give the distibane ($Sb_2H_2Mes_2$) and tetrastibetane (Sb_4Mes_4) can occur. The second reported route to **103Ln** involved the cross-dehydrocoupling reaction of one equivalent of the stibide precursor **102Ln** with one equivalent of $MesSbH_2$ to give one equivalent each of **103Ln** (Ln = Y, quantitative; or Dy, 45%) and mesitylene, and two equivalents of hydrogen gas. Complexes **103Ln** exhibit solid state structures with Ln_3Sb_3 cores akin to the arsinidiide **88Ln** and phosphinidiide **28Ln** analogues, however in **103Ln** the Sb_3 unit is capped with a Sb^{3-} fragment to form a Zintl-like moiety. Complexes **103Ln** feature mean Y–Sb and Dy–Sb bond distances of 3.1211(15)–3.1420(16) Å, and 3.119(1)–3.138(1) Å, respectively. These bond distances are very similar to that of the stibide precursors **102Ln**, which exhibit Ln–Sb bond distances of 3.0987(11)–3.2008(6) and 3.092(6)–3.212(3) Å for Y and Dy, respectively. This observation differs from the analogous pnictinidiide complexes **28Ln** and **88Ln**, where the Ln–Pn distances are shorter than the pnictide precursors; this is likely due to **103Ln** exhibiting $[Sb_4Mes_3]^{3-}$ units as opposed to discrete RSb^{2-} stibinidene ligands. The authors reported that both **102Dy** and **103Dy** show SMM behaviour, with U_{eff} values of 345 and 270 cm^{-1}, respectively, and both complexes exhibiting magnetic hysteresis at 1.8 K.

In 2018, Roesky and co-workers utilised [Sm(Cp*)$_2$] to stabilise a range of samarium polyantimony complexes, Scheme 34.[134] The reaction of [Sm(Cp*)$_2$] with an Sb/Hg amalgam in toluene yielded a mixture of the polyantimony complexes [{Sm(Cp*)$_2$}$_2$(μ-η^2:η^2-Sb$_2$)] (**104**) and [{[Sm(Cp*)$_2$]$_2$Sb}$_2$(μ-Hg)] (**105**), Scheme 34. The product was dependent upon the temperature of the reaction; whilst at room temperature the primary products were **104** and **105**, if the reaction mixture was heated at 60–70 or 120 °C, the polyantimony complexes [{[Sm(Cp*)$_2$]$_3$(Sb$_4$)}$_2$Hg] (**106**) or [{Sm(Cp*)$_2$}$_4$(Sb$_8$)] (**107**) were isolated, respectively. Using a Sb/Hg amalgam however resulted in difficult to separate antimony products, so the authors

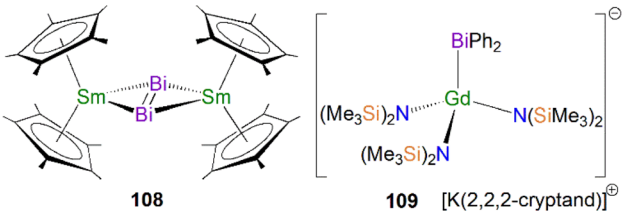

Fig. 10 Lanthanide–bismuth complexes **108** and **109**.

reported an alternate synthetic route to both **104** and **107** *via* the reaction of [Sm(Cp*)$_2$] with antimony nanoparticles. Complex **104** exhibits an Sm–Sb bond distance of 3.2141(9) Å, which is comparable to complex **100**, whereas complex **105** demonstrates significantly shorter Sm–Sb distances of 3.0052(14)–3.0158(13) Å. Complexes **106** and **107** exhibit longer Sm–Sb bond distances of 3.2238(8)–3.3694(8) Å and 3.3134(8)–3.4119(7) Å, respectively. More recently, Roesky and co-workers have shown that [Sm(Cp*)$_2$] can also be used to make 4d/4f polyantimony clusters containing a planar Sb_4-unit that is similar to that seen in **91**.[135]

6.3 Lanthanide bismuth complexes

The first example of a structurally authenticated lanthanide bismuth interaction was reported in 1991 by Evans and co-workers. The reaction of two equivalents of [Sm(Cp*)$_2$] with one equivalent of $BiPh_3$ in toluene afforded [{Sm(Cp*)$_2$}$_2$(μ-η^2:η^2-Bi$_2$)] (**108**) in yields of up to 60%,[136] Fig. 10. The complex is isostructural to the diantimony complex **104** and exhibits Sm–Bi distances ranging from 3.2645(10) to 3.3108(11) Å, which are longer than that the Sm–Sb distances in **104** (3.2141(9) Å). More recent work from the Evans group has shown that the reaction of $BiPh_3$ with the Gd(II) complex [K(2.2.2-cryptand)][Gd{N(SiMe$_3$)$_2$}$_3$] afforded a monomeric Gd(III)-bismuthide complex [K(2.2.2-cryptand)][Gd{N(SiMe$_3$)$_2$}$_3$(BiPh$_2$)] (**109**),[137] Fig. 10, which is the only example of a mononuclear lanthanide–bismuth compound. In the molecular structure of **109**, the Gd–

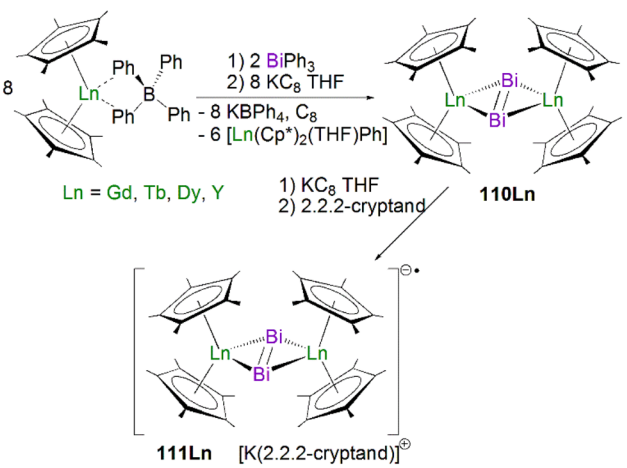

Scheme 35 Synthesis of lanthanide dibismuth complexes **110Ln**–**111Ln**.

Bi bond distance of 3.3516(5) Å is very close to the Sm–Bi bond in **108**.

Very recently, Chilton, Demir and co-workers reported two new sets of lanthanide dibismuth complexes, Scheme 35. The neutral complexes $[\{Ln(Cp^*)_2\}_2(\mu\text{-}\eta^2\text{:}\eta^2\text{-}Bi_2)]$ (**110n**, Ln = Gd, Tb, Dy, Y) were prepared by the one-pot reactions of eight equivalents of $[Ln(Cp^*)_2(BPh_4)]$ (Ln = Gd, Tb, Dy, Y), two equivalents of triphenylbismuth, and eight equivalents of KC_8 at room temperature under argon.[138] Complexes **110Ln** are quite soluble in toluene, thus the poor atom-efficiency of the reaction is overcome by separation from the poorly soluble byproducts. Reduction of **110Ln** using KC_8 in the presence of 2.2.2-cryptand in THF afforded the radical complexes $[K(2.2.2\text{-cryptand})][\{Ln(Cp^*)_2\}_2(\mu\text{-}\eta^2\text{:}\eta^2\text{-}Bi_2^{\bullet})]$ (**111Ln**, Ln = Gd, Tb, Dy, Y).[138] Complexes **111Ln** are the first examples containing the heaviest dinitrogen radical analogues of dibismuth for any d- or f-block metal. The radical nature of **111Ln** are confirmed by the characterisation data and DFT calculations. Reflecting the radical electron in the π-antibonding orbital of the Bi_2 ligand in **111Ln**, the Bi–Bi bond distances of (2.9310(11) to 2.9450(13) Å) are longer than those in neutral **110Ln** (2.8418(10) to 2.8549(9) Å), and the Ln–Bi bond distances are shorter in **111Ln** (3.1865(8) to 3.2064(5) Å) *vs.* **110Ln** (3.2335(2) to 3.2611(8) Å). Magnetic studies have shown that the Bi_2^{3-} radical-bridged **111Tb** and **111Dy** are SMMs with magnetic hysteresis where the Bi_2^{3-} radical as the bridge engenders antiferromagnetic exchange coupling with the paramagnetic lanthanide ions, leading to a ferrimagnetic ground state.

Similar to antimony chemistry there have been a range of lanthanide–bismuth interactions stabilised though the isolation of Zintl anions bound to the lanthanide metal ions. In 2011, Dehnen and co-workers utilised this method to synthesise a mini-fullerene-type Zintl-lanthanide complex, Scheme 36. The reaction of $[K(2.2.2\text{-cryptand})]_2[Sn_2Bi_2]\cdot$en (en = 1,2-ethylenediamine) and $[Eu(C_5Me_4H)_3]$ in toluene gave $[K(2.2.2\text{-cryptand})]_4[Eu@Sn_6Bi_8]$ (**112**) in a 11% yield.[139] The solid-state structure of **112** indicates each position of the cage is occupied by either a Sn or Bi atom in a ratio of 0.76–0.11 and 0.24–0.89, respectively. The Eu-(Sn/Bi) bond distances exhibited by **112** span a wide range of 3.3515(8)–3.5770(9) Å. The Sn/Bi atoms in the non-equatorial positions exhibit shorter mean Eu–Sn/Bi distances (3.4743(11) Å) compared to the equatorial distance (3.5208(15) Å). Complex **112** exhibits a short mean axial Eu–Sn/Bi distance of 3.3418(10) Å.

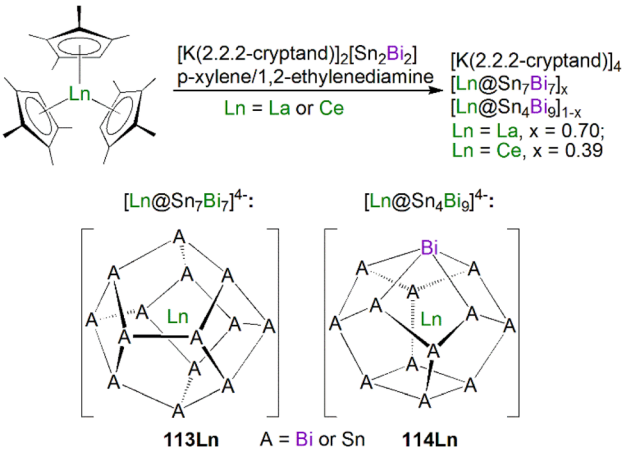

Scheme 37 Synthesis of lanthanide polybismuth Zintl anionic clusters **113Ln** and **114Ln** and representations of the polyhedral architectures. Ln–A interactions are omitted for clarity.

In 2012, Dehnen and co-workers further expanded the range of lanthanide bismuth clusters, Scheme 37; the separate reactions of $[K(2.2.2\text{-cryptand})]_2[Sn_2Bi_2]\cdot$en with $[Ln(C_5Me_4H)_3]$ (Ln = La or Ce) in *p*-xylene gave mixtures of tin–bismuth clusters surrounding lanthanide centres in $[K(2.2.2\text{-cryptand})]_4[Ln@Sn_7Bi_7]_x[Ln@Sn_4Bi_9]_{1-x}$ (Ln = La, x = 0.70; Ln = Ce, x = 0.39).[140] The crystallographic data for both complexes demonstrate two types of cluster, the 14-vertex anion $[Ln@Sn_7Bi_7]^{4-}$ (**113Ln**) and 13-vertex anion $[Ln@Sn_4Bi_9]^{4-}$ (**114Ln**). Like previous Sn/Bi clusters, anions **113Ln** and **114Ln** exhibit disorder of the Sn and Bi atoms occupying the same atomic positions in the cluster. The clusters **113Ln** have similar structures to **112**, exhibiting longer mean Ln–Sn/Bi equatorial distances of 3.539(2) (La) and 3.493(3) Å (Ce) when compared to the non-equatorial distances of 3.433(2) (La) and 3.416(2) Å (Ce). Clusters **113La** and **113Ce** exhibit mean Ln–Sn/Bi axial distances of 3.426(2) and 3.436(2) Å, respectively. The second cluster type, **114Ln**, features Ln–Sn/Bi bond distances over the range of 3.107(4)–3.557(2) and 3.046(12)–3.543(3) Å for La and

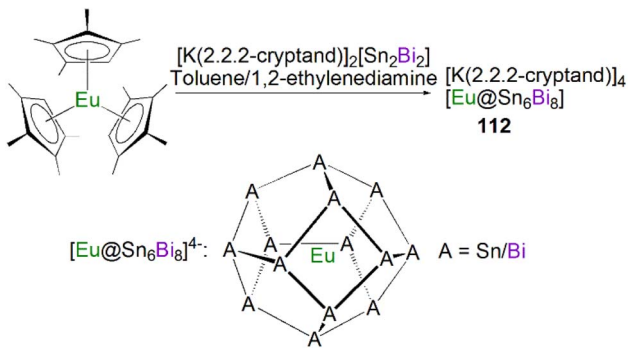

Scheme 36 Synthesis of europium polybismuth Zintl anionic clusters **112**. Eu–A interactions are omitted for clarity.

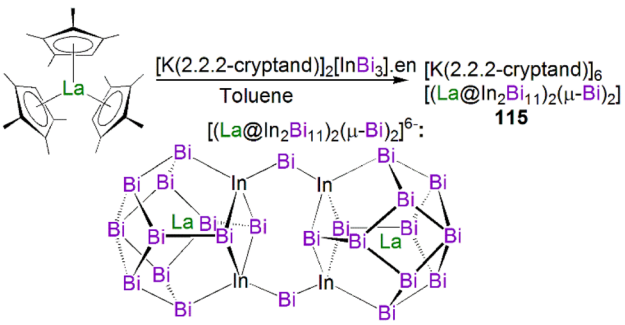

Scheme 38 Synthesis of lanthanum polybismuth Zintl anionic clusters **115** and representation of the polyhedral architecture. La–Bi interactions are omitted for clarity.

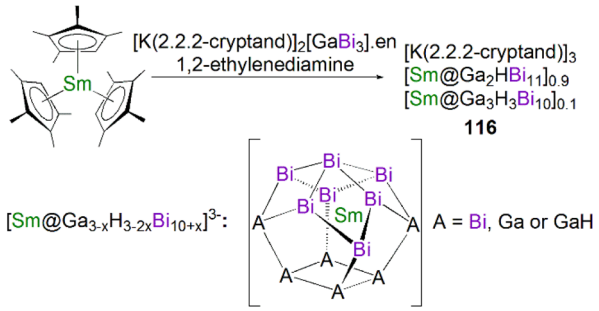

Scheme 39 Synthesis of samarium polybismuth Zintl anionic clusters **116**. Sm–Bi/A interactions are omitted for clarity.

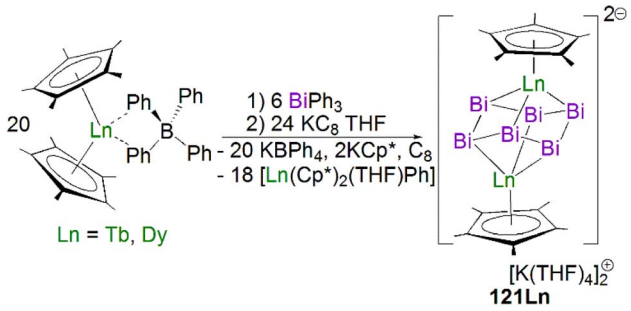

Scheme 41 Synthesis of lanthanide polybismuth anionic clusters **121Ln**.

Ce, respectively. The authors postulated that the differences in Ln–Sn/Bi distances between the La and Ce analogues of **114La** and **114Ce** is most likely a result of the different ionic radii of La(III) and Ce(III).

In parallel work in 2012, Dehnen and co-workers reported the synthesis of the indium metalloid bismuth Zintl cluster, $[K(2.2.2\text{-cryptand})]_6[(La@In_2Bi_{11})_2(\mu\text{-}Bi)_2]$ (**115**) *via* the reaction of $[K(2.2.2\text{-cryptand})]_2[InBi_3]\cdot en$ with $[La(C_5Me_4H)_3]$ in toluene in a yield of 11%,[141] Scheme 38. Complex **115** features two 13-vertex anions connected *via* two bridging bismuth atoms. The La–Bi distances exhibited by **115**, 3.1343(8)–3.5018(9) Å, are similar to that of the anion **114Ln** [3.106(4)–3.557(2) Å].

In 2014, Dehnen and co-workers utilised similar protocols to expand the number of 13-vertex lanthanide–bismuth metalloid clusters to include the gallium-substituted cage $[K(2.2.2\text{-cryptand})]_2[Sm@Ga_2HBi_{11}]_{0.9}[Sm@Ga_3H_3Bi_{10}]_{0.1}$ (**116**) *via* the reaction of $[K(2.2.2\text{-cryptand})]_2[GaBi_3]$.en with $[Sm(C_5Me_4H)_3]$, Scheme 39.[142] The authors reported that the two different trianionic fragments feature disorder similar to the tin analogue **113Ln**, with several of the atomic positions in the cluster being occupied by Bi, Ga and GaH. Formulation of each anionic cluster was determined by the examination of a combination of techniques, namely single crystal diffraction, energy dispersive X-ray and electrospray ionisation mass spectrometry (ESI-MS), which indicated that the two fragments were present in a ratio of 92% to 8% for $[Sm@Ga_2HBi_{11}]$ and $[Sm@Ga_3H_3Bi_{10}]$, respectively. The Sm–Bi/Ga distances in **116** span 3.0464(6)–3.4134(6) Å, which is a similar to the other 13-vertex lanthanide cluster complexes **114Ln** and **115**.

In 2015, Dehnen and co-workers reported the synthesis of a wide range of lead bismuth cages. The separate reactions of the *in situ*-generated Zintl lead precursor $[K(2.2.2\text{-cryptand})]_2[Pb_2Bi_2]\cdot en$ with $[Ln(C_5Me_4H)_3]$ (Ln = La, Ce, Nd, Gd, Sm, Tb) in toluene yielded ten complexes, $[K(2.2.2\text{-cryptand})]_3[Ln@Pb_6Bi_8]_x[Ln@Pb_3Bi_{10}]_{1-x}$, ($x$ = 0.038, 0 or 0.545 for La, Ce or Nd respectively) or $[K(2.2.2\text{-cryptand})]_4$ $[Ln@Pb_7Bi_7]_y[Ln@Pb_4Bi_9]_{1-y}$ (Ln = La; y = 0.038, 0.279 or 0.458; Ln = Nd, Sm or Tb; y = 0), depending on the lanthanide used, Scheme 40.[143] All ten complexes feature a mixture of 14- and 13-vertex anions, $[\{Ln@Pb_6Bi_8\}_x\{Ln@Pb_3Bi_{10}\}_{1-x}]^{3-}$ ($[\mathbf{117Ln}_{x\mathbf{118Ln}1-x}]^{3-}$) and $[\{Ln@Pb_7Bi_7\}_y\{Ln@Pb_4Bi_9\}_{1-y}]^{4-}$ ($[\mathbf{119Ln}_{y\mathbf{120Ln}1-y}]^{4-}$); the structures for the differing anions are analogous to those of **113Ln** and **114Ln**. Like the previously reported lanthanide bismuth cages (**114Ln** and **116**), the anionic clusters **117Ln**–**120Ln** all contain disorder, resulting in both Pb and Bi occupying the same atomic sites.

In 2021, Demir and co-workers reported the synthesis of $[K(THF)_4]_2[\{Ln(Cp^*)_2\}_2(\mu\text{-}Bi_6)]$ (**121Ln**, Ln = Tb, Dy) by one-pot reactions of $[Ln(Cp^*)_2(BPh_4)]$ (Ln = Tb, Dy) with triphenylbismuth in THF, followed by reduction with KC_8 at 45 °C, Scheme 41.[144] The authors proposed that the use of KC_8 induced reduction and bismuth cluster formation. The solid-state structures of **121Ln** revealed $[Ln_2Bi_6]$ cores with lanthanide centres bridged by a rare $[Bi_6]^{6-}$ Zintl ion. Notably, complexes **121Ln** are the first examples of a cyclic bismuth hexamer in an organometallic complex with any metal. The Ln–Bi bond distances for **121Tb** and **121Dy** are 3.055(1)–3.070(1) and 3.042(1)–3.060(1) Å, respectively, which are approximately 0.2 Å shorter than that the Sm–Bi bonds in **108** (3.2645(10)–3.3108(11) Å). The Bi–Bi distances of 3.029(1)–3.042(1) and

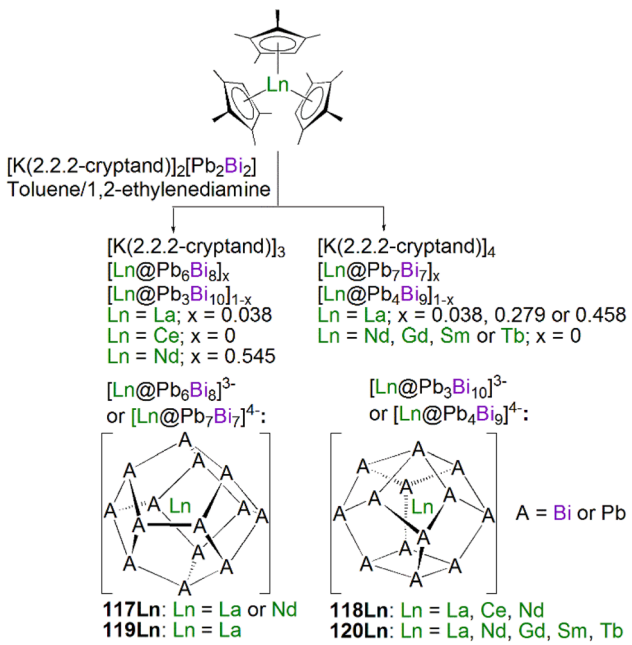

Scheme 40 Synthesis of lanthanide polybismuth Zintl anionic clusters **117Ln**–**120Ln**. Ln–A interactions are omitted for clarity.

3.027(1)–3.036(1) A° for **121Tb** and **121Dy**, respectively, are significantly longer than multiple Bi–Bi bonds (2.82–2.87 A°), and are comparable with Bi–Bi single bonds (>2.99 A°). Magnetic data and quantum calculations indicates strong ferromagnetic interactions between the lanthanide ions facilitated by the Zintl $[Bi_6]^{6-}$ ligands, resulting in magnetic blocking and open hysteresis loops that are rarely observed for super exchange-coupled SMMs containing solely lanthanide ions.

7. Actinide heavier pnictogen complexes

In parallel with lanthanide chemistry, actinide complexes containing heavier pnictogen ligands (from As to Bi) are much rarer than actinide–phosphorus congeners. Again, these complexes tend to form multi-nuclear clusters with the heavier pnictogen ligands bridged by two or more metal centres, thus well-defined mononuclear species are sparse. However, significant advances have been achieved in actinide arsenic multiple bonding chemistry that are discussed in this section. In contrast, there are currently no examples of actinide complexes featuring multiple bonding interactions with antimony or bismuth ligands.

7.1 Actinide arsenic complexes

In 1994, Using a similar synthetic approach used for the preparation of **77**, Scherer and co-workers synthesised the first examples of an actinide polyarsenic complex $[\{Th(Cp^{tt})_2\}_2(\mu^2\text{-}\eta^3\text{-}As_6]$ (**122**) by the treatment of $[(Cp^{tt})_2Th(\eta^4\text{-}C_4H_6)]$ with elemental As_4 in boiling xylene,[145] Fig. 11. Complex **122** is also the first structurally characterised actinide complex containing metal–arsenic bonds, which is isostructural to the polyphosphorus analogue **77**. In the molecular structure of **122**, the Th–As bond distances span the range of 2.913(2) to 3.044(2) Å. However, it would be more than 20 years before more actinide–arsenic complexes started to emerge, reflecting the synthetic challenges of the area.

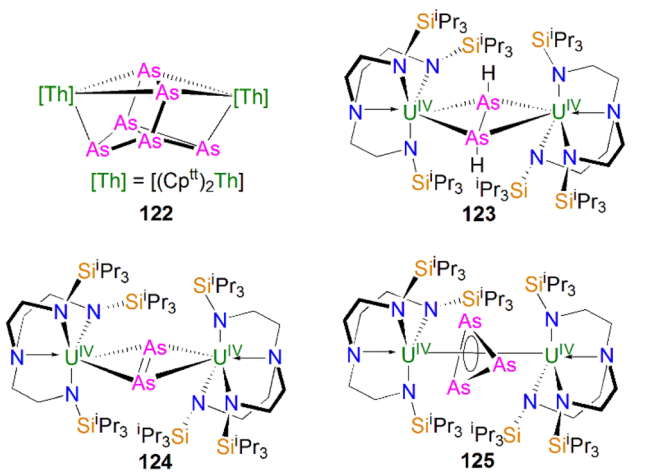

Fig. 11 Examples containing actinide–arsenic bonds **122**–**125**.

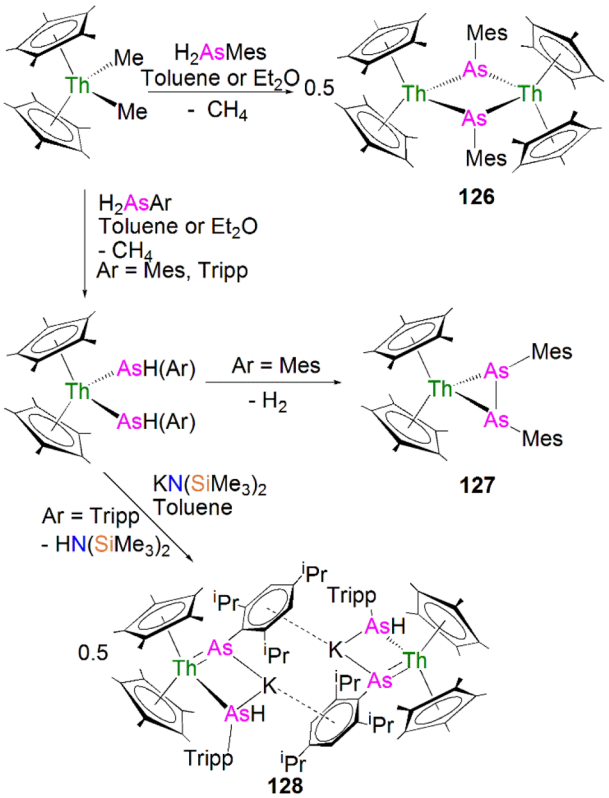

Scheme 42 Synthesis of thorium arsinidiide and diarsene complexes **126**–**128**.

In 2015, Liddle, Scheer, and co-workers reported the diuranium complex $[\{U(Tren^{TIPS})\}_2(\mu\text{-}\eta^2\text{:}\eta^2\text{-}HAsAsH)]$ (**123**)[146] by the reaction of $[U(Tren^{TIPS})(THF)][BPh_4]$ with $KAsH_2$ in 1 : 1.4 ratio *via* a dehydrocoupling process, Fig. 11. On one occasion, the uranium diarsenic complex $[\{U(Tren^{TIPS})\}_2(\mu\text{-}\eta^2\text{:}\eta^2\text{-}As_2)]$ (**124**)[146] was also obtained from the reaction in less than 1% yield, which can be viewed as a fully dehydrocoupled product, Fig. 11. The solid-state structures of **123** and **124** are similar to each other, though the As–As bond distance in **123** (2.4102(13) Å) is longer than that in **124** (2.2568(14) Å), indicating As–As single and As=As double bond characters, respectively. The +4 oxidation state of **123** was confirmed by magnetometry data, so the diarsene ligand has been reduced to its diarsane-1,2-diide form. Complex **123** is the first example of HAsAsH complex for any d- or f-block metal. The characterisation data and theoretical calculations supported the presence of back-bonding-type interactions from uranium to the HAsAsH π*-orbital, indicating the strong π-accepting ability of this ligand. In other work, the authors also reported the structure of $[\{U(Tren^{TIPS})\}_2(\mu\text{-}\eta^3\text{:}\eta^3\text{-}As_3)]$ (**125**),[147] Fig. 11, but the low yield for this compound prevented further characterisation.

In between 2016 and 2021, Walensky and co-workers reported the synthesis of thorium arsenic complexes, Scheme 42. Using methane elimination, the authors prepared the bridging dithorium arsinidiide complex $[\{Th(Cp^*)_2(\mu\text{-}AsMes)_2]$ (**126**) and the arsenide complexes $[Th(Cp^*)_2(HAsAr)_2]$ (Ar = Mes, Tripp) by the reactions of $[Th(Cp^*)_2(Me)_2]$ under different conditions.[148] It

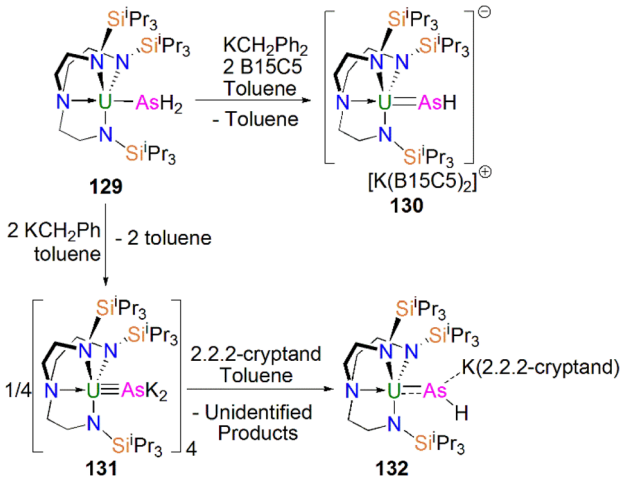

Scheme 43 Synthesis of the uranium arsinidene complexes **130**, arsenido **131**, and arsinidiide **132** from the arsenide **129**.

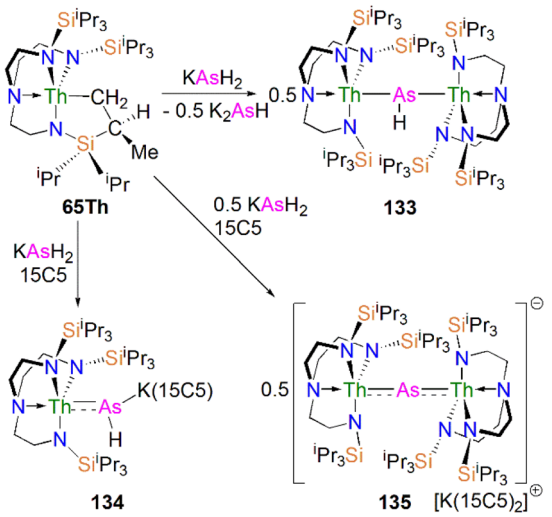

Scheme 44 Synthesis of thorium arsinidiide and arsenido complexes **133–135**.

was found that $[Th(Cp^*)_2(HAsMes)_2]$ is unstable at room temperature and converts to the dehydrocoupled product $[Th(Cp^*)_2(\mu\text{-}As_2Mes_2)]$ (**127**) with the release of H_2 gas. Applying the same synthetic approach, the uranium analogues of **126** and **127** were prepared. With the bulkier substituents on the arsenide group, $[Th(Cp^*)_2(HAsTripp)_2]$ is thermally stable at room temperature and its reactivity with *tert*-butyl isocyanide ^{t}BuNC to give an arsaazaallene product was investigated.[149] The authors reported that deprotonation of $[Th(Cp^*)_2\{AsH(Tripp)\}_2]$ with one equivalent of $KN(SiMe_3)_2$ gave $[Th(Cp^*)_2\{\mu\text{-}As(Tripp)\}\{\mu\text{-}AsH(Tripp)\}K]_2$ (**128**) in yields of 77%.[86] The Th–As bond distances in **126** (2.8787(6) Å) and **127** (2.923(2)/2.971(3) Å) are quite long; by contrast, **128** exhibits a short Th–As distance of 2.7994(4) Å, indicating a multiple bonding interaction. This was probed computationally, revealing a Th=As Wiberg bond index (1.30) nearly twice that of the Th–As single bonds (0.70).

In 2015, Liddle, Scheer, and co-workers adapted the synthetic protocols used for the preparation of the uranium phosphinidene complex **64K**. Deprotonation of **129** with benzyl potassium in the presence of two equivalents of B15C5 produced the analogous arsinidene complex $[K(B15C5)_2][U(Tren^{TIPS})(AsH)]$ (**130**),[147] Scheme 43. Most surprisingly, double deprotonation of **129** by two equivalents of benzyl potassium afforded the arsenido complex $[\{U(Tren^{TIPS})(\mu\text{-}As)(\mu\text{-}K_2)\}_4]$ (**131**).[147] Attempts to abstract the potassium cations from **131** using 2.2.2-cryptand resulted in formation of the arsinidiide $[\{U(Tren^{TIPS})(\mu\text{-}AsH)\}\{K(2.2.2\text{-}cryptand)\}]$ (**132**),[147] with K/H exchange from solvent. The authors additionally reported an As–H stretch in the ATR-IR spectrum of **130** at 1857 cm^{-1}. Complex **131** is a tetramer with an As_4K_6 adamantane-type core, with the bridging potassium ions self-evidently playing an indispensable role in stabilising the arsenido $[As]^{3-}$ centres, *cf.* formation of **132**.

The U–As distance of 2.7159(13) Å in the terminal arsinidene complex **130** is shorter than that seen for the potassium-capped arsinidiide complex **132** (2.7489(10) Å) and the arsenido complex **131** (2.730(2)–2.775(2) Å), which is due to the coordination of the potassium ion (or ions) to the arsenic centre(s). Computational analysis showed highly polarised single, double, and triple uranium arsenic bonding interactions for U–AsH_2 (**129**), U=AsH (**130**) and U≡As (**131**), with substantial 5f orbital contributions to these bonds.

In 2017, Liddle, Scheer, and co-workers adapted the protonolysis chemistry used to access **67**, **70**, and **71**, performing protonolysis reactions of **65Th** with different ratios of $KAsH_2$ both with and without 15C5 to synthesise a range of Th–As complexes, Scheme 44, including the parent arsinidiide $[\{Th(Tren^{TIPS})\}_2(\mu\text{-}AsH)]$ (**133**), the arsinidiide $[\{Th(Tren^{TIPS})(\mu\text{-}AsH)\}\{K(15C5)\}]$ (**134**), and the bridging arsenido $[K(15C5)_2][\{Th(Tren^{TIPS})\}_2(\mu\text{-}As)]$ (**135**), Scheme 44.[150] The authors reported that attempts to prepare a terminal arsinidene $[K(L)_n][Th(Tren^{TIPS})(AsH)]$ (L = crown ethers or 2.2.2-cryptand) under various conditions were unsuccessful. Complex **134** could also be readily prepared in a 70% yield *via* the deprotonation of the parent arsenide $[Th(Tren^{TIPS})AsH_2]$ (the Th analogue of **129**) with one equivalent of benzyl potassium in the presence of one equivalent of 15C5. The ATR-IR spectra of **133** and **134** exhibited As–H stretches of 1930 and 1922 cm^{-1}, respectively. Consistent with the arsenido nature of **135**, no As–H stretch was observed in the ATR-IR spectrum of **135**.

Complexes **133–135** have respective Th–As distances of 2.9619(6)/3.0286(6), 2.8565(7) and 2.8063(14)/2.8060(14) Å, which are shorter than that of the parent arsenide $[Th(Tren^{TIPS})AsH_2]$ [3.065(3) Å]. When compared to the sum of the covalent single and double bond radii of Th and As of 2.96 and 2.57 Å, respectively, these Th–As bonds are relatively long and clearly polarised. An acute Th–As–H bond angle of 79.1(2)° in **134** suggested that a Th···H 'agostic-type' interaction could be present. The solid state structure of **135** is analogous to the thorium phosphido complex **70**, with a symmetrical ThAsTh core and near linear Th–As–Th angle of 177.04(6)°. In line with the multiple bonding interaction in the ThAsTh linkage, the Th–As distances exhibited by **135** (2.8063(14)/2.8060(14) Å) are

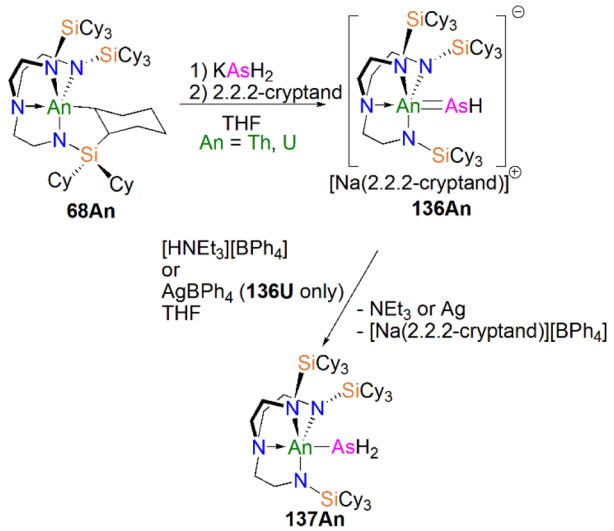

Scheme 45 Synthesis of terminal actinide parent arsinidene and arsenide complexes **136An** and **137An**.

shorter than those in **133** (2.9619(6)/3.0286(6) Å). The authors reported that attempts to prepare a terminal Tren^{TIPS} thorium arsenido Th≡As species using the similar double deprotonation method for **132** proved unsuccessful; indeed, closely related work attempting to construct thorium nitrides supported by Tren^{TIPS} consistently resulted in the formation of parent imido complexes.

In 2022, Liddle, Scheer, and co-workers showed that a terminal parent arsinidene at thorium (and uranium for comparison) could be isolated using the bulky Tren^{TCHS} ligand, Scheme 45. Specifically, reaction of **68An** with $KAsH_2$ in the presence of 2.2.2-cryptand in THF afforded directly, in good yields, [K(2.2.2-cryptand)][An(Tren^{TIPS})(AsH)] (**136An**), Scheme 45.[84] The molecular structures of **136An** confirmed the presence of terminal arsinidene $(AsH)^{2-}$ units that are well-protected by the tricyclohexylsilyl groups. The An–As bond distances of 2.8521(8) Å and 2.7581(6) Å for **136Th** and **136U**, respectively, are statistically invariant to those in **134** and **130**, indicating multiple bonding interactions in these An = AsH linkages that were confirmed by DFT calculations. 'Agostic-type' interactions between the metal ions and arsinidene ligands are observed in both structures, with An–As–H angles of 60.50(12)° and 61.18(12)°, respectively. In addition, ATR-IR spectroscopy revealed As–H stretches at 1867 and 1875 cm^{-1} for **136Th** and **136U**, respectively. The authors found that treatment of **136An** with $[HNEt_3][BPh_4]$ in THF results in the isolation of the parent arsenide complexes [An(Tren^{TCHS})(AsH_2)] (**137An**) in good yields, Scheme 45; oxidation of **136U** also gave the protonated product **137U**.[84]

7.2 Actinide 2-arsaethynolate complexes

Following the aforementioned developments in f-element 2-phosphethynolate chemistry, the chemistry of the corresponding 2-arsaethynolate anion $(OCAs)^-$ is beginning to emerge. In 2018, Meyer and co-workers reported reactions of the U(III) complex [U{(^{Ad,Me}ArO)$_3$N}(DME)] ({(^{Ad,Me}ArO)$_3$N}$^{3-}$ = trianion of tris(2-hydroxy-3-(1-adamantyl)-5-methylbenzyl)amine) with one equivalent of [Na(OCAs)(dioxane)$_3$], and 2.2.2-cryptand giving [Na(2.2.2-cryptand)][{U((^{Ad,Me}ArO)$_3$N)(THF)}(μ-O){U((^{Ad,Me}ArO)$_3$N)(CAs)}].[151] In contrast, using two equivalents of [Na(OCAs)(dioxane)$_3$] yielded the binuclear, μ-oxo bridged diuranium(IV/IV) complex [Na(2.2.2-cryptand)]$_2$[{U((^{Ad,Me}ArO)$_3$N)}$_2$(μ-O)(μ-AsCAs)], which contains a μ:η^1-η^1-coordinated $(AsCAs)^{2-}$ ligand.[151] In 2019, Liddle, Scheer, and co-workers reported the first U–OCAs complex [U(Tren^{TIPS})(OCAs)], and treatment of this complex with KC_8 and 2.2.2-cryptand as an *in situ* electride mixture yielded [K(2.2.2-cryptand)][{U(Tren^{TIPS})}$_2${μ-η^2(OAs):η^2(CAs)–OCAs}] which is the As analogue of **75**, with a highly reduced bent, carbene-like OCAs-ligand.[152] In contrast, reduction or photolysis of [U(Tren^{TIPS})(OCAs)] with [U(Tren^{TIPS})] gave the mixed-valence arsenido complex [{U(Tren^{TIPS})}$_2$(μ-As)], in very low yield, or **123**, respectively.[152] All of these results demonstrate the challenges of using the OCAs ligand to synthesise actinide–arsenic bonds and also that the synthetic methods and ancillary ligands drive the $(OCAs)^-$ bond cleavage chemistry in very different directions.

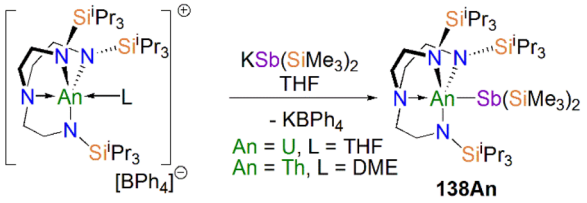

Scheme 46 Synthesis of the actinide–antimony complexes **138An**.

7.3 Actinide antimony complexes

In 2017, Liddle, Scheer, and co-workers reported the isolation and characterisation of the first discrete (*i.e.* not multi-centre) An–Sb bonds (An=U and Th) from the reactions of [An(Tren^{TIPS})(L)][BPh_4] (An=U, L=THF; An=Th, L=DME) and $KSb(SiMe_3)_2$ in THF, yielding [An(Tren^{TIPS}){$Sb(SiMe_3)_2$}] (**138An**), Scheme 46.[153] The closely related uranium complex [U(Tren^{DMBS}){$Sb(SiMe_3)_2$}] with a less sterically bulky supporting ligand could also be prepared using the same synthetic approach.[153]

Complexes **138Th** and **138U** exhibit An–Sb distances of 3.2849(3) and 3.2089(6) Å, respectively. The authors observed a shorter U–Sb bond in **138U** (3.2089(6) Å) compared to [U(Tren^{DMBS}){$Sb(SiMe_3)_2$}] (3.2437(8) Å), likely a result of the differing sterics between the Tren^{TIPS} and Tren^{DMBS} ligand

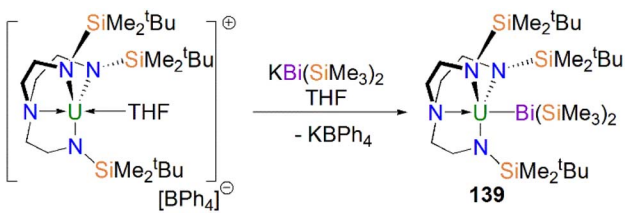

Scheme 47 Synthesis of the uranium–bismuthide complex **139**.

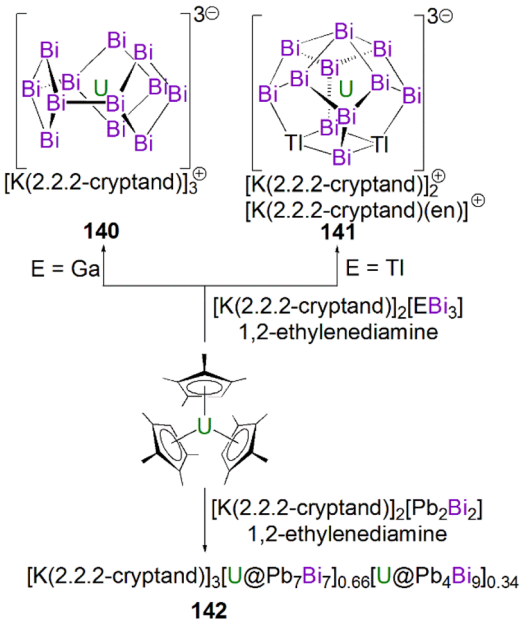

Scheme 48 Synthesis of the uranium–bismuth Zintl anionic clusters **140–142**. U–Bi bonds are omitted for clarity.

systems; the latter results in more orthogonal, and presumably weaker, binding of the stibide ligand. The analogous U–P and U–As complexes were also prepared in that study, revealing increasingly pyramidalised pnictide centres as the group is descended.

7.4 Actinide bismuth complexes

In the same publication describing the work in Section 7.3, Liddle, Scheer, and co-workers also reported the synthesis and characterisation of the first two-centre-two-electron (2c–2e) U–Bi bond, [U(Tren^{DMBS}){Bi(SiMe$_3$)$_2$}] (**139**), by the reaction of [U(Tren^{DMBS})(THF)][BPh$_4$] with KBi(SiMe$_3$)$_2$ in THF, Scheme 47.[153] It was found that the U–Bi bond could not be stabilised using the bulkier Tren^{TIPS} ligands, likely due to steric overload. Complex **139** exhibits U–Bi distances of 3.3208(4) Å which is longer than the above An–Sb bonds. Whilst the U–Bi bond in **139** was isolable, no Th–Bi bond could be isolated with Tren^{TIPS} or Tren^{DMBS}, underscoring the fragility of these linkages. Complex **139** is the only monomeric actinide complex containing a discrete bond to Bi to date.

Dehnen and co-workers reported actinide bismuth clusters in 2016. Reaction of [U(C$_5$Me$_4$H)$_3$] with [K(2.2.2-cryptand)]$_2$[EE′Bi$_2$]·en (E = Ga, Tl, E′ = Bi; E = E′ = Pb) in 1,2-ethlyenediamine gave either [K(2.2.2-cryptand)]$_3$[U@Bi$_{12}$] (**140**), [K(2.2.2-cryptand)]$_2$[K(2.2.2-cryptand)(en)][U@Tl$_2$Bi$_{11}$] (**141**) or [K(2.2.2-cryptand)]$_3$[U@Pb$_7$Bi$_7$]$_{0.66}$[U@Pb$_4$Bi$_9$]$_{0.34}$ (**142**), Scheme 48.[154] The structure of the trianionic fragment of **140** is analogous to the antimony cluster **101Ln**, exhibiting longer equatorial U–Bi bond distances (3.463(3)–3.545(3) Å) than the non-equatorial U–Bi bond distances (3.119(3)–3.167(3) Å). Complex **141** exhibits a 13-vertex cluster that is analogous to **114Ln**, with U–Bi

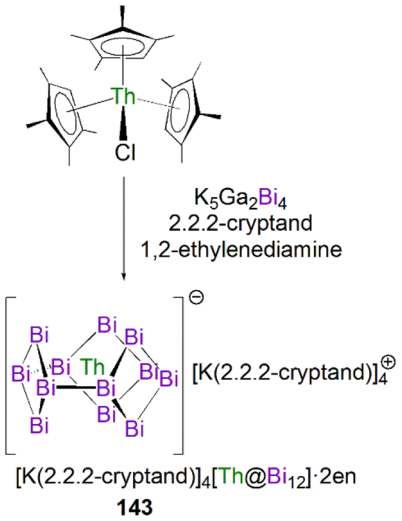

Scheme 49 Synthesis of the thorium–bismuth Zintl anionic clusters **143**. The Th–Bi bonds are omitted for clarity.

distances ranging from 3.068(1) to 3.4515(6) Å. Complex **142** has an isomorphic structure to **118Ln/120Ln**, exhibiting U–Bi bond distances ranging from 2.885(9) to 3.6885(12) Å.

In 2021, Dehnen and co-workers extended this Bi cluster chemistry to include the first example of a thorium bismuth cluster containing Th–Bi bonds, Scheme 49. The authors reported that reaction of [(C$_5$Me$_4$H)$_3$Th(Cl)] with K$_5$Ga$_2$Bi$_4$, which can be used as an *in situ* source of [GaBi$_3$]$^{2-}$ and Bi$_4^{2-}$, in the presence of 2.2.2-cryptand in 1,2-ethlyenediamine afforded [K(2.2.2-cryptand)]$_4$[Th@Bi$_{12}$]·2en (**143**) as black, prismatic crystals, Scheme 49.[155] The structure of **143** was confirmed by single-crystal X-ray diffraction and the Th : Bi ratio within the cluster was verified by micro-X-ray fluorescence spectroscopy. The molecular structure revealed Bi–Bi bond distances over a relatively small range (3.0420(14)–3.132(1) Å) and Th–Bi bond lengths (3.2104(11)–3.5908(9) Å) that are comparable to the An–Bi bonds in **139–142**. Magnetic data and theoretical studies on **143** confirm the formal assignment as Th^{4+} and Bi$_{12}^{8-}$ with a remarkable ring current strength of 24.8 nAT^{-1} for [Th@Bi$_{12}$]$^{4-}$ (and 23.7 nAT^{-1} for Bi$_{12}^{8-}$). This is much larger than in 6π-aromatic benzene (11.4 nAT^{-1}), but close to that in 26π-aromatic porphine (25.3 nAT^{-1}), despite the much smaller number of 2π-electrons involved. The aromatic nature of [Th@Bi12]$^{4-}$ extends aromaticity to the heaviest all-metal inorganic system.

8. Conclusions and outlook

Although f-element heavy pnictogen chemistry initially progressed quite slowly for many decades, with the resurgence of non-aqueous f-element chemistry momentum in this area has increased significantly in recent years, as evidenced by the burgeoning array of novel metal-heavy-pnictogen bond types that are now known. These well-characterised compounds have enabled us to secure new structural motifs and probe the nature of f-element ligand chemical bonds to further deepen our

understanding of chemical bonding with increasingly heavy ions in non-relativistic to relativistic regimes. Overall, f-element heavier pnictogen chemistry is developing well but there are certainly numerous opportunities to advance knowledge and understanding in this burgeoning field.

Looking forward, there are several appealing directions for researchers to explore in this area: (1) in general terms, f-element-phosphorus chemistry is maturing, but arsenic and especially antimony and bismuth are poorly developed – bringing the latter three to the same level of maturity as phosphorus will do much to elucidate periodic trends; (2) there are still relatively few actinide–pnictidene/ido multiple bond complexes and even fewer lanthanide analogues – however, the reports of isolated complexes to date suggests that there is ample scope to secure new Ln and An double and triple bonds to P, As, Sb, and Bi if the right supporting ligands can be identified and coupled with suitable synthetic approaches; (3) heavy analogues of dinitrogen are now known and even as radical species, but examples remain few in number – developing better synthetic approaches would open the area up and provide interesting electronic and physicochemical properties and potential atom-transfer methodologies; and, (4) though relatively few in number, it is already clear that f-element pnictogen clusters can exhibit novel magnetic and aromaticity properties – expanding the range of such compounds can only enhance our understanding of these fundamental phenomena.

Author contributions

J. D., D. P. M. and S. T. L. designed the structure of the review. All authors contributed to the writing of the article.

Conflicts of interest

There are no conflicts to declare.

Acknowledgements

We gratefully acknowledge funding and support from the Royal Society (UF071260, UF110005, RG080285, RG110238), Engineering and Physical Sciences Research Council (EP/K024000/1, EP/M027015/1, EP/P001386/1, EP/P002560/1, EP/S033181/1, EP/T011289/1), European Research Council (CoG-239621, CoG-612724), the Universities of Nottingham, Manchester, Regensburg, and Zhengzhou. S. T. L. thanks the Alexander von Humboldt Foundation for a Friedrich Wilhelm Bessel Research Award.

References

1 J. P. Liu, M. Willard, W. Tang, E. Brück, F. de Boer, E. Liu, J. Liu, C. Felser, G. Fecher, L. Wollmann, O. Isnard, E. Burzo, S. Liu, J. F. Herbst, F. Hu, Y. Liu, J. Sun, B. Shen and A. de Visser, Metallic magnetic materials, in *Handbook of Magnetism and Magnetic Materials*, ed. Coey M. and Parkin S., Springer, Cham, 2021.
2 O. Gutfleisch, M. A. Willard, E. Brück, C. H. Chen, S. G. Sankar and J. P. Liu, *Adv. Mater.*, 2011, **23**, 821–842.
3 Y. Hasegawa and Y. Kitagawa, Lanthanide-based materials for electroluminescence, in *Modern Applications of Lanthanide Luminescence*, ed. de Bettencourt-Dias A., Springer, Cham, 2021, Springer Series on Fluorescence, vol. 19.
4 R. Marin and D. Jaque, *Chem. Rev.*, 2021, **121**, 1425–1462.
5 H. Dong, S.-R. Du, X.-Y. Zheng, G.-M. Lyu, L.-D. Sun, L.-D. Li, P.-Z. Zhang, C. Zhang and C.-H. Yan, *Chem. Rev.*, 2015, **115**, 10725–10815.
6 A. S. Hyre and L. H. Doerrer, *Coord. Chem. Rev.*, 2020, **404**, 213098.
7 G. A. Molander, *Chem. Rev.*, 1992, **92**, 29–68.
8 F. Ortu, *Chem. Rev.*, 2022, **122**, 6040–6116.
9 M. Scharfe, P. A. Lira-Parada, A. P. Amrute, S. Mitchell and J. Pérez-Ramírez, *J. Catal.*, 2016, **344**, 524–534.
10 Z. Zhang, S. Liu, X. Li, T. Qin, L. Wang, X. Bo, Y. Liu, L. Xu, S. Wang, X. Sun, Y. Lu, F. Luo and S. Liu, *ACS Appl. Mater. Interfaces*, 2018, **10**, 22023–22030.
11 S. G. McAdams, A. M. Ariciu, A. K. Kostopoulos, J. P. S. Walsh and F. Tuna, *Coord. Chem. Rev.*, 2017, **346**, 216–239.
12 X. Cheng, J. Zhou, J. Yue, Y. Wei, C. Gao, X. Xie and L. Huang, *Chem. Rev.*, 2022, **122**, 15998–16050.
13 A. Leoncini, J. Huskens and W. Verboom, *Chem. Soc. Rev.*, 2017, **46**, 7229.
14 A. V. Gelis, P. Kozak, A. T. Breshears, M. A. Brown, C. Launiere, E. L. Campbell, G. B. Hall, T. G. Levitskaia, V. E. Holfeltz and G. J. Lumetta, *Sci. Rep.*, 2019, **9**, 1–11.
15 D. A. Atwood, *The Rare Earth Elements: Fundamentals and Applications*, John Wiley & Sons, Ltd, Chichester, UK, 2012.
16 S. T. Liddle, *Angew. Chem., Int. Ed.*, 2015, **54**, 8604–8641.
17 N. P. Bessen, J. A. Jackson, M. P. Jensen and J. C. Shafer, *Coord. Chem. Rev.*, 2020, **421**, 213446.
18 D. Schädle and R. Anwander, *Chem. Soc. Rev.*, 2019, **48**, 5752.
19 M. Keener, L. Maria and M. Mazzanti, *Chem. Sci.*, 2023, **14**, 6493–6521.
20 S. P. Vilanova and J. R. Walensky, *Encyclopedia of Inorganic and Bioinorganic Chemistry*, John Wiley & Sons, Ltd, 2018.
21 C. R. Groom, I. J. Bruno, M. P. Lightfoot and S. C. Ward, *Acta Crystallogr., Sect. B: Struct. Sci., Cryst. Eng. Mater.*, 2016, **72**, 171–179.
22 L.-W. Ye, X.-Q. Zhu, R. L. Sahani, Y. Xu, P.-C. Qian and R.-S. Liu, *Chem. Rev.*, 2021, **121**, 9039–9112.
23 C. Zhu and H. Xia, *Acc. Chem. Res.*, 2018, **51**, 1691–1700.
24 H. Aktaş, J. C. Slootweg and K. Lammertsma, *Angew. Chem., Int. Ed.*, 2010, **49**, 2102–2113.
25 O. T. Summerscales and J. C. Gordon, *RSC Adv.*, 2013, **3**, 6682–6692.
26 T. Li, S. Kaercher and P. W. Roesky, *Chem. Soc. Rev.*, 2014, **43**, 42–57.
27 M. E. García, D. García-Vivó, A. Ramos and M. A. Ruiz, *Coord. Chem. Rev.*, 2017, **330**, 1–36.
28 L. Qiao, C. Zhang, X.-W. Zhang, Z.-C. Wang, H. Yin and Z.-M. Sun, *Chin. J. Chem.*, 2020, **38**, 295–304.

29 L. Giusti, V. R. Landaeta, M. Vanni, J. A. Kelly, R. Wolf and M. Caporali, *Coord. Chem. Rev.*, 2021, **441**, 213927.
30 D. P. Mills and P. Evans, *Chem.–Eur. J.*, 2021, **27**, 6645–6665.
31 L. N. Grant and D. J. Mindiola, *Chem.–Eur. J.*, 2019, **25**, 1–9.
32 M. D. Fryzuk, T. S. Haddad and D. J. Berg, *Coord. Chem. Rev.*, 1990, **99**, 137–212.
33 B. Ramirez, P. Sharma, R. J. Eisenhart, L. Gagliardi and C. C. Lu, *Chem. Sci.*, 2019, **10**, 3375–3384.
34 B. Ramirez and C. C. Lu, *J. Am. Chem. Soc.*, 2020, **142**, 5396–5407.
35 K. Izod, P. O'Shaughnessy, J. M. Sheffield, W. Clegg and S. T. Liddle, *Inorg. Chem.*, 2000, **39**, 4741–4748.
36 K. Izod, S. T. Liddle, W. McFarlane and W. Clegg, *Organometallics*, 2004, **23**, 2734–2743.
37 K. Izod, S. T. Liddle and W. Clegg, *Chem. Commun.*, 2004, 1748–1749.
38 G. W. Rabe, J. Riede and A. Schier, *J. Chem. Soc., Chem. Commun.*, 1995, 577–578.
39 G. W. Rabe and J. W. Ziller, *Inorg. Chem.*, 1995, **34**, 5378–5379.
40 G. W. Rabe, J. Riede and A. Schier, *Organometallics*, 1996, **15**, 439–441.
41 S. Atlan, F. Nief and L. Ricard, *Bull. Soc. Chim. Fr.*, 1995, **132**, 649.
42 F. Nief and L. Ricard, *J. Organomet. Chem.*, 1997, **529**, 357–360.
43 G. W. Rabe, I. A. Guzei and A. L. Rheingold, *Inorg. Chem.*, 1997, **36**, 4914–4915.
44 M. Westerhausen, S. Schneiderbauer, M. Hartmann, M. Warchhold and H. Nöth, *Z. Anorg. Allg. Chem.*, 2002, **628**, 330–332.
45 M. Westerhausen, S. Schneiderbauer, N. Makropoulos, M. Warchhold, H. Nöth, H. Piotrowski and K. Karaghiosoff, *Organometallics*, 2002, **21**, 4335–4341.
46 P. L. Arnold, F. G. N. Cloke and P. B. Hitchcock, *Chem. Commun.*, 1997, 481–482.
47 L. Jacquot, M. Xémard, C. Clavaguéra and G. Nocton, *Organometallics*, 2014, **33**, 4100–4106.
48 A. Jaoul, C. Clavaguéra and G. Nocton, *New J. Chem.*, 2016, **40**, 6643–6649.
49 T. Arliguie, M. Doux, N. Mézailles, P. Thuéry, P. Le Floch and M. Ephritikhine, *Inorg. Chem.*, 2006, **45**, 9907–9913.
50 J. D. Masuda, K. C. Jantunen, O. V. Ozerov, K. J. T. Noonan, D. P. Gates, B. L. Scott and J. L. Kiplinger, *J. Am. Chem. Soc.*, 2008, **130**, 2408–2409.
51 P. Cui, Y. Chen, X. Xu and J. Sun, *Chem. Commun.*, 2008, 5547–5549.
52 P. Cui, Y. Chen and M. V. Borzov, *Dalton Trans.*, 2010, **39**, 6886–6890.
53 B. F. Wicker, J. Scott, J. G. Andino, X. Gao, H. Park, M. Pink and D. J. Mindiola, *J. Am. Chem. Soc.*, 2010, **132**, 3691–3693.
54 Y. Lv, C. E. Kefalidis, J. Zhou, L. Maron, X. Leng and Y. Chen, *J. Am. Chem. Soc.*, 2013, **135**, 14784–14796.
55 J. Zhou, T. Li, L. Maron, X. Leng and Y. Chen, *Organometallics*, 2015, **34**, 470–476.
56 K. Wang, G. Luo, J. Hong, X. Zhou, L. Weng, Y. Luo and L. Zhang, *Angew. Chem., Int. Ed.*, 2014, **53**, 1053–1056.
57 H. Tian, J. Hong, K. Wang, I. de. Rosal, L. Maron, X. Zhou and L. Zhang, *CSD Communications*, Private Communications, 2017.
58 T. Pugh, F. Tuna, L. Ungur, D. Collison, E. J. L. McInnes, L. F. Chibotaru and R. A. Layfield, *Nat. Commun.*, 2015, **6**, 7492.
59 B. Feng, L. Xiang, K. N. McCabe, L. Maron, X. Leng and Y. Chen, *Nat. Commun.*, 2020, **11**, 2916.
60 B. Feng, L. Xiang, A. Carpentier, L. Maron, X. Leng and Y. Chen, *J. Am. Chem. Soc.*, 2021, **143**, 2705–2709.
61 T. E. Rieser, P. Wetzel, C. Maichle-Mössmer, P. Sirsch and R. Anwander, *J. Am. Chem. Soc.*, 2023, **145**, 17720–17733.
62 Y. Lv, X. Xu, Y. Chen, X. Leng and M. V. Borzov, *Angew. Chem., Int. Ed.*, 2011, **50**, 11227–11229.
63 S. N. Konchenko, N. A. Pushkarevsky, M. T. Gamer, R. Köppe, H. Schnöckel and P. W. Roesky, *J. Am. Chem. Soc.*, 2009, **131**, 5740–5741.
64 W. Huang and P. L. Diaconescu, *Chem. Commun.*, 2012, **48**, 2216–2218.
65 T. Li, J. Wiecko, N. A. Pushkarevsky, M. T. Gamer, R. Koeppe, S. N. Konchenko, M. Scheer and P. W. Roesky, *Angew. Chem., Int. Ed.*, 2011, **50**, 9491–9495.
66 T. Li, M. T. Gamer, M. Scheer, S. N. Konchenko and P. W. Roesky, *Chem. Commun.*, 2013, **49**, 2183–2185.
67 C. Schoo, S. Bestgen, R. Köppe, S. N. Konchenko and P. W. Roesky, *Chem. Commun.*, 2018, **54**, 4770–4773.
68 F. Zhang, J. Zhang, Z. Chen, L. Weng and X. Zhou, *Inorg. Chem.*, 2019, **58**, 8451–8459.
69 A. Hauser, L. Münzfeld, S. Schlittenhardt, R. Köppe, C. Uhlmann, U.-C. Rauska, M. Ruben and P. W. Roesky, *Chem. Sci.*, 2023, **14**, 2149–2158.
70 P. G. Edwards, R. A. Andersen and A. Zalkin, *Organometallics*, 1984, **3**, 293–298.
71 B. S. Newell, T. C. Schwaab and M. P. Shores, *Inorg. Chem.*, 2011, **50**, 12108–12115.
72 J. W. Napoline, S. J. Kraft, E. M. Matson, P. E. Fanwick, S. C. Bart and C. M. Thomas, *Inorg. Chem.*, 2013, **52**, 12170–12177.
73 A. L. Ward, W. W. Lukens, C. C. Lu and J. Arnold, *J. Am. Chem. Soc.*, 2014, **136**, 3647–3654.
74 A. J. Ayres, M. Zegke, J. P. A. Ostrowski, F. Tuna, E. J. L. McInnes, A. J. Wooles and S. T. Liddle, *Chem. Commun.*, 2018, **54**, 13515–13518.
75 A. J. Ayres, A. J. Wooles, M. Zegke, F. Tuna and S. T. Liddle, *Inorg. Chem.*, 2019, **58**, 13077–13089.
76 D. Perales, R. Bhowmick, M. Zeller, P. Miro, B. Vlaisavljevich and S. C. Bart, *Chem. Commun.*, 2022, **58**, 9630–9633.
77 M. E. Garner and J. Arnold, *Organometallics*, 2017, **36**, 4511–4514.
78 M. E. Garner, B. F. Parker, S. Hohloch, R. G. Bergman and J. Arnold, *J. Am. Chem. Soc.*, 2017, **139**, 12935–12938.
79 J. M. Ritchey, A. J. Zozulin, D. A. Wrobleski, R. R. Ryan, H. J. Wasserman, D. C. Moody and R. T. Paine, *J. Am. Chem. Soc.*, 1985, **107**, 501–503.
80 P. J. Hay, R. R. Ryan, K. V. Salazar, D. A. Wrobleski and A. P. Sattelberger, *J. Am. Chem. Soc.*, 1986, **108**, 313–315.

81 A. C. Behrle, L. Castro, L. Maron and J. R. Walensky, *J. Am. Chem. Soc.*, 2015, **137**, 14846–14849.
82 B. M. Gardner, G. Balázs, M. Scheer, F. Tuna, E. J. L. McInnes, J. McMaster, W. Lewis, A. J. Blake and S. T. Liddle, *Angew. Chem., Int. Ed.*, 2014, **53**, 4484–4488.
83 E. P. Wildman, G. Balázs, A. J. Wooles, M. Scheer and S. T. Liddle, *Nat. Commun.*, 2016, **7**, 12884–12894.
84 J. Du, G. Balázs, J. A. Seed, J. D. Cryer, A. J. Wooles, M. Scheer and S. T. Liddle, *Angew. Chem., Int. Ed.*, 2022, **61**, e202211627.
85 M. R. Duttera, V. W. Day and T. J. Marks, *J. Am. Chem. Soc.*, 1984, **106**, 2907–2912.
86 T. M. Rookes, B. M. Gardner, G. Balázs, M. Gregson, F. Tuna, A. J. Wooles, M. Scheer and S. T. Liddle, *Angew. Chem., Int. Ed.*, 2017, **56**, 10495–10500.
87 S. P. Vilanova, P. Alayoglu, M. Heidarian, P. Huang and J. R. Walensky, *Chem.–Eur. J.*, 2017, **23**, 16748–16752.
88 P. Rungthanaphatsophon, T. J. Duignan, A. J. Myers, S. P. Vilanova, C. L. Barnes, J. Autschbach, E. R. Batista, P. Yang and J. R. Walensky, *Inorg. Chem.*, 2018, **57**, 7270–7278.
89 M. L. Tarlton, Y. Yang, S. P. Kelley, L. Maron and J. R. Walensky, *Organometallics*, 2021, **40**, 2701–2708.
90 M. L. Tarlton, X. Yu, R. J. Ward, S. P. Kelley, J. Autschbach and J. R. Walensky, *Chem.–Eur. J.*, 2021, **27**, 14396–14400.
91 M. L. Tarlton, S. P. Vilanova, M. G. Kaumini, S. P. Kelley, P. Huang and J. R. Walensky, *Inorg. Chem.*, 2021, **60**, 14932–14943.
92 M. L. Tarlton, Y. Yang, S. P. Kelley, L. Maron and J. R. Walensky, *Organometallics*, 2021, **40**, 2701.
93 C. Zhang, G. Hou, G. Zi, W. Ding and M. D. Walter, *Inorg. Chem.*, 2019, **58**, 1571–1590.
94 *CSD Search by 10-08-2023*.
95 D. S. J. Arney, R. C. Schnabel, B. C. Scott and C. J. Burns, *J. Am. Chem. Soc.*, 1996, **118**, 6780–6781.
96 S. W. Hall, J. C. Huffman, M. M. Miller, L. R. Avens, C. J. Burns, A. P. Sattelberger, D. S. J. Arney and A. F. England, *Organometallics*, 1993, **12**, 752–758.
97 C. Zhang, G. Hou, G. Zi, W. Ding and M. D. Walter, *J. Am. Chem. Soc.*, 2018, **140**, 14511–14525.
98 C. Zhang, G. Hou, G. Zi and M. D. Walter, *Dalton Trans.*, 2019, **48**, 2377–2387.
99 Y. Wang, C. Zhang, G. Zi, W. Ding and M. D. Walter, *New J. Chem.*, 2019, **43**, 9257–9539.
100 D. Wang, W. Ding, G. Hou, G. Zi and M. D. Walter, *Chem.–Eur. J.*, 2020, **26**, 16888–16899.
101 D. Wang, S. Wang, G. Hou, G. Zi and M. D. Walter, *Inorg. Chem.*, 2020, **59**, 14549–14563.
102 D. Wang, G. Hou, G. Zi and M. D. Walter, *Organometallics*, 2020, **39**, 4085–4101.
103 D. Wang, G. Hou, G. Zi and M. D. Walter, *Organometallics*, 2021, **40**, 383–396.
104 S. Wang, T. Li, Y. Heng, G. Hou, G. Zi and M. D. Walter, *Organometallics*, 2021, **40**, 2149–2165.
105 D. Wang, S. Wang, T. Li, Y. Heng, G. Hou, G. Zi and M. D. Walter, *Dalton Trans.*, 2021, **50**, 8349–8363.
106 D. M. King, F. Tuna, E. J. L. McInnes, J. McMaster, W. Lewis, A. J. Blake and S. T. Liddle, *Science*, 2012, **337**, 717–720.
107 D. M. King, F. Tuna, E. J. L. McInnes, J. McMaster, W. Lewis, A. J. Blake and S. T. Liddle, *Nat. Chem.*, 2013, **5**, 482–488.
108 D. M. King, J. McMaster, F. Tuna, E. J. L. McInnes, W. Lewis, A. J. Blake and S. T. Liddle, *J. Am. Chem. Soc.*, 2014, **136**, 5619–5622.
109 R. Magnall, G. Balázs, E. Lu, F. Tuna, A. J. Wooles, M. Scheer and S. T. Liddle, *Angew. Chem., Int. Ed.*, 2019, **58**, 10215–10219.
110 J. Du, G. Balázs, A. J. Wooles, M. Scheer and S. T. Liddle, *Angew. Chem., Int. Ed.*, 2021, **60**, 1197–1202.
111 O. J. Scherer, B. Werner, G. Heckmann and G. Wolmershäuser, *Angew. Chem., Int. Ed. Engl.*, 1991, **30**, 553–555.
112 A. S. P. Frey, F. G. N. Cloke, P. B. Hitchcock and J. C. Green, *New J. Chem.*, 2011, **35**, 2022–2026.
113 A. Formanuik, F. Ortu, R. Beekmeyer, A. Kerridge, R. W. Adams and D. P. Mills, *Dalton Trans.*, 2016, **45**, 2390–2393.
114 D. Patel, F. Tuna, E. J. L. McInnes, W. Lewis, A. J. Blake and S. T. Liddle, *Angew. Chem., Int. Ed.*, 2013, **52**, 13334–13337.
115 B. M. Gardner, F. Tuna, E. J. L. McInnes, J. McMaster, W. Lewis, A. J. Blake and S. T. Liddle, *Angew. Chem., Int. Ed.*, 2015, **54**, 7068–7072.
116 W. Fang, I. Douair, A. Hauser, K. Li, Y. Zhao, P. W. Roesky, S. Wang, L. Maron and C. Zhu, *CCS Chem.*, 2022, **4**, 2630–2638.
117 J. Du, D. Hunger, J. A. Seed, J. D. Cryer, D. M. King, A. J. Wooles, J. van Slageren and S. T. Liddle, *J. Am. Chem. Soc.*, 2021, **143**, 5343–5348.
118 W. J. Evans, T. A. Ulibarri and J. W. Ziller, *J. Am. Chem. Soc.*, 1988, **110**, 6877–6879.
119 H. Schumann, E. Palamidis, J. Loebel and J. Plckardt, *Organometallics*, 1988, **7**, 1008–1010.
120 W. J. Evans, J. T. Leman, J. W. Ziller and S. I. Khan, *Inorg. Chem.*, 1996, **35**, 4283–4291.
121 F. Nief, D. Turcitu and L. Ricard, *Chem. Commun.*, 2002, 1646–1647.
122 T. Pugh, A. Kerridge and R. A. Layfield, *Angew. Chem., Int. Ed.*, 2015, **54**, 4255–4258.
123 T. Pugh, V. Vieru, L. F. Chibotaru and R. A. Layfield, *Chem. Sci.*, 2016, **7**, 2128–2137.
124 N. Arleth, M. T. Gamer, R. Köppe, S. N. Konchenko, M. Fleischmann, M. Scheer and P. W. Roesky, *Angew. Chem., Int. Ed.*, 2016, **55**, 1557–1560.
125 N. Reinfandt, N. Michenfelder, C. Schoo, R. Yadav, S. Reichl, S. N. Konchenko, A. N. Unterreiner, M. Scheer and P. W. Roesky, *Chem.–Eur. J.*, 2021, **27**, 7862–7871.
126 C. Schoo, R. Köppe, M. Piesch, M. T. Gamer, S. N. Konchenko, M. Scheer and P. W. Roesky, *Chem.–Eur. J.*, 2018, **24**, 7890–7895.
127 C. Schöttle, P. Bockstaller, R. Popescu, D. Gerthsen and C. Feldmann, *Angew. Chem., Int. Ed.*, 2015, **54**, 9866–9870.

128 C. Schoo, S. Bestgen, A. Egeberg, J. Seibert, S. N. Konchenko, C. Feldmann and P. W. Roesky, *Angew. Chem., Int. Ed.*, 2019, **58**, 4386–4389.
129 N. Reinfandt, A. Hauser, L. Münzfeld and P. W. Roesky, *Chem. Sci.*, 2022, **13**, 3363–3368.
130 G. Balázs, M. Sierka and M. Scheer, *Angew. Chem., Int. Ed.*, 2005, **44**, 4920–4924.
131 W. J. Evans, S. L. Gonzales and J. W. Ziller, *J. Chem. Soc., Chem. Commun.*, 1992, 1138–1139.
132 X. Min, I. A. Popov, F.-X. Pan, L.-J. Li, E. Matito, Z.-M. Sun, L.-S. Wang and A. I. Boldyrev, *Angew. Chem., Int. Ed.*, 2016, **55**, 5531–5535.
133 T. Pugh, N. F. Chilton and R. A. Layfield, *Chem. Sci.*, 2017, **8**, 2073–2080.
134 C. Schoo, S. Bestgen, A. Egeberg, S. Klementyeva, C. Feldmann, S. N. Konchenko and P. W. Roesky, *Angew. Chem., Int. Ed.*, 2018, **57**, 5912–5916.
135 N. Reinfandt, C. Schoo, L. Dütsch, R. Köppe, S. N. Konchenko, M. Scheer and P. W. Roesky, *Chem.–Eur. J.*, 2021, **27**, 3974–3978.
136 W. J. Evans, S. L. Gonzales and J. W. Ziller, *J. Am. Chem. Soc.*, 1991, **113**, 9880–9882.
137 A. B. Chung, A. J. Ryan, M. Fang, J. W. Ziller and W. J. Evans, *Inorg. Chem.*, 2021, **60**, 15635–15645.
138 P. Zhang, R. Nabi, J. K. Staab, N. F. Chilton and S. Demir, *J. Am. Chem. Soc.*, 2023, **145**, 9152–9163.
139 F. Lips, R. Clérac and S. Dehnen, *Angew. Chem., Int. Ed.*, 2011, **50**, 960–964.
140 F. Lips, M. Hołyńska, R. Clérac, U. Linne, I. Schellenberg, R. Pöttgen, F. Weigend and S. Dehnen, *J. Am. Chem. Soc.*, 2012, **134**, 1181–1191.
141 B. Weinert, F. Weigend and S. Dehnen, *Chem.–Eur. J.*, 2012, **18**, 13589–13595.
142 B. Weinert, F. Müller, K. Harms, R. Clérac and S. Dehnen, *Angew. Chem., Int. Ed.*, 2014, **53**, 11979–11983.
143 R. Ababei, W. Massa, B. Weinert, P. Pollak, X. Xie, R. Clérac, F. Weigend and S. Dehnen, *Chem.–Eur. J.*, 2015, **21**, 386–394.
144 P. Zhang, F. Benner, N. F. Chilton and S. Demir, *Chem*, 2022, **8**, 717–730.
145 O. J. Scherer, J. Schulze and G. Wolmershäuser, *J. Organomet. Chem.*, 1994, **484**, C5–C7.
146 B. M. Gardner, G. Balázs, M. Scheer, A. J. Wooles, F. Tuna, E. J. L. McInnes, J. McMaster, W. Lewis, A. J. Blake and S. T. Liddle, *Angew. Chem., Int. Ed.*, 2015, **54**, 15250–15254.
147 B. M. Gardner, G. Balázs, M. Scheer, F. Tuna, E. J. L. McInnes, J. McMaster, W. Lewis, A. J. Blake and S. T. Liddle, *Nat. Chem.*, 2015, **7**, 582–590.
148 M. L. Tarlton, O. J. Fajen, S. P. Kelley, A. Kerridge, T. Malcomson, T. L. Morrison, M. P. Shores, X. Xhani and J. R. Walensky, *Inorg. Chem.*, 2021, **60**, 10614–10630.
149 A. C. Behrle and J. R. Walensky, *Dalton Trans.*, 2016, **45**, 10042–10049.
150 E. P. Wildman, G. Balázs, A. J. Wooles, M. Scheer and S. T. Liddle, *Nat. Commun.*, 2017, **8**, 14769–14777.
151 C. J. Hoerger, F. W. Heinemann, E. Louyriac, M. Rigo, L. Maron, H. Grützmacher, M. Driess and K. Meyer, *Angew. Chem., Int. Ed.*, 2019, **131**, 1693–1697.
152 R. Magnall, G. Balázs, E. Lu, M. Kern, J. van Slageren, F. Tuna, A. J. Wooles, M. Scheer and S. T. Liddle, *Chem.–Eur. J.*, 2019, **25**, 14246–14252.
153 T. M. Rookes, E. P. Wildman, G. Balázs, B. M. Gardner, A. J. Wooles, M. Gregson, F. Tuna, M. Scheer and S. T. Liddle, *Angew. Chem., Int. Ed.*, 2018, **57**, 1332–1336.
154 N. Lichtenberger, R. J. Wilson, A. R. Eulenstein, W. Massa, R. Clérac, F. Weigend and S. Dehnen, *J. Am. Chem. Soc.*, 2016, **138**, 9033–9036.
155 A. R. Eulenstein, Y. J. Franzke, N. Lichtenberger, R. J. Wilson, H. L. Deubner, F. Kraus, R. Clérac, F. Weigend and S. Dehnen, *Nat. Chem.*, 2021, **13**, 149–155.
156 E. R. Pugliese, F. Benner and S. Demir, *Chem.–Eur. J.*, 2023, e202302687.
157 E. R. Pugliese, F. Benner and S. Demir, *Chem. Commun.*, 2023, DOI: **10.1039/d3cc04520j**.
158 Q. Wen, B. Feng and Y. Chen, *Acc. Chem. Res.*, 2023, DOI: **10.1021/acs.accounts.3c00429**.